Degradable Microchannel Nerve Guidance Scaffolds for Central and Peripheral Nerve Repair- From Soft to Rigid

by

Dena Shahriari

A dissertation submitted in partial fulfillment
of the requirements for the degree of
Doctor of Philosophy
(Macromolecular Science and Engineering)
in The University of Michigan
2016

Doctoral Committee:

Associate Professor Jeff S. Sakamoto, Chair
Assistant Professor Geeta Mehta
Professor Mark H. Tuszynski
Professor Alan S. Wineman

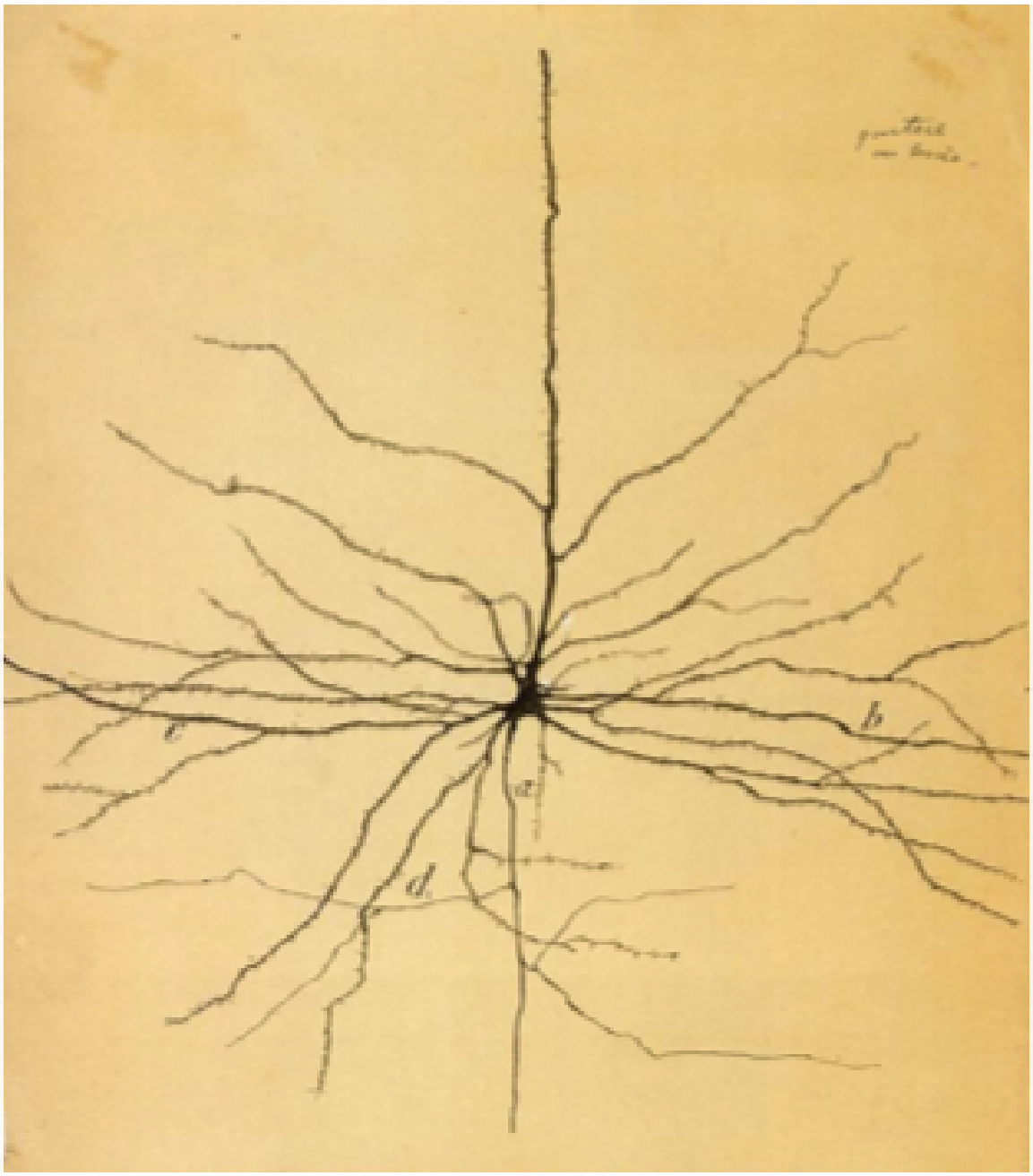

One of the first drawings of a neuron by Santiago Ramón y Cajal who once said: "In adult centers the nerve paths are something fixed, ended, immutable. Everything may die, nothing may be regenerated. It is for the science of the future to change, if possible, this harsh decree." 1928.

To those with paralysis. And to my family and my love who so beautifully support me to reach higher for my dreams and turn them into reality.

ACKNOWLEDGEMENTS

I, for most, thank my mother, Roya, who is the symbol of care, warmth and hard work for me. My siblings, Mahzad, Shabnam, Shirzad and Shabahang have been my pillars through the years. My family's continuous support and love have fostered my ambitions and spirit for hard work. It is also the encouragement and support of my love, Philipp, who believes in me and patiently comforts me.

I appreciate the support of my amazing friends through the years. Oishi and Shoeleh who have always supported me and having long conversations on topics from science to women's rights never get old. It was also together with Asma, Regina and Yunsung that we could form a pyramid of encouragement for each other and make great memories. Dan and Kayla are other dear friends who made working on this project both joyful and valuable.

My PhD advisor, Prof. Jeff Sakamoto is greatly appreciated. This work would have not been possible without him. His intelligence and stimulating ideas shaped me as a scientist, which I am very much thankful for.

I appreciate Prof. Mark Tuszynski for his vast expertise, intelligence and kind support through the years. It has been an invaluable opportunity learning from him.

Prof. Wendy Campana is sincerely appreciated for her great knowledge, intelligence and warm spirit. She is a successful female figure I admire.

I am grateful for our invaluable collaboration with Prof. Mark Tuszynski, Prof. Wendy Campana and their lab members. Their stimulating thoughts, advice and contributions were pivotal to this work. In addition, all the animal studies presented

in this dissertation including but not limited to surgical procedures and *in vivo* characterizations were obtained by Prof. Mark Tuszynski as the main PI for the spinal cord projects and Prof. Wendy Campana as the main PI for the peripheral nerve work. Dr. Kobi Koffler form Prof. Mark Tuszynski's lab is specially acknowledged for performing all the spinal cord surgeries and characterizations. Drs. Kenichi Murakami, Masataka Shibayama and Go Kubota from Prof. Wendy Campana's lab are appreciated for performing all the peripheral nerve surgeries and evaluations.

Dr. Dan Lynam is acknowledged for his important and invaluable contribution to Chapters III, V and VI and the Appendix. Kayla Wolf is appreciated for her original ideas and hard work on Chapters IV and VI and the Appendix. I also thank Christopher Scott for his hard work on Chapter V.

I thank all my committee members, Profs. Jeff Sakamoto, Geeta Mehta, Mark Tuszysnki and Alan Wineman for their support and great insight.

Lastly, this work would have not been possible without the generous funding sources. The work was funded by the NIH (R01 EB014986), the Veterans Administration and the Dr. Miriam and Sheldon G. Adelson Medical Research Foundation. I also greatly acknowledge the National Science Foundation for their Graduate Research Fellowship as well as the Macromolecular Science and Engineering department at the University of Michigan for a fellowship.

TABLE OF CONTENTS

LIST OF FIGURES

Figure

LIST OF TABLES

Table

LIST OF ABBREVIATIONS

BJH Barrett-Joyner-Halenda

BET Brunauer, Emmett, Teller

BSA bovine serum albumin

SEM scanning electron microscopy

BDNF brain-derived neurotrophic factor

$CaCl_2$ calcium chloride

CNC computer numerical control

HP high-purity

LbL layer-by-layer

LP low-purity

MCFB multicomponent fiber bundles

NaCl sodium chloride

NaOH sodium chloride

NGS nerve guidance scaffold

PAA poly(acrylic acid)

PBM planetary ball-milling

PCL poly caprolactone

PDL poly-D-lysine

PEG poly(ethylene glycol)

PEGDA poly(ethylene glycol) diacrylate

PEO polyethylene oxide

PFA paraformaldehyde

PGA poly(glycolic acid)

pHEMA poly 2-hydroxyethyl methacrylate

PLA poly(lactic acid)

PMMA poly(methyl methacrylate)

PNI peripheral nerve injury

PNS peripheral nervous system

PS polystyrene

rcf relative centrifugal force

RCL reactive cell layer

RO reverse osmosis

rpm revolutions per minute

SCI spinal cord injuries

TBS Tris-buffered saline

TrKB tropomyosin receptor kinase B

ABSTRACT

Degradable Microchannel Nerve Guidance Scaffolds for Central and Peripheral Nerve Repair- From Soft to Rigid

by

Dena Shahriari

Traumatic nerve injury is generally permanent and debilitating. There is no available therapy primarily owing to the lack of spontaneous axon growth in the adult human central nervous system. In this doctoral work, an interventional technology was investigated to promote and guide axons through nerve gaps to provide nerve repair.

Previously, agarose hydrogel microchannel scaffolds linearly guided axons through lesion gaps of spinal cords in rats. However, these scaffolds were non-degradable. In this work, first the efficacy of degradable hydrogels such as alginate, chitosan and poly(ethylene glycol) (PEGDA) as nerve guidance scaffolds was studied. All the hydrogels, however, were concluded unstable *in vivo* and provided limited axon growth.

To fabricate scaffolds effective for nerve repair poly caprolactone (PCL) with slow degradation rate (reported over 8 months) was selected and investigated. In addition, to increase the open volume of scaffolds, a novel scaffold architecture and fabrication process were introduced in which, both the channels open space and the interstitial

space between the channels could be utilized for axon growth. A salt-leaching process was developed to optimize PCL properties such as porosity, stiffness and cell adhesion. The scaffold design entailed the fabrication of PCL tubes and their assembly inside a PCL outer tube resulting scaffolds with >60% open volume (a 3-fold improvement to state-of-the-art microchannel scaffolds). When implanted in transected spinal cords in rats, linear axon growth inside and between the channels was observed.

The PCL scaffolds, with 3 orders of magnitude higher stiffness than the nerve tissue, provided the highest axon integration and growth in close proximity to the scaffold walls when compared to soft hydrogels. This observation is contradictory to the general belief that an implant with stiffness more closely matching the tissue is more effective. Indeed, this doctoral work is the first study that suggests axon/implant integration is enhanced *in vivo* when the substrate stiffness is orders of magnitude higher than the host tissue.

This technology was translated to poly lactic-co-glycolic acid (PLGA), for a higher degradation rate, and was fabricated to clinically-relevant dimensions. Overall, this dissertation introduces a promising microchannel scaffold for its translation to human nerve repair.

CHAPTER I

Rationale and Aims

Paralysis caused by traumatic nerve damage is generally permanent and debilitating. A cure does not exist mainly since spontaneous nerve regeneration particularly in the adult mammalian spinal cord is disorganized and limited. To guide growing axons and stimulate axon growth toward their distal targets, interventional techniques are under investigation. Microchannel scaffolds combined with drug delivery have previously proven advantageous in promoting a high density of axonal growth in the spinal cords lesion cavities of rats. However, there is still a need for biocompatible and month-long degradable microchannel scaffolds that are functionalized with an acellular drug delivery technique. In this dissertation, materials synthesis and characterization as well as scaffold architectures and fabrication techniques for generating an effective microchannel scaffold are investigated. The development of acellular drug delivery systems are also studied. The specific aims of the dissertation are briefly described below.

1.1 Alginate hydrogel scaffolds

In Chapter III, alginate hydrogel was investigated as the scaffold material. *In vitro* degradation of alginate was quantified using rheology, which showed the hydrogel stiffness decreases by more than 96% in 2 days. Alginate scaffolds with linear

channels were engineered by expanding a fiber-optic templating technology and were implanted in the transected spinal cords of rats. Although some linear axon growth was observed, the implanted scaffolds degraded within 14 days before complete axon growth could occur. Therefore, the studied alginate hydrogel degraded at a higher rate than required for nerve repair.

1.2 Dense alginate scaffolds

It was next hypothesized that dense alginate with significantly reduced porosity has a slower degradation rate than porous alginate hydrogel investigated in Chapter III. To test this hypothesis, in Chapter IV, alginate films with minimal porosity were generated. To functionalize the films with a drug delivery technique, proteins were incorporated with the films and a sustained protein release for 50 days was obtained. The films could also provide a gradient release of proteins. In addition, the bioactivity of the released protein was confirmed. Lastly, a scaffold fabrication technique was introduced to produce microchannel scaffolds. However, when implanted in transected spinal cords of rats, scaffolds degraded within 28 days, which was not sufficient time for axons to grow through the entire length of the nerve gap (2 mm). Reactive cell layers (RCL) were also formed at the ends of the scaffold and the necrosis (unnatural cell death) of the host spinal cord occurred, indicating the inflammatory response of the material.

1.3 Poly(ethylene glycol) diacrylate (PEGDA) hydrogel scaffolds

In Chapter V, a slower degrading hydrogel, PEGDA, was investigated as the scaffold material. The change in the stiffness of the material was studied based on its $weight\%$ ($wt.\%$) and uv cross-linking time. Upon selecting a PEGDA composition

with optimum stiffness (30.6 kPa), the hydrogel was modified with RGD peptides to reduce inflammatory response and improve cell adhesion properties. In addition, the PEGDA scaffolds were functionalized with a layer-by-layer (LbL) drug delivery technique to release brain-derived neurotrophic factor (BDNF), which occurred for 8 days. PEGDA scaffolds were fabricated using the fiber-optic templating technology. The scaffolds were implanted in the transected spinal cords of rats and remained intact for at least 28 days. However, PEGDA hydrogel scaffolds swelled *in vivo* to the degree that less than 14% open volume was available for nerve growth. Therefore, to obtain a scaffold with higher open lumen volume, an alternative approach was needed.

1.4 Agarose hydrogel microdrilled scaffolds with poly caprolactone (PCL) supporting conduits

Chapter VI focuses on a unique scaffold architecture specifically designed for the peripheral nervous system (PNS). Unlike the spinal cord which is protected by the vertebra, peripheral nerves are surrounded by soft tissue and subjected to relatively large dimensional displacement when limbs move. Therefore, when a guidance scaffold is implanted in the PNS, it is necessary to secure the scaffold to the nerve stumps to minimize its movement and to provide mechanical reinforcement. Therefore, the goal of Chapter VI was to fabricate a supporting conduit that can be placed around a microchannel scaffold and be sutured to the nerve stump. PCL was investigated as the conduit material owing to its high strength. To tailor its mechanical properties, porosity was introduced to enhance flexibility and suture-ability. Agarose was investigated as the scaffold material since its efficacy for axon growth was perviously confirmed. Microchannel agarose scaffolds were produced using a microdrill and were inserted into the PCL conduits. The scaffolds were implanted in 1 cm-long nerve gaps in rats sciatic nerves and the PCL conduit was sutured to the nerve stumps. Scaffolds

remained stable in the nerve tissue for at least 56 days. In addition, axon penetration and Schwann cells were observed inside the channels. Overall, PCL conduits were concluded biocompatible and effective in securing a microchannel scaffold in *cm*-long peripheral nerve gaps.

1.5 Poly caprolactone (PCL) scaffolds with high open volume

The work introduced in Chapter VII is aimed to develop the next generation of biocompatible and degradable scaffolds exhibiting a significant increase in open volume. State-of-the-art microchannel scaffolds have a lumen volume less than 45% with the rest of the space occupied by the matrix between the channels. To maximize the scaffold open volume, a new scaffold design was introduced in which, microtubes were assembled inside an outer tube creating interstitial space in between the tubes. To produce the scaffolds, PCL tubes introduced in Chapter VI were modified and used for scaffold fabrication. A salt-leaching technique was developed to optimize pore size, stiffness and cell attachment properties of PCL. Scaffolds with over 60% open volume were implanted in rats transected spinal cords for 28 days. Axonal penetration and linear growth were observed both inside the innertubes and in the interstitial space between the innertubes. In addition, the inflammatory response was the lowest observed compared to agarose, alginate, chitosan and PEGDA scaffolds and is therefore considered the most promising microchannel scaffold compared to the investigated scaffolds.

1.6 Impact and summary

The focus of Chapter VIII was to first confirm the clinical translation of the microchannel scaffolds. Attempts are taken to confirm the PCL technology described in

Chapter VII can be translated to other FDA-approved materials. PLGA was investigated since it is one of the most commonly used biomaterials in tissue engineering and also becasue it degrades faster than PCL (4-8 months as opposed to 1-3 years). PLGA inner tubes with optimized pore size and stiffness were synthesized and inserted inside a PCL conduit. Preliminary data indicates the potential of these scaffolds for nerve repair. Next, the viability of producing microchannel scaffolds with clinically-relevant dimensions were shown and their performance was tested in the sciatic nerve gap of a large animal model (minpig). 10 mm-long PCL microchannel scaffolds with 8 mm diameter were produced without limitation to increase the dimensions. Although further characterization is necessary, preliminary work showed some motor and sensory functional recovery. Overall, the viability of translating the technology introduced in Chapter VII to human clinical applications is suggested.

Next, the criteria for an ideal nerve guidance scaffold are discussed. In addition, some of the discoveries of the dissertation are summarized and compared to analyze the effect of stiffness on nerve growth in spinal cord injury. It is suggested that, unlike the common dogma of "softer is better", a higher rate and density of axon growth occurs on rigid polymers compared to soft hydrogels *in vivo*. Finally, future directions are discussed.

CHAPTER II

Introduction

2.1 Spinal cord injury Overview

2.1.1 Spinal cord injury

Individuals with spinal cord injuries (SCI) generally lose sensation and function at and below the point of injury. Every year about 12,500 new cases of SCI occur in the USA alone [26, 123]. In 2014, approximately, 276,000 individuals with an average age of 42 years lived with SCI [123]. SCI are generally caused by vehicular accidents (39.08%), falls (29.54%), violence (14.4%), and sports and recreational activities (8.39%) (Fig. 2.1) [123]. The condition is debilitating and is considered permanent since less than 1% of the individuals fully recover [35, 45, 123]. In addition, the health complications of SCI progresses over time and about one third of the individuals need re-hospitalization at least once a year [45, 123]. The life expectancy of individuals with SCI after the injury is on average 14 years and has remained constant since the 1980s [26, 123]. In addition, the employment and educational status of individuals is often affected with SCI as shown in Table 2.1 [35, 123]. Overall, there is a compelling need to develop a treatment for SCI.

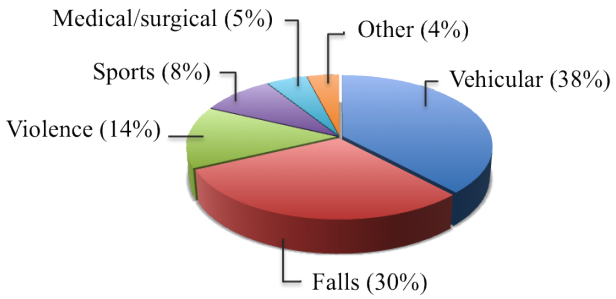

Figure 2.1: Causes of SCI. Chart is reproduced from [123].

Status (%)	At injury	Year 1	Year 10	Year 20	Year 30	Year 40
Empolyed	58.1	12.2	27.9	34.4	32.9	18.5
Student	15.3	16.1	7.2	2.7	0.7	0.0

Table 2.1: The table shows the percentage of individuals with SCI that are employed or are students based on the number of years after the injury. Graph is reproduced from [123].

2.1.2 Acute phase after an injury

The penetration of a damaged vertebrate or an object into the spinal cord can bruise, crush or transect the spinal cord axons and causes SCI. The first few hours (about 3 hours) after an injury are crucial to reduce the severity of the injury due to the immediate swelling of the tissue, which causes secondary damage to the spinal cord. Depending on the level of the injury, surgeries are generally necessary and performed as quickly as possible to remove foreign debris and vertebra fragments [47]. In addition, steroids such as methylprednisolone may reduce inflammation [154]. Orthopedic devices are also often used to stabilize the spine to prevent further damage. On average, the individual is hospitalized for 11 days [123]. The patient may regain slight functional motor and/or sensory recovery within 6 months after the injury owing to some degree of spontaneous spinal cord repair.

2.1.3 Rehabilitation phase after an injury

After the effects of the acute stage, when trauma has subsided and the patient's health is stabilized, rehabilitation may begin. The main purpose of rehabilitation is to help the individual (and the family members) adjust and learn about healthcare options, re-establish independence, and prepare for vocational opportunities as/if the level of injury allows. A variety of health aspects need to be addressed during rehabilitation. When 3187 individuals with SCI were surveyed in 11 different studies, data indicated that the functions most important to the individuals were bowel/bladder control, sexual function, upper limb mobility/sensation, and pain [156]. Other studies have aimed to understand the quality of life aspects most important to the individuals; factors such as friend/family relationships, general health/function, employment, and leisure/recreation were among the aspects individuals preferred more rehabilitation on [156]. In 2014, the rehabilitation stage took an average of 36 days in the USA [123].

2.2 Axons and axon regeneration

2.2.1 SCI at the anatomical level

The information-processing components of the nervous system are neurons. Generally, a neuron receives electrical signals from its dendrites and passes it to another neuron or a muscle through its axon (Fig. 2.2) [83]. In mammals, the spinal cord consists of thousands of linearly-oriented (rostral to caudal) axons, supporting neural cells and capillaries that are physically protected by vertebrae. Spinal cord axons begin from the occipital bone and end between the first and second lumbar vertebrae. When SCI occurs, the axons are transected/injured and the information cannot be transmitted, which causes motor and sensory functionality loss at and below the injury. Neurons of transected spinal cord may survive the injury and minimally re-

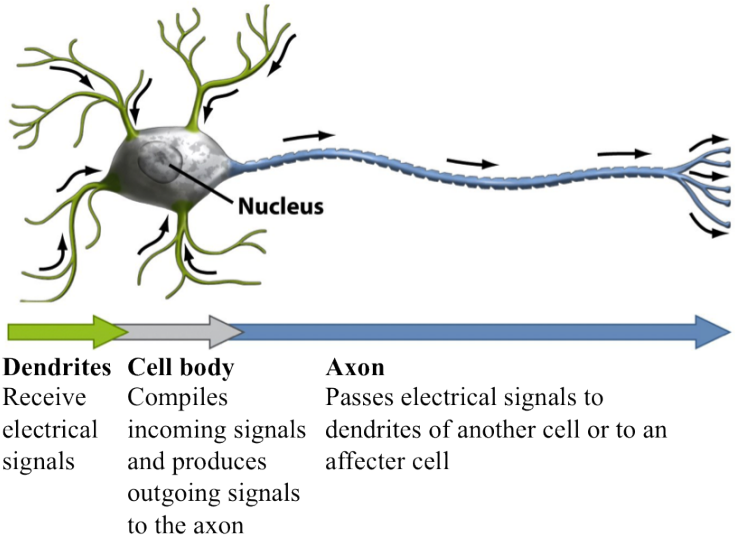

Figure 2.2: Image of an axon. The arrows show the direction of information flow through a neuron: from dendrites to cell body to axons. Image is from [51].

generate by releasing growth factors and cytoskeletal proteins [150].

2.2.2 Axon regeneration mechanism

Axon regeneration can be defined as "1) the growth of a cut axon and 2) extension into or beyond a lesion" [173]. To enable spinal cord repair, the long tract axons of the motor and sensory neurons need to regenerate. It is generally believed that an axon cannot grow or regenerate without a growth cone, which is the tip of a growing axon and the extension of the filopodium (a cell component also important for cell migration) (Fig. 2.3). Axons use growth cones to read signals and select a growth direction [63, 101]. One hypothesis for growth cone translocation and axon extension is the myosin-based clutch theory. When actin filaments at the tip of the growth cone are linked to a substrate and extend toward a target, they are used as "clutches" to pull the central part of the growth cone forward and therefore extend the axons (Fig. 2.4) [164].

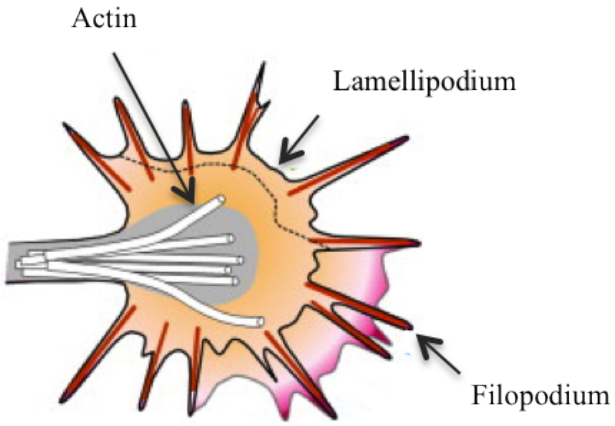

Figure 2.3: The image illustrates the growth cone of an axon with some of its main components: actin, lamellipodium and filopodium. Image is from [89].

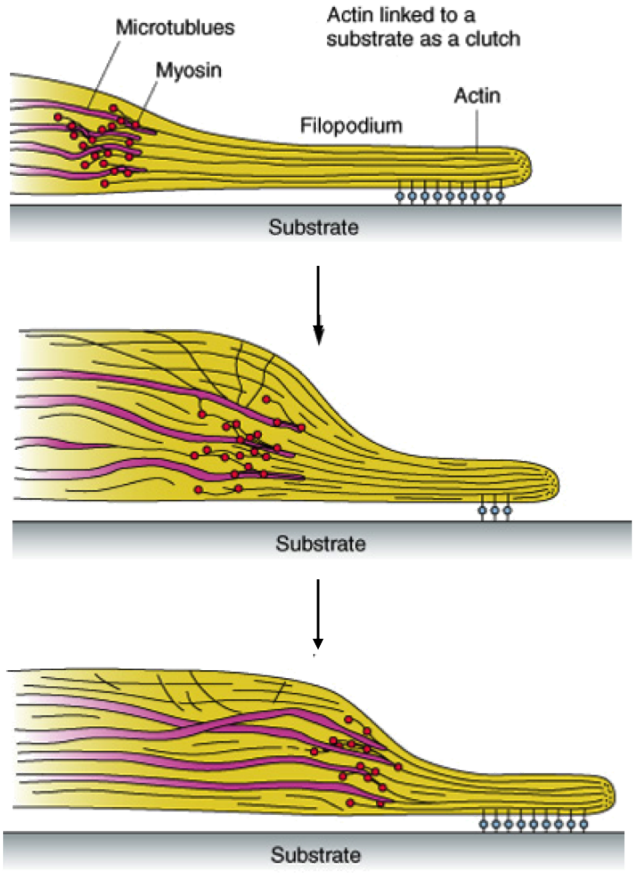

Figure 2.4: The clutch hypothesis for growth cone translocation and axon growth. The actin-based motor, myosin, anchored to ends of microtubules, pulls actin filaments toward the central domain. Image is from [146].

2.2.3 Inhibitory environment of SCI for axon growth

A traumatic injury to the spinal cord triggers a series of secondary responses that significantly limit the growth of axons (Fig. 2.5). The accumulation of inflammatory molecules is one of the immediate responses that is both beneficial and detrimental to axon regeneration [38]. After SCI, an influx of neutrophils occurs within hours followed by macrophages within days to remove cellular debris [135]. Simultaneously, microglia migrate and proliferate in the lesion in the first few hours of injury and often form an inhibitory glial layer within 2 weeks [135]. In addition, since cystic cavities form after severe SCI, meningeal cells and oligodendrocytes fill the lesion to reduce edema, ischemia, hemorrhage, and change in electrolyte level [94, 166]. Consequently, the lesion swells with fluid, reducing tissue density below a point that can provide a permeable matrix for axon growth [138, 166, 174]. Two weeks post-SCI, inhibitory molecules such as oligodendrocytes, reactive astrocytes and chondroitin sulfate proteoglycans (CSPGs) [49, 77, 144] fill the lesion and create an inhibitory environment for axon growth. Overall, since a permeable matrix is necessary for axon growth [174], spontaneous axon growth is limited after SCI.

2.3 Peripheral nerve injury overview

2.3.1 PNI impact

According to Christopher and Dana Reeve Foundation, about 1.4% of the US population with an average age of 52 $\pm$ 18 years live with peripheral nerve injury (PNI) [26]. About 20,000 procedures are performed annually to help repair peripheral nerve injury [125]. Following a PNI, peripheral neuropathy (nerve disease or damage) may occur which affects the somatosensory system [170]. Neuropathy symptoms include, but are not limited to, tingling or numbness, burning or stabbing pain, muscle weakness and extreme sensitivity to touch [14]. About 66% of individuals

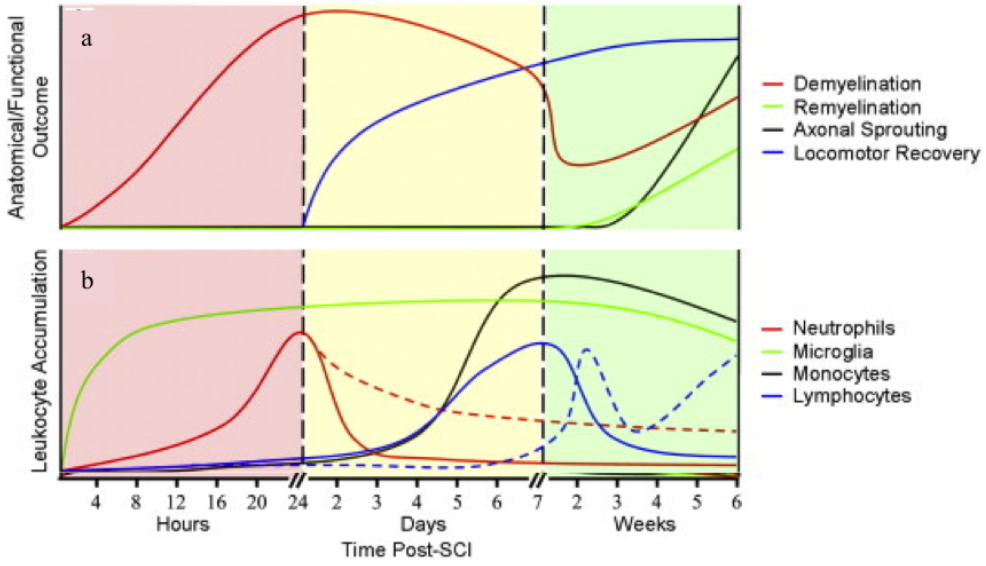

Figure 2.5: The temporal (a) anatomical and functional results and (b) inflammatory responses in SCI rodents [38].

with PNI live with pain and 50% with neuropathy pain [27]. Extreme neuropathic pain often has a more negative impact on the life quality than the disability itself [27]. Because of the pain as well as the loss of body movement and sensation, more workdays are lost and financial burden is high [27, 45]. Individuals with paralysis report a lower quality of life and higher depression rates [27, 45].

2.3.2 Axon regeneration in the peripheral vs. central nervous system

Unlike in SCI, axons can regenerate through a PNI and form functional neural relays after a process called Wallerian degeneration (Fig. 2.6). Several factors distinguish the post-trauma lesion environment in SCI compared to PNI. First, myelin debris is removed immediately after a PNI, but have a delayed removal in SCI, which causes an inhibitory environment for axon regeneration [148]. Second, the axon regenerating genes are silenced in the spinal cord but can be upregulated upon injury in the peripheral nerves [48]. Third, a PNI lacks the inhibitory molecules that are present in SCI. Instead, Schwann cells form a guiding structure called Bünger bands that support axon regeneration through the PNI [92, 129]. Forth, Schwann cells

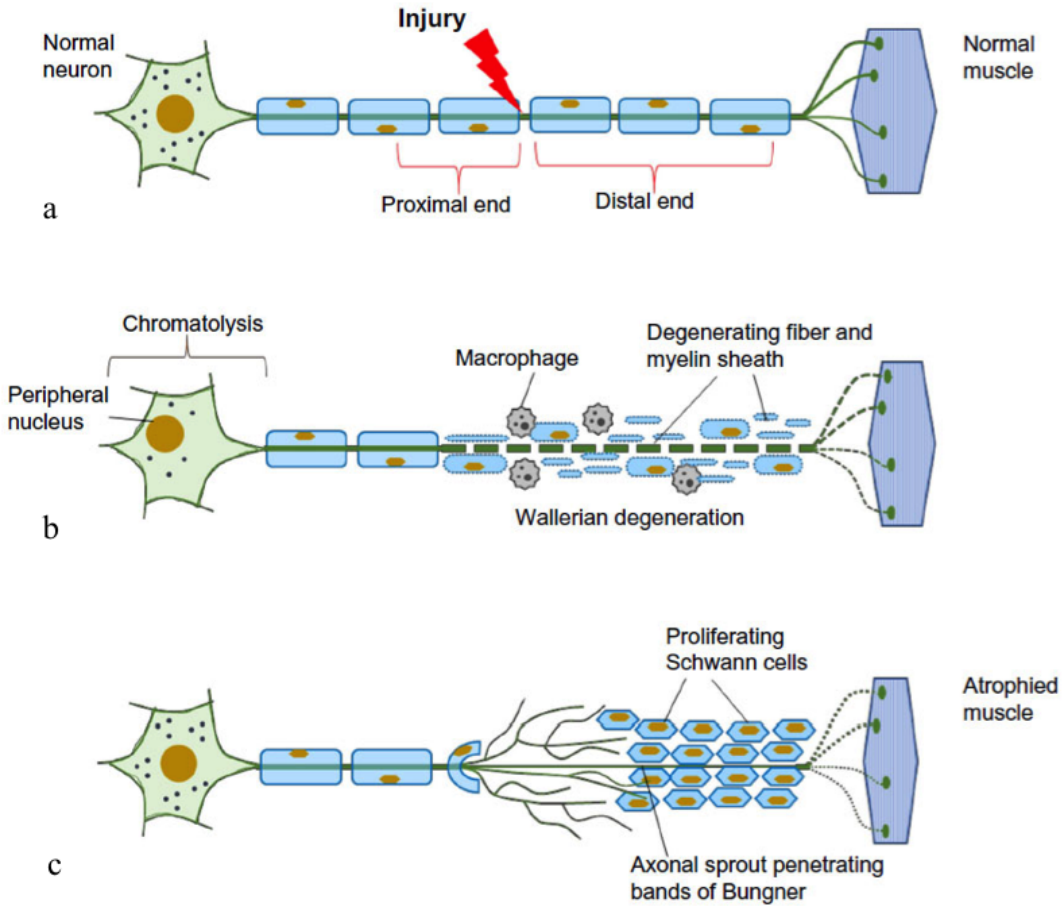

Figure 2.6: Cascade of cellular events after an injury to a peripheral nerve during Wallerian degeneration. (a) Upon injury, the axon cytoskeleton and myelin degenerates. (b) Within 1-3 days, Schwann cells and macrophages start removing the axon and myelin debris. (c) 10-20 days later, Schwann cells form Bünger bands for axons to regenerate along. Images are from [5].

release growth factors after PNI, which induce axon regeneration.

2.3.3 Approaches to peripheral nerve repair

Peripheral nerve repair can occur if the nerve end epineuria are sutured together to connect a severed peripheral nerve [29]. However, when the nerve gap is larger than $\sim$4 mm, suturing the nerve stretches the nerve and diminishes axon regeneration [145]. Currently, autologous grafts are the most prevalent treatment [76, 120] and are considered the"gold standard" approach for acute PNI. They, however, have

practical limitations such as donor site morbidity and painful neuroma formation and are not always possible [11, 95]. Therefore, synthetically engineered grafts are under investigation as an alternative approach. The main purposes of these grafts are to circumvent the disadvantages of autologous grafts while achieving comparable at worst or superior at best clinical outcomes compared to autologous nerve grafts. These grafts are discussed in section 2.5.

2.4 Biomaterials used for nerve guidance scaffolds

2.4.1 Biomaterials selection criteria

The material choice for a nerve implant is critical for its design and performance. Not only should the material be bioinert and degradable, it must also be compatible with a nerve guidance scaffold fabrication technique. Ideally, the material should also allow for the integration of a drug delivery technology. Moreover the implant material should have adequate mechanical properties to survive the rigors of scaffold fabrication process, implantation and patient motion during recovery particularly for the highly mobile regions such as sciatic nerves. Consequently the mechanical properties of a material play an important role in the development of effective nerve guidance scaffold technology. Commonly used biomaterials are divided into biological polymers, natural hydrogels and synthetic polymers and are described in more details below.

2.4.2 Biological polymers

Biological polymers are derived from living systems and are bioresorbable. Collagen, a component of the extracellular matrix [8], is a common example used in nerve scaffolds [39, 149] but it requires cross-linking chemicals that can be toxic [124]. Fibrin is another biomaterial commonly used as tissue adhesives that is derived from blood

[155]. Fibrin primarily consists of fibrinogen, which, in conjunction with platelets, forms blood clots [13, 70]. Thrombin enzymatically breaks fibrinogen to initiate fibrin formation [13, 70] after which a 3-dimensional network is formed [155]. Other examples include gelatin and hyaluronic acid. Biological polymers, however, generally do not have adequate mechanical integrity to sustain a scaffold fabrication technique or implantation process. Overall, it is generally challenging to engineer natural polymers into scaffolds [21]. In addition, since they are driven from the body, they may induce immune response [21].

2.4.3 Polysaccharide hydrogels

Natural hydrogels are polysaccharides generally isolated from sea products and are commonly tested for nerve repair because: 1) they are typically inert, 2) have high water contents similar to tissue, and 3) their mechanical properties can generally be controlled. One example is agarose hydrogel previously used as nerve scaffolds [55, 65, 158]. However, agarose is non-degradable in the body and is generally known to have poor cell adhesion properties. Chitosan is another natural hydrogel widely used for nerve repair [3, 52, 132, 176, 178] and depending on its chemical structure can degrade between a few days to more than 3 months [52, 142]. Despite the advantage of having a tunable degradation, its elastic modulus is reported to be approximately 40 kPa [37], which may limit the fabrication of a scaffold with the necessary mechanical integrity to maintain linear channels. Alginate hydrogel, on the other hand, has adjustable mechanical properties and can have a stiffness of 300 kPa [134], which is sufficient for maintaining linear channels as previously demonstrated [103, 158]. This hydrogel can be ionically cross-linked with earth Alkalines such as calcium [82] and is reported to degrade within 2 months [84] through the leaching of the cross-linking cations. However, the degradation rate of ionically cross-linked alginate has not been accurately characterized for its performance in the nerve tissue.

2.4.4 Synthetic polymers

Synthetic polymers are artificially produced; therefore, their properties and functionality are more controllable and predictable than natural materials. For example, their chemical structure can be tailored to obtain a wide range of mechanical and chemical properties [21]. The most common synthetic scaffold polymers are saturated aliphatic polyesters such as poly(lactic acid) (PLA), poly(glycolic acid) (PGA) and their copolymers [143]. Among this class of polymers, the behavior can vary significantly, owing to their unique composition. For example, the degradation mechanism of these polymers is based on the hydrolysis or the cleaving of ester bonds [109]. The degradation rates depend on the ratio of PLA and PGA since PLA is more hydrophobic and degrades slower. Overall, the degradation rate is more or less unaffected by the *in vivo* environment [143]. However, if an inflammatory response occurs, the pH changes and the hydrolysis rate (and therefore degradation rate) is affected [21]. One example of aliphatic polyester copolymers is PEG (poly(ethylene glycol) or polyethylene oxide (PEO) which is a particularly hydrophilic substrate that results in poor cell and/or protein attachment and can lower the inflammatory response [21]. However, if cell/protein adhesion is desired, PEG can be modified with different peptides such as RGD, IKVAV and YIGSR [66, 186]. In addition, the mechanical properties of PEG can be controlled by changing the PEG weight% [17, 66]. Another polyester previously used for nerve repair applications is poly caprolactone (PCL) [23, 90, 149]. Similar to PEG, PCL does not allow cell attachment [136, 147] likely because of its hydrophobic structure and non-porous morphology. Moreover, PCL is a relatively slow degrading polyester (degradation period reported from 1 year up to 3 years [34, 54]).

2.5 Nerve grafts for axon guidance

2.5.1 The significance of linear axon guidance

Regenerating axons have limited sense of directionality; as a result, they lack the ability to spontaneously grow toward distal targets. However, interventional technologies such as a nerve guidance scaffold can provide physical cues to linearly guide axons. Since axons grow in bundles, guiding individual axons toward distal targets is not only impractical, it is ineffective. Instead, nerve fascicles, integrated with support cells and capilaries, can be linearly guided by nerve guidance scaffolds [46]. A nerve fascicle, in this context, is a group of axons that move toward the distal target [175]. In principal, if the nerve fascicle is confined to a space with a matching diameter, though there may be some misalignment between the native proximal and distal axonal tracts, recapitulation within native nerve tracts is feasible [72, 163, 168, 188]. Thus, nerve guidance scaffolds consisting of linearly-arranged microchannels are a viable approach to guide axonal regeneration.

2.5.2 Nerve grafts designs

Nerve grafts consisting of a range of architectures and designs have been widely investigated. The role of the grafts is to provide a supporting substrate to promote and guide regenerating axons into and beyond nerve gaps (Fig. 2.7). The idea of nerve implants first started in the late 1800s. Later, veins and arteries [179, 180], followed by plastics [56] and metals [40] were studied and even implanted in damaged peripheral nerves in humans. Although some of these grafts enabled nerve growth, they all caused neural impairment and some trigged immune system rejection. Similarly, the use of biological nerve grafts in the PNI from the individual or a cadaver causes damage to the donor nerve, has limited availability and can induce immune rejection [10, 189]. Hollow conduits have been investigated for peripheral nerve re-

pair [132, 181, 182, 185]. In addition, different types of FDA-approved conduits such as Surgisis® [71, 157], Neurotube® [79], NeuroMatrix® [79], Neuroflex® [96] and NeuraGen® [4, 85] are currently available for PNI. Filling the nerve gap with a gel or a matrix is another approach to promote the penetration and growth of axons. For example, collagen gels were transplanted in the transected rats spinal cords and some axon growth through the matrix was observed [110]. Hashimoto *et al.* compared alginate, collagen and fibrin gels for axon growth in sciatic nerve gaps [69]. To further enhance the degree of linear guidance, electrospun fibers are under investigation and the presence of supporting neural cells and some axonal growth were observed [25, 74, 117]. In addition, electrospun fibers may be embedded in a conduit for improved ease of handling during surgery [178]. Other designs such as seeding Schwann cells on a collagen sheath and rolling the sheath has also been investigated [64]. Overall, although some axon growth is observed with myriad designs, linear guidance of axons is generally poor and the majority of axons do not reach their distal targets. To further improve linear axon guidance, multilumen scaffolds are under development.

Extensive research has been conducted to develop a process for fabricating multilumen scaffolds. For example, non-degradable agarose [55, 65, 158] and chemically cross-linked alginate [131, 137] scaffolds as well as degradable poly 2-hydroxyethyl methacrylate (pHEMA) [50] and poly lactic-co-glycolic acid (PLGA) [172] scaffolds with linear microchannels were fabricated. These multilumen scaffolds provided linear directionality for growing axons; however, the microchannel scaffolds occupied more than 55% of the lesion volume. The low lumen volume drastically limits nerve regeneration as well as vascularization and is therefore non-ideal. Another important criterion for a nerve scaffold is for it to have a month-long degradation rate to allow complete axon growth through the lesion. Overall, further modifications are needed to improve the current multilumen scaffold designs.

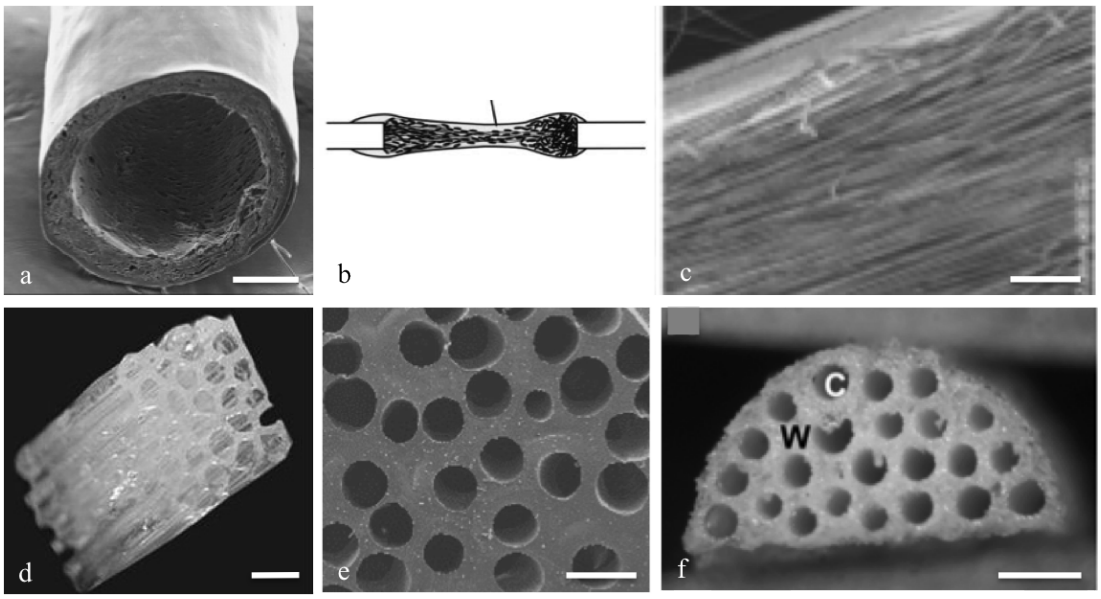

Figure 2.7: Examples of different nerve grafts. (a) Chitosan conduit [3], (b) alginate hydrogel [69], (c) electrospun poly-L-lactic acid fibers [74], and microchannel scaffolds from (d) agarose [158], (e) pHEMA [50] and (f) PLGA [169]. The scale bar in (c) is 50 μm. All the other scale bars are 500 μm

2.5.3 Criteria for nerve guidance scaffolds

When designing a scaffold, several criteria must be simultaneously satisfied. First, the scaffold material must be biocompatible and exhibit month-long degradation rates (for example, one month of regeneration was required to guide axons for 2 mm in spinal cord cavities [158]). Second, the scaffold channel diameter should be large enough for axon bundles (nerve fascicles) to grow into but small enough to provide linear guidance. There is a debate on the optimum channel diameter, which is reported from 20 μm by Pawar *et al.* [131] to 200 μm by Stokols *et al.* [158]. Third, even though it has not been definitively demonstrated, scaffold walls may require interconnected porosity to allow nutrients, waste and oxygen to permeate laterally between microchannels and the scaffold periphery, but small enough to prevent axon cross-over [20, 75]. Fourth, to maximize lumen volume and therefore regeneration, the scaffold channel wall thickness should be minimized. Lastly, it should be possible to manufacture clinically relevant cm-long scaffolds.

2.6 Growth factor delivery

A sustained supply of growth-promoting neurotrophic factors, at a sufficient dosage, can substantially promote axon regeneration and nerve growth [9, 53, 171]. An approach to deliver these factors is to virally transfect or genetically modify cells to produce nerve growth factors [55, 65, 158]. Though effective in stimulating the regeneration of axons, the cellular drug delivery approach can cause tumor formation, spread outside of the injury site, and raise ethical controversies. To avoid these issues, alternative approaches involving acellular drug delivery are under development.

One acellular drug delivery technique is to coat the implant with proteins by immersion in a protein solution [133, 162]. However, this method causes initial burst release and fast protein degradation [98, 152]. Drug delivery systems such as polymeric microspheres can prolong the bioactivity of proteins by encapsulating and delivering drugs, yet they also cause initial burst release and require a secondary carrier to remain in the lesion site and are therefore non-ideal [19].

Protein immobilization on a nerve graft is another approach in which proteins are covalently bonded to the scaffold walls. However, this technique limits the scaffold material to substances with specific functional groups suitable for protein binding. In addition, there are still contradicting results regarding the efficacy of a protein for nerve regeneration when it is bound to a surface and cannot be internalized by neurons [2, 61, 107, 108].

Another drug delivery technique is the layer-by-layer (LbL) drug delivery system. LbL is based on the alternating assembly of materials and the sequential incorporation of drugs on a matrix through complementary interactions [31, 32]. The use of carboxylic acid-based polyelectrolytes allows the assembly of such layers through hydrogen bonding at a pH below the pK_a of the polymers and later releasing the layers in a less acidic environment (Fig. 2.8) [22, 160, 161, 177]. Studies on pH sensitive LbL assembly on agarose hydrogel have shown the release of lysozyme for at least 4 weeks

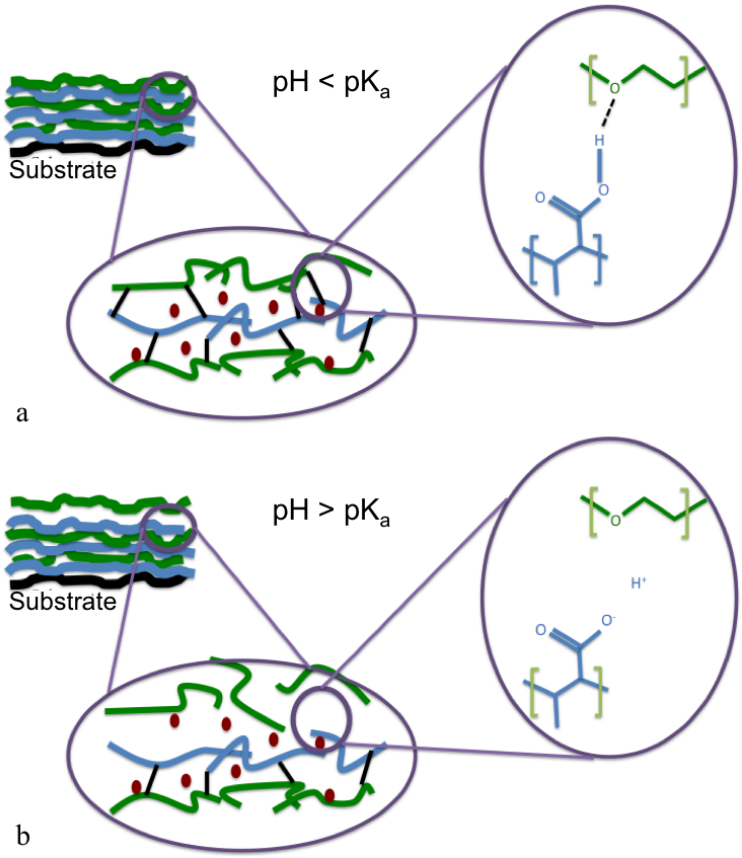

Figure 2.8: (a) Assembly and (b) release of poly (acrylic acid) (PAA) and poly (ethylene glycol) (PEG) alternating layers on a substrate. One layer acts as the hydrogen donor and another as the hydrogen acceptor. Hydrogen bonds are formed at a pH below the pK_a of the polymers. The layers are gradually dissociated when the pH rises above the pK_a. Proteins (red dots) can be taken up in between the polymeric layers and therefore slowly released upon pH rise.

[115] and brain-derived neurotrophic factor (BDNF) for 2 weeks [105]. Furthermore, increasing the surface area of the material causes a higher protein uptake and release [104, 115]. Overall, the LbL drug delivery technique has promising potential for use with nerve implants.

Despite the progress in the fields of neuroscience, materials synthesis and processing, scaffold engineering and drug delivery systems, no therapy exists for SCI as well as few *cm*-long PNI. An approach that combines the findings and discoveries of all these fields may significantly propel the progress in nerve repair. Numerous

research groups currently work on developing such combinatorial therapies. However, there is yet to be reported a nerve guidance scaffold with favorable biocompatibility and degradation rate functionalized with a local and sustained drug release, which stimulates nerve growth and linearly guides the axons through nerve gaps.

CHAPTER III

Characterizing the Degradation of Alginate Hydrogel for Use in Microchannel Scaffolds for Spinal Cord Repair

3.1 Abstract

Alginate was studied as a degradable nerve guidance scaffold material *in vitro* and *in vivo*. *In vitro* degradation rates were determined using rheology to measure the change in shear modulus vs time. The shear modulus decreased from 155 kPa to 5 kPa within 2 days; however, alginate samples maintained their superficial geometry for over 28 days. The degradation behavior was supported by materials characterization data showing alginate consisted of high internal surface area (400 m^2/g), which likely facilitated the release of cross-linking cations resulting in the rapid decrease in shear modulus. To assess the degradation rate *in vivo*, microchannel scaffolds were fabricated using a fiber templating technique. The scaffolds were implanted in a 2 mm-long T3 full transection rodent spinal cord lesion model for 14 days. Although there was some evidence of axon guidance, in general, alginate scaffolds degraded before axons could grow over the 2 mm-long lesion. Enabling alginate-based scaffolds for nerve repair will likely require approaches to slow its degradation.

3.2 Introduction

Agarose hydrogel scaffolds with linear channels were previously fabricated and scaled to *cm*-long scaffolds for spinal cord repair [55, 65, 158]. However, these implants are non-degradable and inflammation is frequently observed at the scaffold-host tissue interface [65]. The ideal nerve guidance scaffold (NGS) should have the following characteristics: 1) be biocompatible [28, 128]; 2) have high channel volume and/or thin walls to maximize open space for axonal growth; 3) have linear channels to guide axons and maintain their organization in the spinal cord [1, 158]; 4) have channel diameters between 25 μm and 200 μm [131, 158]; 5) degrade after nerve regeneration to avoid permanently occupying the spinal cord [1] and 6) be cost-effective [1].

In this work, a calcium cross-linked alginate hydrogel was investigated as a guidance scaffold material for axonal regeneration owing to its biocompatibility with nerve tissue [91, 122, 127, 165], wide range of elastic moduli (1 kPa to 320 kPa) [86, 113, 134], and tunable degradation rate [86, 134]. Ionically cross-linked alginate degrades through the release of divalent cross-linking cations such as calcium, and their exchange with monovalent cations such as sodium [91].

The *in vitro* degradation of alginate has been previously studied. For example, McKay *et al.* studied the change in the shear modulus of 0.25 $wt.\%$ and 0.5 $wt.\%$ alginate hydrogel after 2 days of *in vitro* degradation [113]. Other studies have performed cell attachment studies on alginate for up to 10 weeks and suggested techniques such as adding NaCl to preserve material integrity [111, 112]. However, to date there have been no studies that correlate the change in the shear modulus of calcium cross-linked alginate in week-long experiments.

Previous *in vivo* works on alginate such as Prang *et al.* and Suzuku *et al.* studied the efficacy of covalently cross-linked microchannel alginate scaffolds and calcium cross-linked alginate hydrogel sponges for spinal cord repair, respectively [137, 165]. However, there have been no studies to evaluate the *in vivo* degradation of calcium

cross-linked alginate hydrogel scaffolds for spinal cord repair. To determine if alginate hydrogel is a viable nerve guidance scaffold material, it is important to understand its degradation behavior *in vitro* and to test its efficacy *in vivo*.

This study entailed a two-pronged approach to characterize the degradation of calcium cross-linked alginate hydrogel. First, the *in vitro* degradation was measured using rheology, and by assessing the specimen for macroscopic deterioration. Second, *in vivo* degradation was characterized by fabricating and implanting microchannel alginate scaffolds in rodent T3 full transections to determine if adequate integrity is maintained to effectively guide axons over two weeks. To achieve shear moduli similar to that of previously reported 3 $wt.\%$ agarose hydrogel scaffolds [55, 65, 158], a 3 $wt.\%$ alginate hydrogel composition cross-linked with 100 mM calcium chloride ($CaCl_2$) was chosen, which is reported to have the same modulus as 3 $wt.\%$ agarose [134]. It was observed that the shear modulus of the alginate hydrogel decreased by 97% within 3 days *in vitro*. In addition, *in vivo* tests demonstrated that while scaffolds may initially maintain channels to guide axons, the scaffold was not visible through optical and fluorescent imaging after two weeks of *in vivo* testing.

3.3 Experimental

Both high-purity (HP) alginate suitable for *in vivo* studies and the more commonly used low-purity (LP) alginate were used (Provona UP MVG and Provona MVG, respectively. FMC Nova Matrix; Philadelphia, PA). Both alginate grades had more than 60% guluronate monomer. All other chemicals were purchased from Sigma (St. Louis, MO) unless otherwise mentioned.

Alginate was dissolved in reverse osmosis (RO) water (3 $wt.\%$) and cross-linked in a 100 mM $CaCl_2$ solution to form a hydrogel.

3.3.1 Fabrication of alginate hydrogel

To make homogeneous alginate hydrogels, a 1-dimensional (1-D) cross-linking technique was developed to improve uniformity Fig. 3.1. A glass microfiber filter paper (Whatman grade GF/A) was placed between two 2024 alloy aluminum rings (7.6 cm inner diameter, 8.9 cm outer diameter. McMaster; Aurora, OH). The tubes and filter paper were adhered together using double-sided tape forming a reservoir to contain the alginate precursor during the cross-linking process. Alginate solution was poured on top of the filter paper, but was too viscous to permeate through it. The reservoir assembly was placed in a 100 mM $CaCl_2$ solution (Alfa Aesar; Ward Hill, MA) to allow the calcium ions to permeate through the filter paper and into the alginate solution. A 6.4-mm diameter hole was made in the bottom ring, approximately 3 mm below the filter paper, to release air bubbles. After 24 hr of immersion to cross-link the alginate solution, disks were cut from the alginate hydrogel using a custom punch consisting of 0.8 mm wall thickness, titanium 6 aluminum-4 vanadium alloy (McMaster) tube, sharpened to a knife edge (11.4 mm inner diameter). Alginate hydrogel faces were cut with a razor blade to produce 5 mm-tall samples with flat and parallel opposing surfaces.

To compare cross-linking techniques, the conventional radial cross-linking method was also used to fabricate alginate disks. Briefly, plastic mesh (1 mm opening size, McMaster) was shaped into cylindrical tubes about 25 mm in diameter. The tubes were immersed in alginate solution, where the longitudinal axis was oriented vertically, and immediately transferred to and kept in a 100 mM $CaCl_2$ solution, after which the hydrogels remained for 24 hr. The alginate hydrogels were cut perpendicular to the longitudinal axis using a razor blade to produce disks about 5 mm tall and 11.4 mm in diameter.

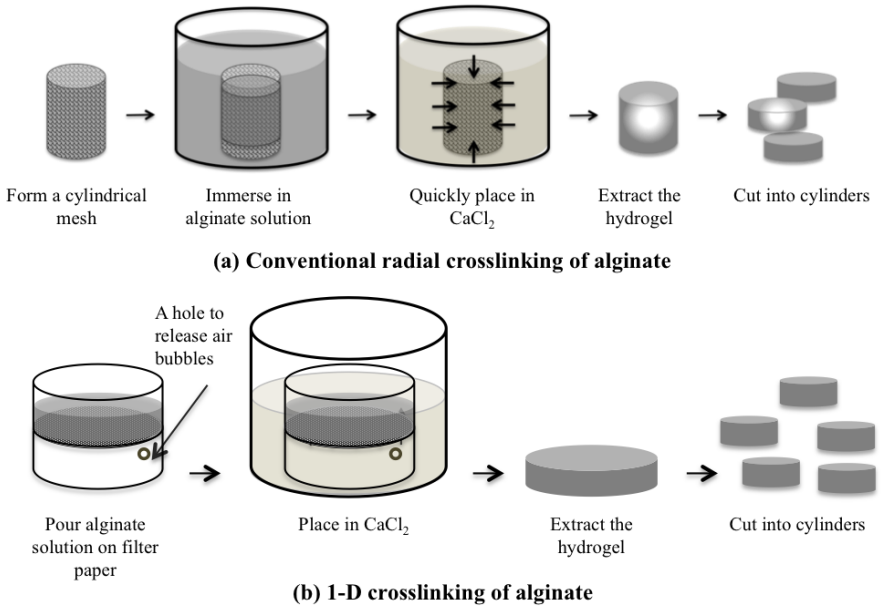

Figure 3.1: (a) Conventional radial and (b) 1-D cross-linking of alginate. Unlike radial cross-linking, 1-D cross-linking produces uniform disks for up to 15 mm tall samples.

3.3.2 Shear modulus measurements

Parallel 2024 aluminum plates (11.4 mm diameter) were custom-made and inserted in an Ares rheometer (TA instruments; Schaumburg, IL) for shear modulus testing. Sand paper (1200 grit) was adhered to the parallel plates using double-sided tape to avoid sample slippage during testing (as suggested by Meyvis *et al.* [118]). First, the initial contact point, and thus the height of the sample, was measured upon the initial detection of normal force. Since the shear modulus of hydrogels changes with the frequency of the shear strain [7, 93, 100, 118], the frequency was fixed at 1 Hz for all rheology experiments. To optimize the shear strain rate, a range of 0.01% to 50% shear strain was applied and the shear modulus was recorded. Since the shear modulus of alginate continuously decreased at dynamic shear strains higher than 0.5%, a dynamic shear strain of 0.5% was chosen for all experiments. In general, the procedure by Meyvis *et al.* was followed to measure the shear moduli [118].

Briefly, the shear modulus was recorded after 50 s of applied dynamic shear strain with a frequency of 1 Hz. Each disk was then compressed for a distance of 25-100 μm (0.5-2.0% compression strain), and the modulus was measured. Subsequent compression was applied until the shear modulus did not change; full contact with the sample was established and the shear modulus was recorded ($n = 5$). In addition, to confirm 1-D cross linking was uniform, the shear modulus measurements were conducted on both faces of a cylindrical specimen to ensure the modulus was the same on each face.

3.3.3 Assessing the *in vitro* degradation rate of alginate disks

The HP and LP alginate disks, made using the 1-D and radial cross-linking methods ($n = 5$), were stored in $37°C$ 1xDPBS with a volume equivalent to five times the volume of each disk. The solution was exchanged daily. Images of the alginate disks were taken to qualitatively assess swelling and degradation. To characterize the swelling of alginate, the diameters of the disks were measured using electronic calipers (Mitutoyo; Aurora, IL). The heights of the HP alginate disks were measured daily until day 6 using the initial contact point detected by the rheometer. The diameter and height measurements were used to determine the volume and hence track the degree of swelling. The shear modulus of the disks were measured daily until the modulus decreased to less than 3% of the original value.

3.3.4 Pore characterization

Cross-linked HP alginate was supercritically dried to preserve the pore structure. The procedure was the same as previously reported by Lynam *et al.* [104]. The hydrogel was immersed in 100% ethanol (Decon Labs, Inc.; King of Prussia, PA) for 3 days and the ethanol was changed every day. The samples ($n = 3$) were then washed with liquid CO_2 over 2 days followed by supercritical extraction. Scanning electron microscopy (SEM) (JOEL 7500F; Peabody, MA) was used to characterize the poros-

ity. Brunauer, Emmett, Teller (BET) (Micromeretics ASAP 2020; Norcross, GA) was used to measure surface area and pore size distribution as described elsewhere [104]. Briefly, water was removed under vacuum (10-6 $torr$) at 80°C for 12 hr before each nitrogen sorption test. Free space and surface area were measured through the quantification of the adsorption/desorption behavior using ultra high purity helium and nitrogen, respectively and were correlated using Barrett-Joyner-Halenda (BJH) desorption method.

3.3.5 Scaffold fabrication

HP alginate scaffolds were fabricated using a fiber templating technique [103, 158]. Briefly, multicomponent fiber bundles (MCFB) of hexagonally-packed polystyrene (PS) fibers with 167 μm diameter separated by a poly(methyl methacrylate) (PMMA) matrix with 67 μm spacing were used (Paradigm Optics; Vancouver, WA). After templating, alginate scaffolds contracted longitudinally and expanded laterally when immersed in physiological solutions, likely caused by an osmotic effect. To account for these dimensional changes, the MCFBs were made 5% longer in the longitudinal direction and 10% shorter in the lateral dimensions, resulting in 2 mm long and 1.8 mm by 1.8 mm wide scaffolds. The MCFBs were bonded to PS caps, and the PMMA matrix was removed using a 80:20 vol/vol propylene carbonate:acetonitrile solution. Templates were then soaked in 3 $wt.\%$ HP alginate solution and centrifuged at 1000 revolutions per minute (rpm) (9 relative centrifugal force (rcf)) for 30 s to facilitate hydrogel permeation between the PS fibers. To ensure complete permeation, templates were kept in an alginate solution overnight at room temperature, and centrifuged at 1000 rpm (9 rcf) for another 30 s before cross-linking in 100 mM $CaCl_2$ for 4 hr. Excess alginate hydrogel along the template periphery was trimmed off using a razor blade. The alginate-permeated templates were immersed in 37°C cyclohexane under agitation for 2 days to selectively etch away the PS fibers. The alginate scaffolds

with linear channels were then washed with 100 mM $CaCl_2$ to remove any remaining residue.

Alginate scaffolds were placed in 1 ml of 1xDPBS at 37°C and the solution was replaced every 24 hr. Optical images of the scaffolds were taken on days 1, 3, 7, 14, 21 and 28 to ensure the channels and the bulk geometry of the scaffolds were maintained *in vitro*. Agarose (3 $wt.\%$) hydrogel was selected as a control scaffold material, because it is known to be non-degradable and its efficacy for spinal cord repair has been studied [55, 65, 158]. Agarose scaffolds were prepared similar to alginate scaffolds following the protocol first described by Stokols *et al.* [158]. Briefly, fiber templates were cut to 2.0x1.8x1.8 mm, bonded to PS caps and reinforced with PS lateral supports as explained above. Agarose (3 $wt.\%$) was heated to 70°C to produce a molten agarose solution. The fiber template was placed in the molten agarose and centrifuged at 1000 rpm (9 rcf) for 45 s to remove air bubbles and promote fiber wetting. Upon cooling to room temperature and gelling, the fiber templates were extracted from agarose and any extra agarose was trimmed from the template using a razor blade. The fiber template permeated with agarose construct was placed in tetrahydrofuran (Alfa Aesar, Ward Hill, MA), at 37°C for 3 days under agitation while exchanging the solution every day. The scaffolds were then washed in RO water.

3.3.6 Surgical procedures and *in vivo* characterization

Details regarding the animal handling and surgeries are described elsewhere [81]. Briefly, adult female Fischer 344 rats (150-200 g) were used in this study according to the NIH guidelines for laboratory animal care and safety. A combination (2 ml/kg) of ketamine (25 mg/ml), xylazine (1.3 g/ml), and acepromazine (0.25 mg/ml) was used to anesthetize the animals. T2-T4 laminectomies were performed. Micro scissors were used to create 2 mm-long lesion cavities in the T3 spinal cord segments. The

lesions were cleared using micro aspiration. Animals were divided into three experimental groups ($n = 3$ per group): Group 1 received no treatment; Group 2 received non-degradable agarose hydrogel scaffolds; and Group 3 received alginate hydrogel scaffolds (alginate hydrogel scaffolds were soaked in 1 ml of phosphate buffer (pH 7.4) for 20 min prior to implantation).

To examine scaffold degradation *in vivo*, animals were sacrificed 2 weeks post-implantation and perfused with 4% paraformaldehyde (PFA) in 100 mM phosphate buffer at 4 C. Segments (2 cm-long) centered above the lesion sites were separated and post-fixed in 4% PFA overnight at $4°C$, and then in 30% sucrose (w/v) in 100 mM phosphate buffer at $4°C$ for another 48 hr prior to cryosectioning. Longitudinal sections at a thickness of 30 μm were collected on a cryostat. For immunolabeling, slides were suspended in proteinase K (1:20, antigen retrieval) (Millipore; Darmstadt, Germany) for 20 min followed by postfix with methanol for 5 min at room temperature. Slides were blocked using 5% goat serum in Tris-buffered saline (TBS) containing 0.25% Triton X-100 for 1 hr. The slides were then incubated overnight with mouse-anti-Neurofillament 200 for axons staining (Millipore) with a 1:500 dilution. The sections were washed with TBS and labeled with secondary antibody: goat-anti-chicken 647 (1:250, for 2.5 hr in dark at room temperature) (Life Technologies, Carlsbad, CA). The slides were then washed with TBS, labeled with Fluoromount G (Southern Biotechnology Associates, Inc.; Birmingham, Alabama) and imaged using a fluorescent microscope (Olympus BX53; Center Valley, PA).

3.4 Results

3.4.1 *In vitro* degradation testing

Images of the conventional and 1D cross-linked gels after immersion ion 1xDPBS are shown in Fig. 3.2. The radially cross-linked alginate hydrogel disks fragmented

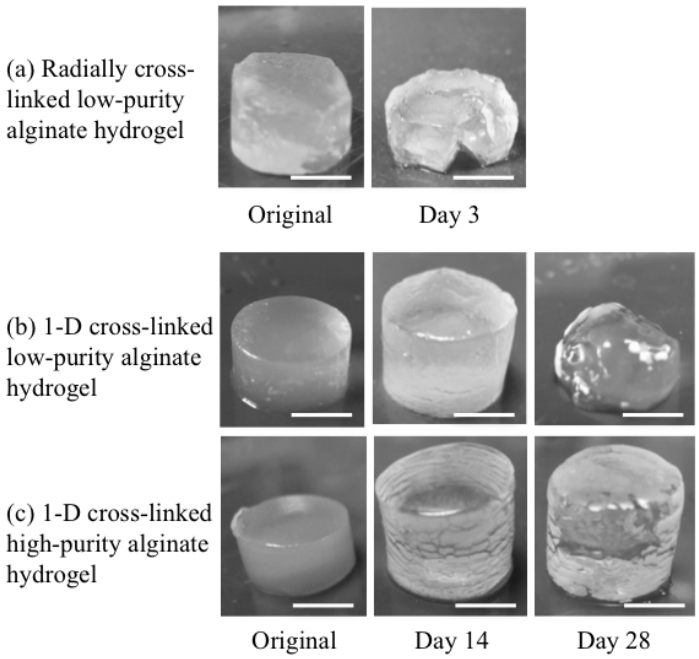

Figure 3.2: Visual changes of 11.4 *mm*-diameter (a) radially cross-linked low-purity alginate and 1D cross-linked (b) low-purity and (c) high-purity alginate during *in vitro* degradation. Unlike radially cross-linked hydrogels, 1D cross-linked alginate does not fragment and exhibits uniform degradation. Scale bars are 5 *mm*.

within 3 days, thus it was not possible to make dimensional measurements as a function of time (Fig. 3.2). Conversely, the alginate hydrogel disks fabricated by the 1-D cross-linking technique maintained their geometry making it possible to quantitatively assess the change in physical properties as a function of time (Fig. 3.1). Thus, only 1-D cross-linked samples were considered for quantitative degradation characterization. Since only the HP alginate would be implanted, only HP swelling was characterized. Negligible changes in the diameters of the samples were measured. The majority of the changes in height (and therefore swelling) occurred between days two and three, after which the volume increase subsided, e.g. between days three and six (Fig. 3.3).

To accurately characterize and quantify the degradation of alginate hydrogel disks, changes in shear moduli were measured using rheology. The shear moduli of HP and LP alginate hydrogel were 155 $\pm$ 21 kPa and 186 $\pm$ 20 kPa, respectively. The

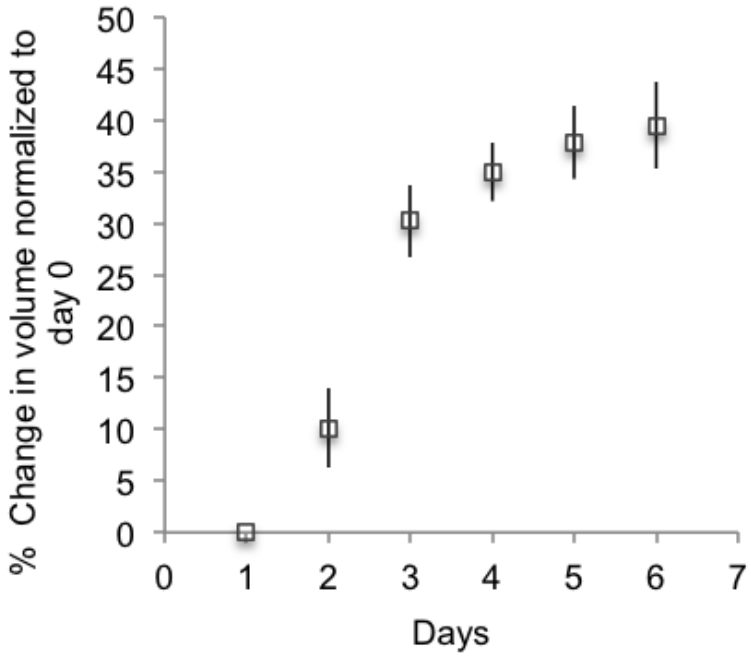

Figure 3.3: The change in the volume of HP alginate disks during degradation. The data are normalized to the volume of the samples from day 0. The disks swell to about 40% by day 6.

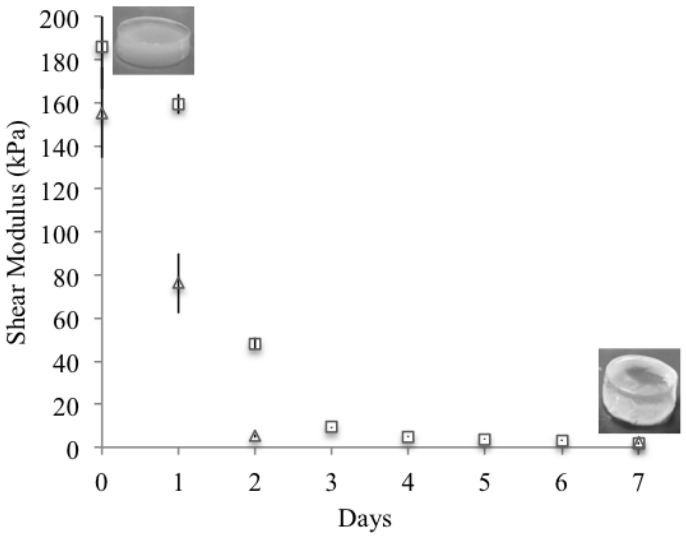

Figure 3.4: Rheology measurements for low-purity (□) and high-purity (△) alginate, including optical images of the high-purity samples (with a diameter of 11.4 mm) on days 0 and 7. While the shear modulus drops by 97% within 3 days, the superficial geometry is maintained.

different moduli may have resulted from the different purities; regardless, the shear moduli of both HP and LP alginate hydrogel disks decreased by approximately 97% by day three (Fig. 3.4).

3.4.2 Pore characterization

SEM images showed 3 $wt.\%$ alginate hydrogel consisted of cross-links in the 10-20 nm range and interconnected pores in the tens of nanometer range (Fig. 3.5). The BJH method on nitrogen desorption data on supercritically dried 3 $wt.\%$ alginate hydrogel corroborates the SEM analysis, indicating that most pores fell within the 25-35 nm diameter range with a total surface area of 415.7 $\pm$ 12.0 m^2/g ($n = 3$) (Fig. 3.6). These data are consistent with similar studies on supercritically dried 3 $wt.\%$ agarose and 2 $wt.\%$ alginate hydrogels [104, 139].

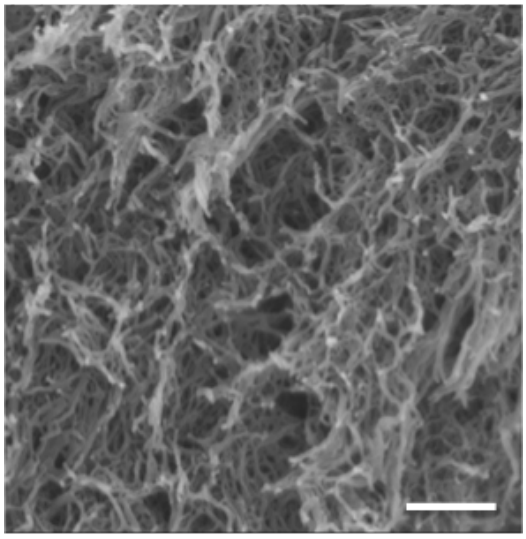

Figure 3.5: SEM image of supercritically dried 3 $wt.\%$ alginate showing interconnected pores, which are in the tens of nanometer range. Scale bar is 200 nm.

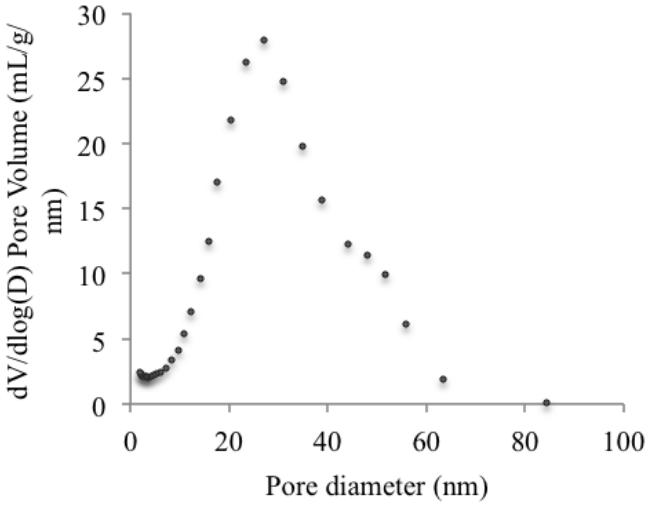

Figure 3.6: Nitrogen desorption data of supercritically dried alginate showing that the majority of nanopores are 25-35 nm in diameter.

3.4.3 Scaffold characterization and *in vivo* testing

Images of a template and an alginate scaffold are shown in Fig. 3.7. The average template fiber diameter and the spacing between fibers were 219.7 ± 16.0 μm and 95.7 ± 9.1 μm, respectively. The alginate hydrogel scaffold matched the template pattern and had an average channel diameter and scaffold wall thickness of 197.5 ± 25.4 μm and 83.5 ± 35.6 μm, respectively. Contraction during cross-linking may explain the slight reduction in dimensions compared to the templates. Differences between template-to-scaffold channel diameter and wall thickness was 10.1% and 14.6%, respectively. This was comparable to fiber templated agarose hydrogel scaffolds exhibiting 14.2% and 22.0% channel diameter and wall thickness template-to-scaffold shrinkage, respectively. Optical images (not shown) demonstrated that alginate scaffolds generally maintained their channels for at least 28 days.

Histology sectioning 2 weeks post-implantation showed that non-degradable agarose hydrogel scaffolds were intact and the channels were distinguishable (Fig. 3.8a). Some linear axonal growth was observed throughout the agarose hydrogel scaffolds. However, the channels and the alginate hydrogel scaffolds were not, in general, distinguishable in the histology (Fig. 3.8b). Nevertheless, there was some evidence of linear axonal regeneration in Fig. 3.8b and Fig. 3.8c, suggesting that some microchannels could maintain integrity long enough to guide axons up to approximately 0.5 mm (Fig. 3.8c).

3.5 Discussion

Alginate hydrogel was investigated as a degradable nerve scaffold for spinal cord repair owing to its reported biocompatibility and tunable degradation rate [86, 91, 122, 127, 134]. After developing a technique to fabricate uniform disks, the degradation of alginate hydrogel was quantified *in vitro* by monitoring the change in its

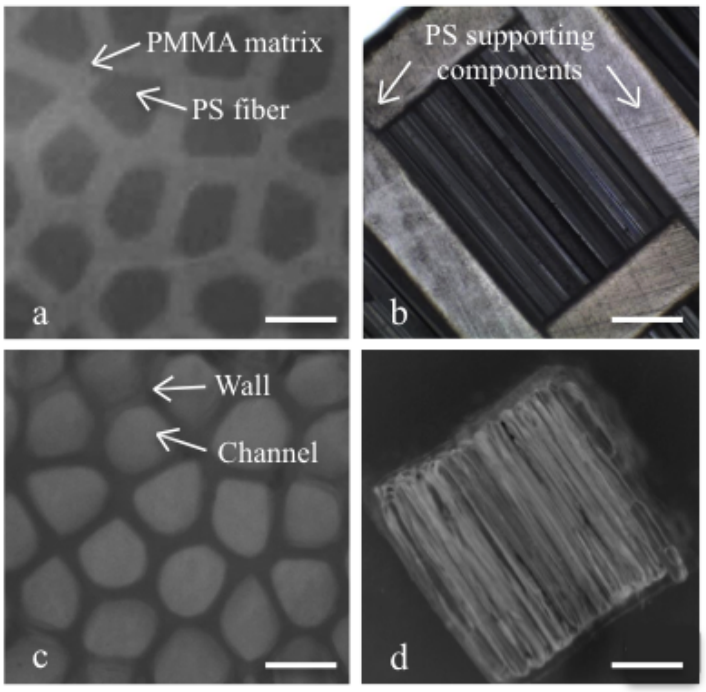

Figure 3.7: (a) Cross-section and (b) longitudinal view of a multicomponent fiber bundle template consisting of a PMMA matrix and PS fibers. The PS components (b) maintain PS fiber linearity after the PMMA matrix is etched. Templated alginate scaffold cross-section and side view (c) and (d), respectively. Scale bars in (a) and (c) are 400 μm and in (b) and (d) are 500 μm.

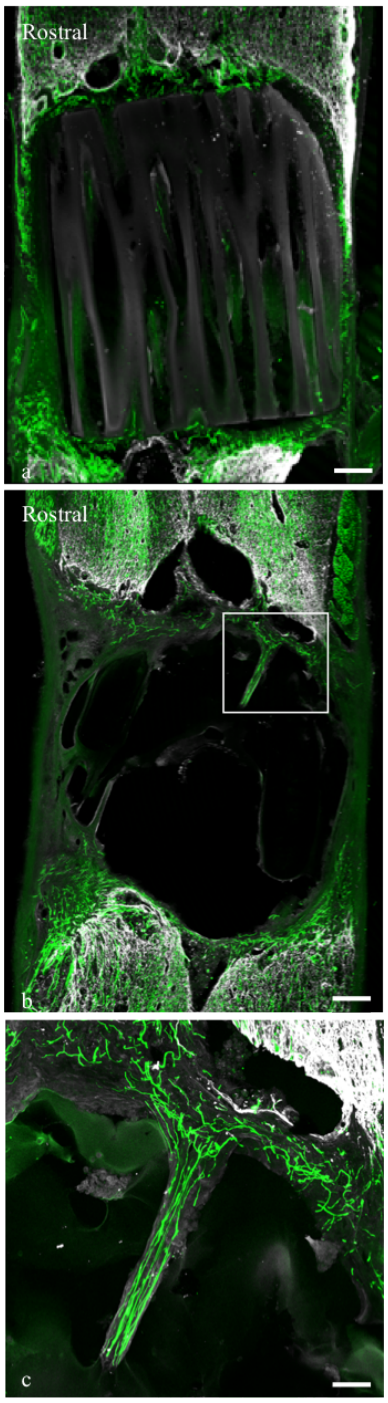

Figure 3.8: Representative images of neurofilament (green) labeling of a completely transected rat spinal cord 2 weeks post-implantation: (a) agarose scaffold and (b) alginate scaffold. The agarose hydrogel scaffold remained intact while the alginate scaffold mainly degraded. Some axonal growth into the agarose scaffold is observed. A higher magnification image (c) shows some axonal growth at the rostral end of the alginate scaffold. The Scale bars in (a) and (b) are 200 μm and the scale bar in (c) is 50 μm.

shear modulus over time. Scaffolds with linear channels were then fabricated and implanted in rodent spinal cords to test their efficacy for axonal guidance *in vivo*.

To measure the change in the shear modulus during degradation, first a technique for fabricating homogeneous alginate hydrogel disks was developed. Conventional radial cross-linking was initially attempted, but samples fragmented within 3 days likely due to the non-uniform permeation of calcium ions. To achieve uniform cross-linking, a novel 1-D cross-linking technique was developed. The uniformity of samples with a height less than 15 mm was confirmed since the same modulus was obtained when performing rheometry on the top and on the bottom of the disks (with the bottom of the disk being the side against the filter paper).

Once a technique was established to fabricate homogenous alginate hydrogel disks, rheometry was used to characterize their degradation *in vitro*. Rheometry was selected because, unlike techniques such as uniaxial compression testing, swelling during loading (the "barreling effect") is minimized [119]. The barreling effect can cause deformation and sometimes rupture, which prevents the re-testing of the same sample as it degrades. In this study, rheology was used to measure the shear modulus to characterize the degradation rate *in vitro*. Applying a dynamic sinusoidal shear stress minimizes the barreling effect and yields information about both the shear and the viscous behavior by providing shear and loss moduli, respectively. The initial shear modulus on day zero was in agreement with the previously reported value [134], but had relatively lower standard deviations (generally below 10%) compared to previous work [93, 100, 126, 134]. The 1-D cross-linked samples maintained their integrity to allow for mechanical testing beyond day 1, unlike samples obtained by radial cross-linking. These results confirmed the effectiveness of rheology for quantifying the degradation of hydrogels, which was previously suggested by Meyvis and co-workers [118].

Rheological analysis showed that the shear modulus of HP alginate hydrogel dra-

matically decreased from 155 kPa to 5 kPa in 2 days, while no change in the superficial geometry was observed for over 28 days. The exchange of cross-linking calcium cations with monovalent sodium cations is the main cause of degradation of calcium cross-linked alginate hydrogel [80, 91, 139]. The combination of high internal surface area (415.7 $\pm$ 12.0 m^2/g) and nano scale interconnected porosity (Fig. 3.2), likely facilitated calcium ion loss and swelling (Fig. 3.2 and Fig. 3.3), which decreased the shear modulus and later caused fragmentation.

The observed degradation behavior suggested that alginate hydrogel undergoes bulk degradation. Since alginate hydrogel maintained its superficial geometry *in vitro* for over 1 month, alginate was considered a promising candidate for degradable nerve guidance scaffolds. To test this hypothesis, microchannel alginate hydrogel and non-degradable agarose hydrogel (control) nerve guidance scaffolds were fabricated using a fiber templating technique [158]. The fiber template construction resulted in alginate permeation from two opposing faces (Fig. 3.7b shows one of only two open template faces that the alginate solution could permeate). Thus, upon immersion in the $CaCl_2$ solution, the cross-linking direction was one-dimensional. The degradation of alginate scaffolds was first studied *in vitro* and it was confirmed that the scaffolds generally maintained their channels and bulk geometry for at least 28 days. In light of the promising *in vitro* data both on alginate disks and scaffolds, the scaffolds were implanted in a T3 full transection rodent model to test their efficacy *in vivo*. The approach used to characterize degradation was based on a qualitative assessment of the lesion cavity two weeks post implantation (Fig. 3.8). In agreement with previous work [55, 65, 158], linear walls and channels are clearly discernable in the lesion containing the agarose scaffold. However, compared to the agarose scaffolds, there was no clear evidence of linear walls or channels in the lesion containing the alginate scaffold, aside from a few linear axons on the proximal and distal ends of the cavity; perhaps evidence that initially the alginate scaffold guided axons before it degraded

away. Though the details of the degradation mechanism are difficult to determine, it is believed that the images in Fig. 3.8 indicate that the alginate scaffold was not present/functional after two weeks post implantation.

3.6 Conclusions

Alginate hydrogel was evaluated as a nerve guidance scaffold material. The degradation rate of alginate was measured *in vitro* using rheology. A methodology was developed to fabricate uniformly cross-linked alginate hydrogel disks to measure the shear modulus as a function of time. It was determined that the shear modulus of alginate hydrogel decreased by 97 % in 2 days, but no change in the superficial geometry of the hydrogel was observed in 28 days. *In vivo* studies demonstrated, qualitatively, that calcium cross-linked alginate hydrogel did not maintain adequate mechanical integrity to guide axons toward distal targets over a 2 mm T3 full transection spinal cord injury model. It is possible that if alginate hydrogel scaffold walls degraded slower, linear guidance to the distal targets may have occurred. In future work, approaches to decrease the degradation rate of alginate should be pursued to make it a viable scaffold material for nerve regeneration scaffolds.

CHAPTER IV

Dense Alginate Films Fabricated into Microchannel Scaffolds and Functionalized for a Gradient Protein Release

4.1 Abstract

This work investigates the synthesis of an alginate-based material with lower degradation rate compared to alginate hydrogel. Alginate solution was dried to dense films and cross-linked with calcium chloride ($CaCl_2$). Possibly due to the increase in surface roughness, the NIH 3T3 fibroblast cells adhered to alginate in its dense form but not in its hydrogel form. It was shown that the tensile elastic modulus of the films increased from 76.1 MPa to 552.2 MPa as the concentration of $CaCl_2$ changed from 100 mM to 1000 mM. In addition, to obtain continuous drug release from dense alginate films, proteins (lysozyme or brain-derived neurotrophic factor (BDNF)) were incorporated with the hydrogel solution prior to dehydration and cross-linking. A sustained protein release was obtained *in vitro* for at least 50 days and the BDNF bioactivity released from the films was confirmed. Next, two novel techniques were introduced to fabricate mm-long disks. The disks were microdrilled into microchannel scaffolds and implanted in 2 mm-long transected rats spinal cords. It was observed that the dense alginate scaffolds degraded within 4 weeks *in vivo*. Overall, further

modifications are necessary for alginate to be used as a viable nerve guidance scaffold for spinal cord repair.

4.2 Introduction

To linearly guide axons through the lesions of spinal cord, microchannel scaffolds were investigated [55, 65, 131, 158]. These scaffolds, however, were not degradable. Alginate hydrogel microchannel scaffolds were investigated as an alternative degradable material (Chapter III). However, alginate hydrogel degraded before complete axon regeneration occurred in the spinal cord cavity. The hydrogel had high surface area and interconnected porosity, which likely facilitated degradation. In this study, it was hypothesized that a significant reduction in the alginate porosity may decrease the leaching of cross-linking calcium ions and consequently prolong the degradation of alginate. Overall, the goal of this study was to produce non-porous dense alginate that can be fabricated into microchannel scaffolds. The scaffolds were aimed to 1) allow cell attachment, 2) can be functionalized for month-long drug release, and 3) linearly guide axons through spinal cord lesion sites.

Alginate was fabricated into dense films. Tensile testing was performed to quantify the effect of cross-linker concentration ($CaCl_2$) on the elastic modulus of the films. Similar to a previous report by Leroux *et al.* [93], the modulus increased by increasing the $CaCl_2$ concentration. In addition, upon significantly reducing the porosity, the cell adhesion properties of the films were increased compared to alginate hydrogels, which is likely due to the increase in surface roughness of dense alginate.

In addition to providing linear guidance for growing axons in a lesion cavity, it is necessary to stimulate axonal growth. Therefore, providing a sustained drug release is necessary [12, 174]. In addition, a gradient protein release can further facilitate cell growth and guidance [33, 78, 121]. Proteins were therefore incorporated with alginate films to obtain a sustained gradient release. In addition to obtaining a 50-day release

profile, the bioactivity of the released protein was confirmed.

Lastly, the films were fabricated into microchannel scaffolds and implanted in the transected T3 spinal cords of rats. Sectioning and immunolabeling were performed after 4 weeks. Inflammatory response was observed and the scaffolds had fragmented into debris within 4 weeks. Therefore, similar to alginate hydrogel, dense alginate microchannels did not have the adequate degradation rate. It is possible that the degradation rate of dense alginate was slower than alginate in its hydrogel form; nevertheless, the degradation rate was not long enough to allow nerve growth through the 2 mm-long spinal cord lesion cavity in rats.

4.3 Experimental

4.3.1 Alginate film fabrication

Alginate (Provona UP MVG) was purchased from FMC Nova Matrix (Philadelphia, PA). To fabricate films, 16 g of 3 $wt.\%$ alginate/RO water was poured on a 130 mm-diameter polystyrene petri dish (VWR; Radnor, PA) and air-dried for 18 hr (Fig. 4.1). All alginate films were cross-linked with $CaCl_2$ solution at 100 mM concentrations for 4 hr unless specified otherwise.

4.3.2 Material characterization

The cross-linked alginate films were fractured in liquid N_2. The surface fracture of the films were coated with 3 nm-thick gold (SPI Supplies; West Chester, PA) and imaged under scanning electron microscopy (SEM) (ZEISS AURIGA FIB; Thornwood, NY).

To characterize the change in the elastic modulus of alginate films versus cross-linking concentration, alginate films were cross-linked with $CaCl_2$ at 100, 200, 300 to 1000 mM. Alginate films were cut to 30 x 8 mm rectangular pieces and tensile

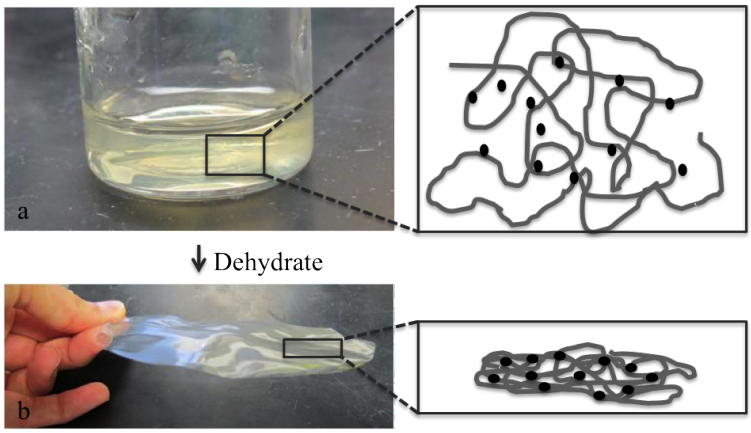

Figure 4.1: Fabricating dense alginate films. (a) The top picture on the left shows alginate hydrogel and (b) the bottom left shows alginate collapsed film after dehydration. The gray schematics on the right correspond to predicted macroscopic structure of alginate in either form. The black dots represent the optional addition of protein molecules temporarily immobilized by the alginate.

testing was performed at 1.5 N/min load rate ($n = 5$) (Instron; Norwood, MA).

To study the change in cell attachment based on porosity, NIH 3T3 fibroblasts were cultured on both alginate hydrogel (Chapter III) and the dense alginate films ($n = 3$). Cells were imaged after 48 hr using a contrast microscope.

4.3.3 Protein incorporation and bioactivity measurements

Alginate powder (1 $wt.\%$) was added to 1 mg/ml lysozyme/RO water solution. The solution (5 ml) was poured in a 6 well-plate (VWR) and air-dried for 18 hr ($n = 3$) to produce films. The films were cross-linked with 100 mM of $CaCl_2$ for 4 hr. Excess $CaCl_2$ was removed in 1xDPBS for 15 min and films were stored in 1 ml of 1xDPBS at 37°C. The solution was collected and exchanged daily for 50 days. To measure the protein concentration of the collected solutions, a Micro BCA^{TM} protein assay kit (Thermo Fisher Scientific; Wayne, MI) was used and the protocol by the manufacturer was followed.

To obtain a gradient release profile, a barrier was placed at the center of a

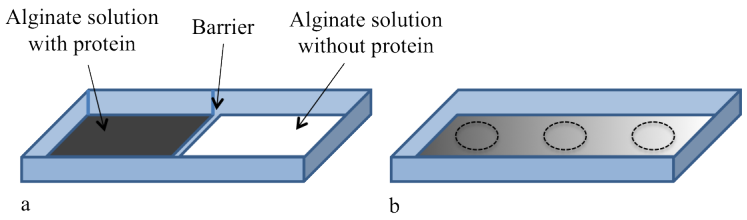

Figure 4.2: Fabricating dense alginate films with gradient protein release. (a) Using a barrier, two reservoirs were created in a rectangular-shape container and filled with alginate solution- one with and one without protein. (b) The barrier was removed and the solution was air-dried. Three pieces of the film as shown with the dashed circles in (b) were extracted for protein release measurements.

rectangular-shape reservoir (60 x 20 mm). Each reservoir was filled with 5 ml of 1 $wt.\%$ alginate solution with or without lysozyme (1 mg/ml) (Fig. 4.2(a)). The barrier was then removed and the solutions were air-dried for 18 hr. Three 10 mm-diameter circles as shown in Fig. 4.2(b) were extracted from the film and cross-linked with 100 mM $CaCl_2$ solution for 4 hr. Each film was rinsed with 1xDPBS for 15 min and stored in 1 ml of 1xDPBS with the solution collected and refreshed daily. Micro BCA^{TM} assay was used to measure the protein concentrations ($n = 3$).

BDNF-incorporated films were fabricated to characterize the bioactivity of the released protein. 6 ml of a 1.2 $wt.\%$ alginate solution with 29 μg of human BDNF (ProSpec; Rehovot, Israel) was poured in a 6 well-plate ($n = 3$). To reduce the adhesion of BDNF to well-plate walls, an ultra low-adhesion well-plate (Corning; Corning, NY) was used. The alginate/BDNF solutions were dried for 18 hr to produce films. Films were cross-linked with 100 mM $CaCl_2$ for 4 hr. 1xDPBS was used for 15 min to wash the films. The films were stored in a defined culture medium prepared according to the protocol described by Lynam *et al.* [105]. The solutions were exchanged daily and stored at $4°C$. The bioactivity of the released BDNF for the first 6 days was tested by applying the solution on transfected NIH 3T3 cell line that expressed BDNF-recognition tropomyosin receptor kinase B (TrKB). The cells were seeded at a concentration of 5 x 10^4 $cells/ml$. Contrast imaging and cell counting

was performed after five days and normalized to the cell count obtained from control group treated with 50 ng/ml of fresh BDNF.

4.3.4 Dense alginate disk and scaffold fabrication

Two techniques were used to fabricate alginate disks. In the first technique, alginate films were rolled and cross-linked to fabricate a solid dense disk. Alginate films were prepared as explained in 4.3.1. The films were then rolled around a 1 mm-diameter steel rod for a final diameter of 1.8 mm. The alginate roll was then inserted in a 2 mm inner diameter plastic tube. The steel rod was gently removed from the film and the assembly was placed inside a 100 mM $CaCl_2$ solution for 4 hr for the alginate to cross-link and fully fill the tube. The alginate disk was cut to 2 mm-long pieces. In the second technique, incremental amounts of alginate solution was poured on top of alginate films to produce disks. Specifically, 17 g of 6 $wt\%$ alginate was poured in a well of a 12 well-plate and air-dried for 4 hr. The process was repeated until a 2 mm-long disk was fabricated.

Alginate disks were microdrilled in a hexagonal pattern using a computer numerical control (CNC) machine (US Digital, Vancouver, WA) and a patterning program (Artsoft Software Inc.; Livermore Falls, ME). A microdrill bit of size 0.30 mm was used to microdrill channels with a spacing of 0.20 mm at a feed-rate of 0.020 mm/min. The scaffolds were sterilized in 50:50 vol ratio of ethanol (Decon Labs, Inc.; King of Prussia, PA) and RO water for 15 min; rinsed with autoclaved RO water and stored dry.

4.3.5 Surgical procedure and *in vivo* characterization

The NIH guidelines for laboratory animal care and safety was followed. The implantation protocol and characterization are described elsewhere [81]. Briefly, 150-200 g adult female Fischer 344 rats were deeply anesthetized using a combination

of ketamine (25 mg/ml), xylazine (1.3 mg/ml), and acepromazine (0.25 mg/ml). Laminectomy on T2-T4 sections were performed and 2 mm-long lesion cavities in the T3 sections of spinal cords were performed. Scaffolds from section 4.3.4 were inserted into lesions upon micro-aspiration and cleaning ($n = 4$).

Animals were perfused with 4% paraformaldehyde (PFA) 4 weeks post-implantation. Segments (2 cm-long) were post-fixed in 4% PFA overnight at $4 \circ C$ followed by 48 hr storage in 30% sucrose (w/v) in 100 mM phosphate buffer at $4°C$. Longitudinal sections (0.03 mm-thick) were cryosectioned. Slides were stored in proteinase K (1:20, antigen retrieval) for 20 min and methanol for 5 min. Goat serum (5%) in Tris-buffered saline (TBS) was used to block the slides for 1 hr. Mouse-anti-Neurofillament 200 with a 1:500 dilution for axons staining was used overnight. Slides were washed with TBS and stored in secondary antibody: goat-anti-chicken 647 for 2.5 hr in dark and washed with TBS. Slides were then labeled with Fluoromount G and imaged (Olympus BX53; Center Valley, PA).

4.4 Results and Discussion

4.4.1 Material properties

To compare the difference between the porosity of alginate hydrogel and alginate dense films, the SEM image of supercritically dried alginate hydrogel from Chapter III was compared to the cross-sectional image of a dense alginate film (Fig. 4.3). The images confirm the loss of pores in the dense alginate film. In addition, the change in porosity was hypothesized to reduce solution exchange in dense alginate film and prolong its degradation.

Since $CaCl_2$ is the cross-linking solution, it was expected that the elastic modulus of the films increases with the increase in the cross-linkers concentration [93]. To confirm and quantify the change, alginate films with varying concentrations were

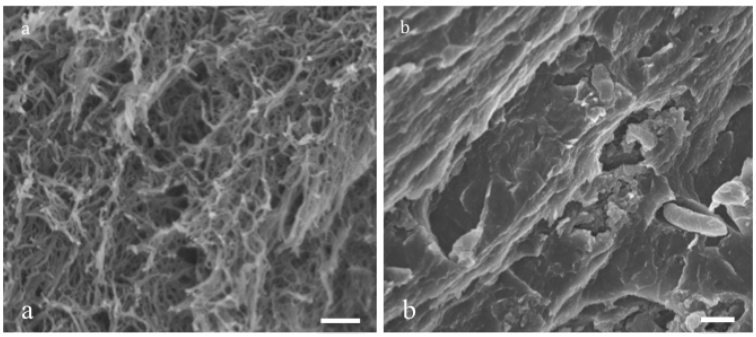

Figure 4.3: SEM images of (a) highly porous supercritically dried alginate hydrogel versus (b) collapsed alginate film. Scale bar in (a) is 0.15 μm and in (b) is 1 μm.

prepared and tensile testing was performed. As shown in Fig. 4.4, the elastic modulus of films increases from 76.1 MP to 552.2 MPa by changing the cross-linkers concentration from 100 mM to 1000 mM. To better match the elastic modulus of a nerve tissue (1-3 kPa), 100 mM concentration was chosen through this study. It was noted that robust films were not successfully produced with a $CaCl_2$ concentration below 100 mM.

It was predicted that cell adhesion may improve on dense alginate compared to its hydrogel form due to the change in its morphology. Previous reports on peptide-modified dense alginate films confirmed cell attachment [36, 57]. In this study, the cell attachment of NIH 3T3 fibroblasts was tested on alginate hydrogel versus dense alginate films. The results confirm the enhancement in cell adhesion on alginate films versus alginate hydrogel (Fig. 4.5).

4.4.2 Protein release measurements and bioactivity characterization

To obtain a sustained protein release from alginate films, proteins were incorporated with alginate solution prior to drying and cross-linking. Lysozyme was initially used due to its similarity in size to BDNF as well as its low-cost. The lysozyme release profile showed a sustained release for 50 days with a total amount of 277 μg released protein per cm^2 of alginate film (Fig. 4.6). In addition, unlike conventional

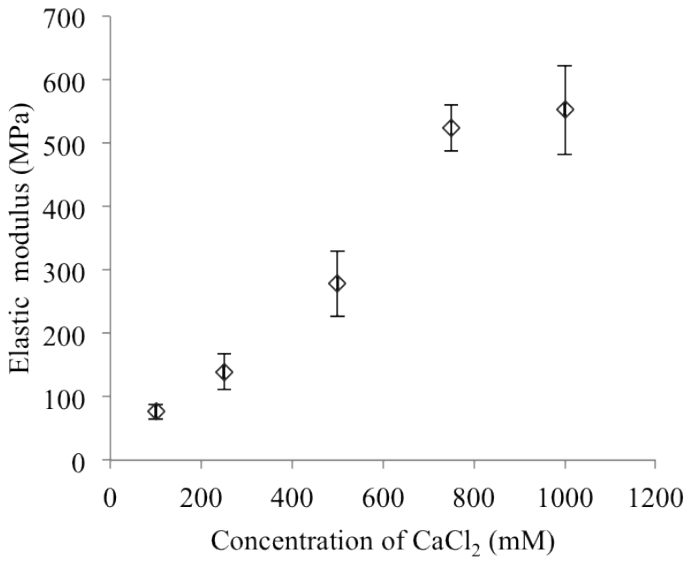

Figure 4.4: The elastic modulus of dense alginate films increased by raising the concentration of the cross-linking solution ($CaCl_2$).

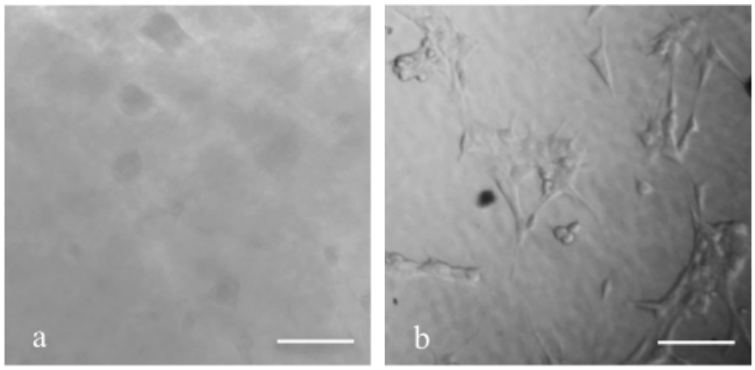

Figure 4.5: NIH 3T3 fibroblasts do not attach on (a) hydrogel form of alginate but attach on (b) dense alginate films. Scale bars are $30\mu m$.

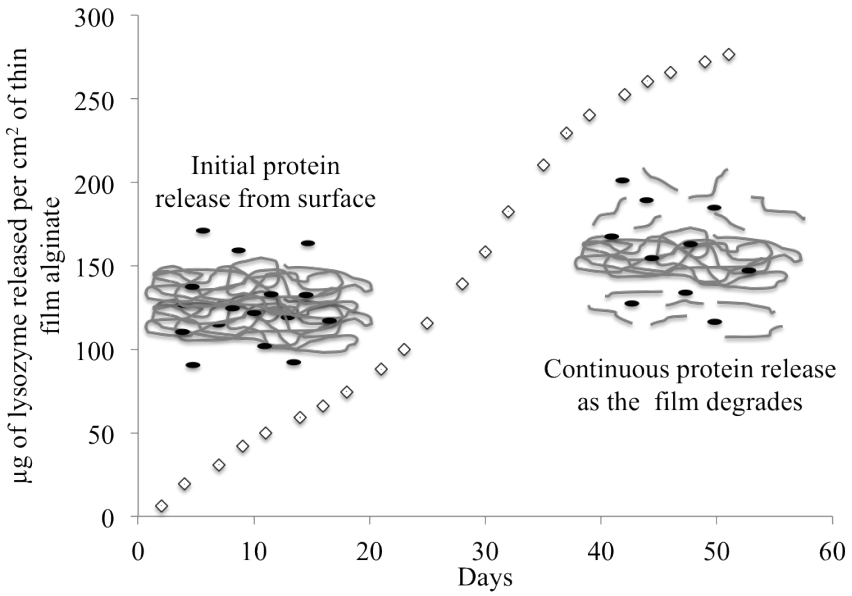

Figure 4.6: The graph shows a 50-day sustained release from a lysozyme-loaded dense alginate film. The schematics represent a dense alginate film (gray) with protein molecules (black) incorporated. The schematic on the left demonstrate that, due to the dense alginate structure, the protein is initially primarily released from the outer layers of alginate. As the film degrades (schematic on the right), protein can be released from inner layers.

drug delivery techniques, no burst release was observed. As the schematics in Fig. 4.6 show, the non-porous structure of alginate might have aided in the controlled release of protein by the gradual release of protein molecules as the film degrades.

Next, attempts were made to produce alginate films with a gradient protein release. Alginate solutions with and without lysozyme were used to fabricate a continuous film (Fig. 4.2). Fig. 4.7 shows release profiles from both ends of the film as well as the center. Protein was not detected from the portion of the film that did not initially have protein incorporated. This observation indicated that the diffusion of proteins through the alginate solution minimally occurred. In addition, there was a clear difference between the release profiles from the center and the segment of the film with the initial high amount of protein, which indicated a gradient release profile was obtained. Overall, it was concluded that a continuous film could be fabricated using the reservoir-fabrication system with molecules minimally diffusing through al-

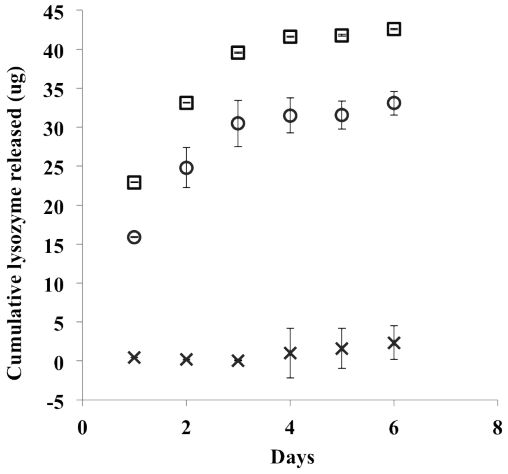

Figure 4.7: The graph shows the cumulative release profile of a lysozyme-gradient alginate film described in Fig. 4.2. (□) is the release profile of the section with lysozyme while (x) is from the section without lysozyme. (○) is the release profile from the center of the film. The comparison between the profiles shows a gradient release profile can be achieved.

ginate solution. Thus, separate alginate solutions containing increasing amounts of protein can be used on a mulit-reservoir system to potentially produce a film with a robust gradient release.

Upon obtaining promising lysozyme release data, BDNF release was tested. However, one of the concerns of protein release from dense alginate films was that the protein may become inactive during dehydration and/or cross-linking in $CaCl_2$ solution. To test the bioactivity of protein released from dense alginate, BDNF was incorporated with alginate films for a targeted daily release of 50 ng/ml (a concentration optimum for axon growth). A proliferation assay using TrKB-expressing cells was used to assess the bioactivity of released BDNF. As Fig. 4.8 shows, cells proliferated when treated with the solution released from the dense alginate/BDNF film on day 1. To quantify the bioactivity of BDNF and confirm its bioactivity for the following days, the number of cells present after 5 days of proliferation were normalized to the positive control treated with 50 ng/ml of fresh BDNF (Fig. 4.9). The proliferation of the cells responding to the released BDNF was between 10-70% compared

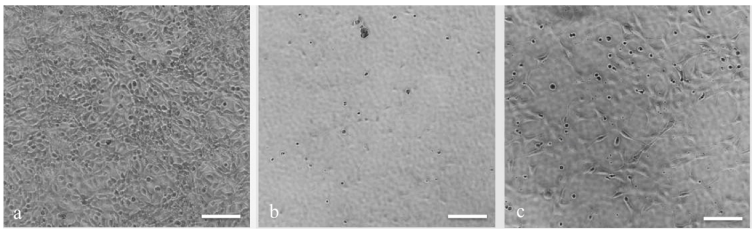

Figure 4.8: The cell proliferation images after 5 days of culturing with cells treated with (a) 50 ng/ml fresh BDNF as positive control, (b) no BDNF as negative control, and (c) solution released from dense alginate/BDNF film on day 1. Positive control confirms the proliferation of cells while only few cells were present on the negative control. Cells had proliferated when treated with solution released from dense alginate/BDNF film confirming the bioactivity of released BDNF. The scale bars are 50 μm.

to 50 ng/ml of fresh BDNF for the first 6 days of release suggesting that the BDNF bioactivity was at least partially preserved. The lower proliferation rate of the experimental group could be because the bioactivity of BDNF was partially lost and/or the release concentration was below the optimum value of 50 ng/ml. In future work, the released BDNF concentration is measured to better understand this phenomena.

The presented drug delivery technique can be used for the delivery of one or multiple molecules/proteins as long as the bioactivity of the drug is maintained. In addition, the released concentration can be controlled by simply changing the initial amount of drug incorporated in the dense film. The gradient release profile is yet another advantage of this novel technique since it is known that a gradient release of drugs can act as a chemoattractant and further stimulate cell growth [33, 78, 121]. To the knowledge of the author, this is the first report of a drug delivery technique that provides sustained month-long drug release with control over the release concentration and capability to have a gradient release.

4.4.3 Scaffold characterization

As shown in Fig. 4.10(a) and Fig. 4.10(b), rolled alginate films can form a disk. The disks were successfully microdrilled into microchannel scaffolds (Fig. 4.10(c)). It

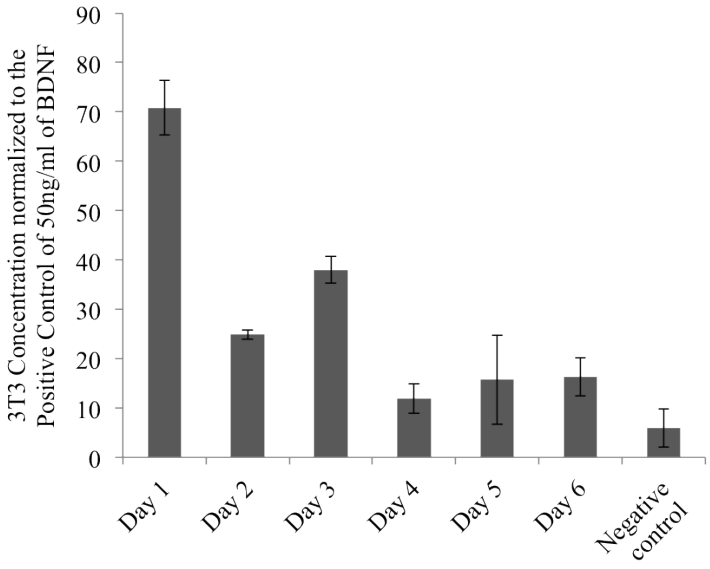

Figure 4.9: The graph shows the bioactivity results of a BDNF-incorporated alginate film using cellular assay on transfected TrkB 3T3 cells. Proliferation results are normalized to the cell count from 50 ng/ml fresh BDNF-treated cells. Data show that the released BDNF is at least partially active.

was, however, observed that the scaffolds dissociated into pieces when stored in RO water for 2 days. A different technique was, therefore, developed to fabricate more robust alginate disks and scaffolds. Careful subsequent drying of alginate solution on previously dried alginate films led to the fabrication of alginate disks with desired lengths. The disks were then microdrilled (Fig. 4.10(d)) into scaffolds with 0.30 mm diameter channels and a spacing of 0.20 mm.

4.4.4 *In vivo* results

While valuable information can be obtained about cell attachment and degradation of dense alginate films *in vitro*, *in vivo* studies are necessary to assess the biocompatibility and degradation of dense alginate in the nerve tissue. Scaffolds were, therefore, implanted in the transected T3 section of rats spinal cords. Fig. 4.11 shows alginate scaffold immunolabeled for neurofilaments 4 weeks post-implantation. Massive inflammatory response and necrosis (cell death) of the host spinal cord oc-

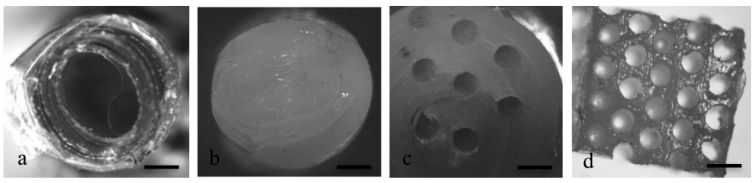

Figure 4.10: Dense alginate scaffolds fabricated via two different techniques. 1) (a) Alginate films were rolled, (b) cross-linked with $CaCl_2$ into a disk and (c) microdrilled to obtain microchannel scaffolds. 2) Subsequent amounts of alginate solution was dehydrated on top of alginate films until the disk reached a targeted hight. (d) The alginate disks were then microdrilled into scaffolds with channel diameters of 300 μm. The scale bars are 300 μm.

curred indicating that the biocompatibility of dense alginate microchannel scaffolds ought to be optimized for future *in vivo* applications. In addition, the scaffold had fragmented and debris were observed (Fig. 4.11). Thus, this study demonstrated that the fabricated dense alginate scaffold did not have adequate degradation rate for nerve repair. Overall, further modifications are necessary for alginate to be used for nerve repair.

4.5 Conclusions

Dense non-porous alginate was fabricated which, unlike alginate hydrogel, allowed cell attachment. To functionalize the films for drug release, lysozyme was incorporated and a sustained protein release for at least 50 days was observed. When BNDF was used, the released BDNF was at least 10-70% bioactive for 6 days. Furthermore, the films could be fabricated to have a gradient protein release. The introduced drug delivery technique is, therefore, a simple yet promising technique for a sustained month-long gradient release of proteins and/or molecules with the capability to control the released concentration. In addition, by developing a novel technique, *mm*-long disks and microchannel scaffolds were produced. However, the dense alginate scaffolds caused inflammatory response in the spinal cord and degraded too

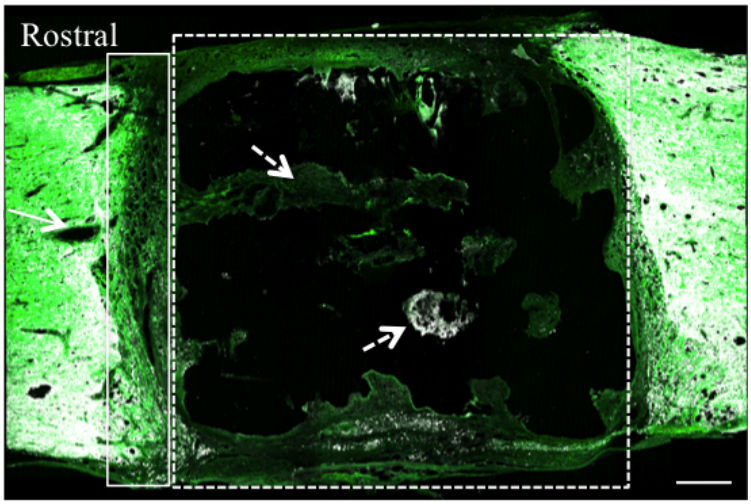

Figure 4.11: Dense alginate scaffold implanted in a transected T3 rat spinal cord and immunostained for neurofilaments (green) after 4 weeks. The box with dashed lines shows the transected spinal cord. The box with solid lines demonstrate a 250 μm-thick layer of scar tissue formed at the rostral end. Scar tissue is also formed at the distal end of the scaffold. Necrosis of the host spinal cord was also observed (an example is shown by the solid arrow on the left). In addition, the dashed arrows point to the scaffold debris indicating that the scaffold fragmented in less than 4 weeks. The scale bar is 250 μm.

quickly before complete axon growth could occur. Further modifications are necessary to improve the biocompatibility of dense alginate and reduce its degradation rate.

CHAPTER V

Poly(ethylene glycol) diacrylate (PEGDA) Microchannel Scaffolds for Spinal Cord Repair Functionalized with Layer-by-Layer Controlled Protein Release

5.1 Abstract

The goal of this work was to fabricate month-long degradable nerve guidance scaffolds that are functionalized with an acellular drug release technique. Poly(ethylene glycol) diacrylate (PEGDA) hydrogels modified with RGD peptides were selected as the scaffold material owing to their reported biocompatibility to the nerve tissue as well as month-long degradation rates. By increasing the weight% (wt.%) of PEGDA from 5 $wt.\%$ to 20 $wt.\%$, the elastic modulus increased from 2.6 kPa to 130.1 kPa. Next, PEGDA/RGD microchannel scaffolds were fabricated by modifications to a previously reported fiber optic templating technique. The scaffolds provided linear axon growth after 28 days when implanted in 2 mm-long transected T3 rat spinal cords. However, the material swelled by over 50% and had reduced open volume. To further improve the scaffolds and promote higher density axon growth, the scaffolds were functionalized with a layer-by-layer drug delivery technique. The release

of brain-derived neurotrophic factors (BDNF) was confirmed *in vitro* for 8 days with a concentration above 50 ng/ml of a microchannel volume. While further work is needed to increase the open volume of the scaffolds, PEGDA/RGD scaffolds are a promising approach as a degradable microchannel scaffold functionalized with an acellular drug release.

5.2 Introduction

Spontaneous spinal cord repair scarcely occurs in adult humans because of the random and limited axon regeneration [18]. Thus, providing spinal cord repair requires 1) guiding growing axons through the lesion and 2) increasing the density of axons [12]. Microchannel scaffolds have linearly guided axons through transected spinal cords in rats [55, 65, 137, 158, 169]. In addition, non-degradable microchannel agarose scaffolds filled with genetically engineered or transfected cells to release brain-derived neurotrophic factor (BDNF) [55, 158] or NT-3 [65], respectively, showed a high density of axons linearly growing in lesions of rats spinal cords. However, cellular drug delivery has possible disadvantages such as ethical issues, immune response, and tumor formation. To eliminate the drawbacks of cellular approach, acellular drug delivery systems are being developed. One example is a layer-by-layer (LbL) drug delivery technique, which involves the bonding of alternating layers of polyelectrolytes and proteins on a material [31, 32]. When carboxylic acid-based electrolytes are used, hydrogen bonds are formed between the layers at a pH below the pKa of the layers [160, 161]. All the layers including the protein are slowly disassembled at a pH above the pKa resulting in a continues pH-controlled drug release. Agarose microchannel scaffolds have previously been functionalized with LbL system to release BDNF for at least 2 weeks and the bioactivity of the released BDNF was confirmed [105].

Leveraging the efficacy of nerve guidance scaffolds (NGS) in linearly guiding axons, this work aims to produce degradable microchannel scaffolds functionalized with

the LbL system. *uv* crosslinkable poly(ethylene glycol) diacrylate (PEGDA) was selected as the scaffold material since it is FDA-approved for applications such as drug delivery, has tunable mechanical properties [17, 66] and has a favorable degradation rate [16, 140]. In addition, the inflammatory response of PEGDA can be reduced by incorporating RGD peptides [106].

In this work, the mechanical properties of PEGDA was characterized and optimized based on its *wt.*% and *uv* crosslinking time. A fiber optic templating technique [103, 158] was modified to fabricate PEGDA-containing RGD scaffolds with linear microchannels. The *in vivo* performance of the scaffolds was tested in transected T3 spinal cords in rats. In addition, the PEGDA scaffolds were functionalized with the pH-responsive LbL drug delivery system to obtain over a week release of brain-derived neurotrophic factor *in vitro*. This work, therefore, introduces a combinatorial approach to both guide and promote the growth of axons for spinal cord repair.

5.3 Experimental

5.3.1 Mechanical testing

The mechanical properties of PEGDA with *wt.*% of 5, 10, 15 and 20 crosslinked for 20, 35 and 50 *min* under *uv* light (365 *nm*) were characterized using compression testing. All samples were prepared by dissolving 0.75 *wt.*% photo initiator (2-Hydroxy-4'-(2-hydroxyethoxy)-2-methylpropiophenone. Sigma; St. Lois, MO) and the corresponding amount of PEGDA (*MW* 8,000. Alfa Aesar; *MW*) in deionized water (DI water). The cylinders were formed by crosslinking 15 *ml* of PEGDA/photo initiator solution in the wells of a 12-well plate (Corning; Corning, NY). Cylinders with parallel surfaces were obtained by sanding the top surfaces with an 800 grit-sand paper (McMaster; Aurora, OH). Compression testing was performed using an Instron (Instron; Norwood, MA) at 1.5 mm/min compression rate ($n = 5$).

5.3.2 Scaffold fabrication

PEGDA/RGD scaffolds were fabricated by modifications to a templating technique [158]. Hexagonally packed multicomponent fiber bundle (MCFB) templates composed of 0.167 mm-thick polystyrene (PS) fibers with claddings of poly methyl methacrylate (PMMA) (0.067 mm-thick) were used. Since PEGDA swells in water after crosslinking, the scaffolds templates were undersized and cut to 1.6 mm-high and 1.45 x 1.45 mm cross-sections to produce 2.0 mm-high and 1.8 x 1.8 mm wide scaffolds. The PS fibers of the cut MCFBs were chemically bonded to PS pieces matching the cross-section of the template using $40°C$ cyclohexane (Alfa Aesar). Two opposing sides of the MCFBs were also bonded to PS caps to further support the PS fibers. The PMMA claddings were removed in 80:20 volume ratio of propylene carbonate:acetonitrile mixture at $60°C$ in 3 days under agitation. The templates were washed in ethanol for 2 hr followed by a wash in deionized (DI) water for 1 hr, and then air-dried. Following the protocol by Browning *et al.* [16] RGD peptides with a sequence of Cys-Arg-Gly-Asp-Ser were prepared by American Peptide Company (Sunnyvale, CA) and dissolved in DI water for a 1.5 mM concentration. PEGDA (5, 10 and 15 $wt.\%$) and the photo initiator (0.75 $wt.\%$) were dissolved in the 1.5 mM RGD/DI water solution. The templates were immersed in the PEGDA mixture and centrifuged for 45 s at 1000 revolutions per minute (rpm). The PEGDA-containing templates were crosslinked under 365 nm uv light for 35 min. For scaffolds used in animal studies, sterile conditions were maintained from this point. Upon crosslinking, the hydrogel surrounding the template was carefully removed by passing a razor blade parallel to the template on each side. The templates were then placed in cyclohexane for 2 days at $37°C$ to remove the PS fibers and produce PEGDA scaffolds with empty channels. Autoclaved reverse osmosis (RO) water was used to rinse and store the scaffolds with.

5.3.3 Surgical procedure, sectioning and immunolabeling

All animal procedures were handled according to the NIH laboratory protocol for animal care and safety. The *in vivo* work and characterization was followed by a previously reported protocol [158]. Adult female Fischer 344 rats (150-200 g) went under anesthetics using a solution of ketamine (25 mg/ml), xylazine (1.3 mg/ml) and acepromazine (0.25 mg/ml). Laminectomy on the T2-T4 section of the spinal cord of rats was performed. T3 segment of the spinal cord (2 mm) was removed and micro-aspirated. RGD-containing PEGDA (10 $wt.\%$) scaffolds were inserted in the transected spinal cords ($n = 7$). Using 4% paraformaldehyde (PFA) at $4°C$, animals were perfused and the implantation site was cut and placed in 30:70 $wt.$ ratio sucrose:1xDPBS for 48 hr. Longitudinal sections (30 μm thick) were cryosectioned for $n = 5$ of the animals and stored in proteinase K:antigen retrieval (1:20) (Millipore; Darmstadt, Germany) for 20 min. Slides were then placed in methanol for 5 min and placed in 5% of goat serum in Tris-buffered saline (TBS) with 0.25% Triton X-100 for 60 min. Mouse-anti-Neurofillament 200 (1:500) (Millipore) was used to stain neurofilaments overnight. Slides were then placed in the secondary antibody, goat-anti-chicken 647 (1:250) (Life Technologies; Carlsbad, CA), for 2.5 hr followed by labeling with Fluoromount G (Southern Biotechnology Associates, Inc.; Birmingham, Alabama). For $n = 2$ of the animals, toluidine blue staining was performed on 1 μm-thick cross-sections and gold-sputtered prior to electron microscopy.

5.3.4 LbL deposition and release

The protocol by Lynam *et al.* [105] was used for LbL assembly on PEGDA/RGD scaffolds fabricated from 10 $wt.\%$ PEGDA described in section 6.3.2. Briefly, poly(acrylic acid) (PAA) (MW 15,000. Sigma) and poly(ethylene glycol) (PEG) (MW 10,000. Sigma,) were dissolved in DI water for a concentration of 1 mg/ml. DI water was used as wash baths. The pH of all the solutions was adjusted to 3.5 using acetic

acid (Sigma). Human BDNF (ProSpec; Rehovot, Israel) was dissolved in 1xDPBS solution (Invitrogen; Carlsbad, CA) (1 $\mu g/ml$). The pH of the 1xDPBS solution was adjusted to 3.5 using acetic acid and contained 1% bovine serum albumin (BSA). BSA was added with the recommendation of the BDNF manufacture's protocol to enhance the stability of BDNF and to act as a blocking agent to reduce the adhesion of BDNF to the walls of the container. Layers of PAA, PEG and BDNF were assembled by dipping PEGDA scaffolds in polymer or protein bath for 30 min followed by one or two 10 min dips with agitation in wash baths (pH 3.5 of DI water). 30.5 bilayers were coated by assembling five bilayers of PAA/PEG followed by five bilayers of PEG/BDNF, repeating this cycle three times and ending LbL deposition with one final PAA layer. These steps were done automatically using Thermo Scientific Varistain 24-4 Automatic Slide Stainer (Waltham, MA). After LbL assembly, the scaffolds were rinsed with neutral pH DI water for 2 minutes. To obtain BDNF release profile, samples were then stored at $37°C$ in 1 ml of 1xDPBS solution. The 1xDPBS solution was collected and refreshed daily for a total of 14 days. The BDNF concentration from each day was measured using an ELISA assay (Boster Immunoleader; Pleasanton, CA). BDNF release from 2 scaffolds was studied and the protein release from each day was measured twice using ELISA. To relate the BDNF release measurements to the BDNF concentration released inside the lumen of a scaffold, the ELISA measurements were normalized to the scaffold lumen volume (3.5 mm^3). The normalized values with a unit of $ng/ml_{mllumen}$ allow a better estimate of how much protein may be available for axon growth in the microchannels of the scaffold *in vivo*.

5.4 Results and Discussion

5.4.1 Mechanical properties of PEGDA

The elastic modulus of 5, 10, 15 and 20 *wt.*% PEGDA samples crosslinked for 20, 35 and 50 *min* are shown in Fig. 5.1(a). The graph shows that changing the crosslinking time from 20 *min* to 50 *min* minimally affected the elastic moduli. However, increasing the *wt.*% of PEGDA increases the elastic modulus. Fig. 5.1(b). shows the linear increase of the elastic modulus of samples crosslinked for 35 *min* as their *wt.*% is increased. Since the PEGDA concentration is 50 times more than the RGD peptides concentration, the affect of RGD on the mechanical properties of PEGDA was considered insignificant. Therefore, no RGD was added to the PEGDA samples used for compression testing.

To our knowledge, there is no study that characterizes the effect of *uv* crosslinking time on the mechanical properties of PEGDA. Measuring the change in the elastic modulus of PEGDA with changing *uv* crosslinking time may help understand the penetration of *uv* light. On the other hand, PEG and PEGDA mechanical properties based on their *wt.*% were quantified in previous works [16, 17, 66]. However, the mechanical properties of a hydrogel may change based on its *MW*. Therefore, in addition to understanding the effect of *uv* crosslinking time on the elastic modulus of PEGDA, the change in the modulus based on *wt.*% was quantified.

5.4.2 Scaffold fabrication

Studies such as Gunn *et al.* [66] have shown PC12 cells neurite extension increases on softer PEGDA surfaces. Therefore, the scaffolds were aimed to have the lowest elastic modulus to improve nerve growth. However, while 5 *wt.*% PEGDA demonstrated the lowest elastic modulus among all the studied *wt.*%, 5 *wt.*% PEGDA scaffolds did not have adequate mechanical properties to maintain linear channels. Thus, 10 *wt.*%

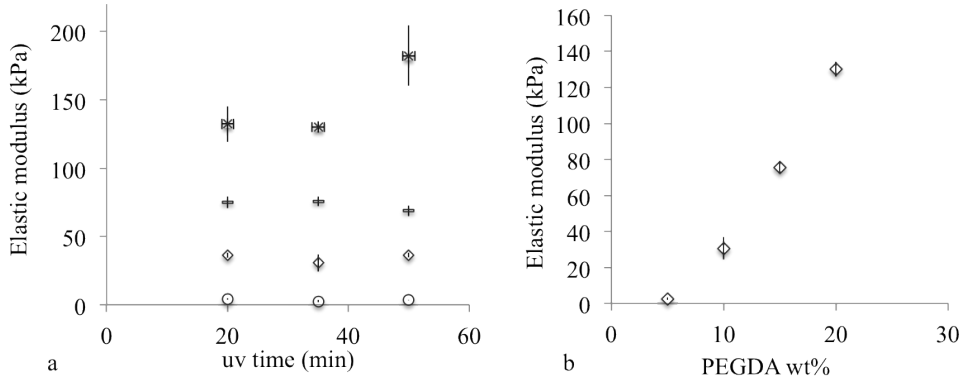

Figure 5.1: The change in the elastic modulus of PEGDA based on its $wt.\%$ and uv crosslinking time. (a) shows the modulus of 5 $wt.\%$ ($\circ$), 10 $wt.\%$ ($\diamond$) and 15 $wt.\%$ (-) did not significantly change when the uv crosslinking time was increased, while the modulus of 20 $wt.\%$ (x) PEGDA increases when crosslinked for 50 min. Increasing $wt.\%$ increased the elastic modulus as more closely shown in (b) in which a 35 min uv-crosslinking time was used while varying the $wt.\%$ of the PEGDA.

PEGDA scaffolds were used to fabricate scaffold. In addition, it was noted that although the change in the uv crosslinking time did not significantly change the elastic modulus (Fig. 5.1(b)) or the strain to failure (data not shown) of PEGDA cylinders, scaffolds crosslinked at 20 min uv crosslinking did not have linear channels while 50 min crosslinking made the scaffolds brittle. These results suggest limitations for the penetration of uv light into cm-long disks. Therefore, 35 min uv crosslinking time was used through the rest of the study. Overall, the data suggests that the mechanical properties of scaffolds may be different than PEGDA cylinders possibly due to the geometrical and dimensional differences.

When scaffolds were removed from cyclohexane upon PS matrix etching, the scaffolds had the same dimensions as the templates (1.6 x 1.45 x 1.45 mm). However, within an hr of placement in RO water, the scaffolds were 2.0 x 1.8 x 1.8 mm while still mimicking the linear structure of the templates (Fig. 5.2). The scaffolds also maintained the same hexagonal pattern of the templates and had 44% channel volume with an average channel diameter of 160 μm. It was noted that the dimensions

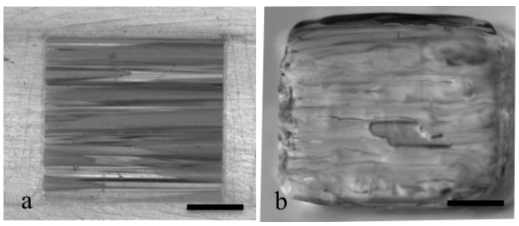

Figure 5.2: The longitudinal view of the template (a) and PEGDA scaffold (b) shows the scaffold matches the structure of the template with microchannels. The scale bars are 0.5 mm.

of the scaffolds did not change in RO water within 1 week after the initial swelling *in vitro*.

5.4.3 *In vivo* performance

Since no growth factors were introduced in the lesion site, a low axon growth density was expected. Nevertheless, all the scaffolds ($n = 5$) provided linear axon growth through some of their channels (Fig. 5.3). In addition, serotonergic (5HT) axons were observed in the scaffold channels (Fig. 5.4). When 5HT axons are present in a damaged spinal cord, it is difficult to verify if transected serotonergic axons regenerated or the surrounding undamaged axon terminals sprouted into the scaffold [173]. However, since a full spinal cord transection was performed, it is highly likely that all axons were cut during the injury and that the increase in the serotonergic axons is because of regeneration and not sprouting.

To further characterize the *in vivo* behavior of PEGDA scaffolds, the cross-sections of the scaffolds were stained with toluidine blue (Fig. 5.5). The open volume of the scaffolds were ∼13.8% which translates to over 50% swelling after 4 weeks of implantation in the spinal cord. Similarly, Browning *et al.* [16] shows that 10 *wt.*% PEGDA subcutaneously swells for 45% within 12 weeks. Swelling of PEGDA is likely because of the crosslink cleavage and the reduction in the crosslink density [12, 16].

Finally, it was also noted that PEGDA scaffolds did not degrade *in vivo* 1 month post-implantation. Previous work on templated hydrogel scaffolds focused on non-

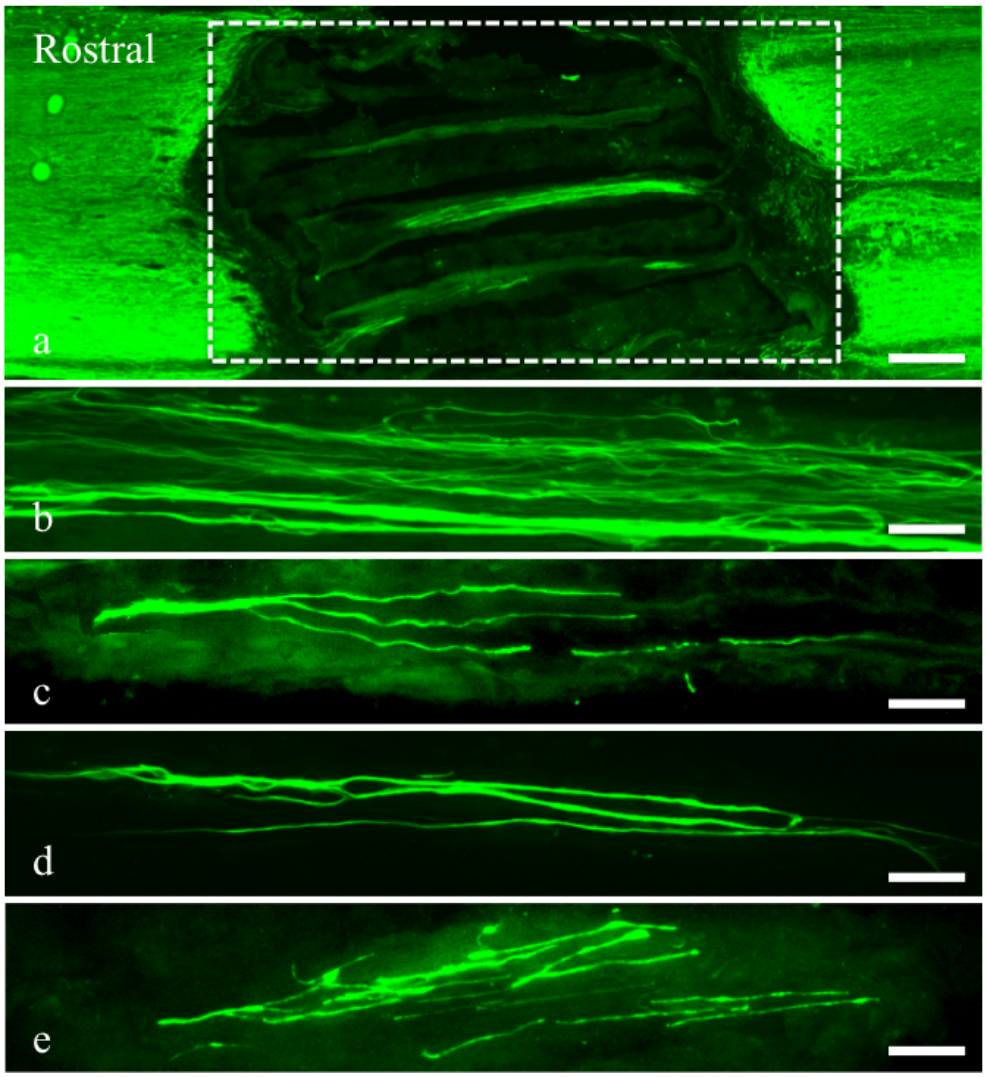

Figure 5.3: Linear axon growth is observed through some of the PEGDA scaffold channels. Neurofilaments are stained in green. Figure (a) shows a representative image of a PEGDA scaffold 4 weeks post-implantation in the T3 transected rat spinal cord. The boxed region in (a) is the nerve gap where the scaffold was inserted. Figures (b), (c), (d) and (e) are the most axon-dense channels of 4 different implants and highlight the reproducibility and efficacy of PEGDA microchannel scaffolds in linearly guiding axons along the nerve gap. The scale bar in (a) is 0.25 mm and the scale bars in (b), (c) and (d) are 0.04 mm.

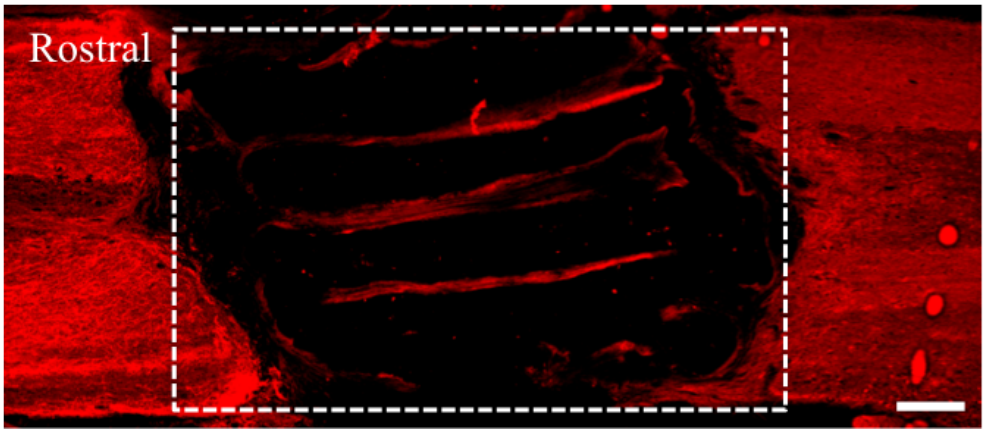

Figure 5.4: Serotonergic axon presence and regeneration in the nerve gap. The boxed region shows the transected T3 spinal cord in a rat with the scaffold implanted for 4 weeks. 5HT serotonergic axons grew linearly along some of scaffold channels. The scale bar is 0.25 mm.

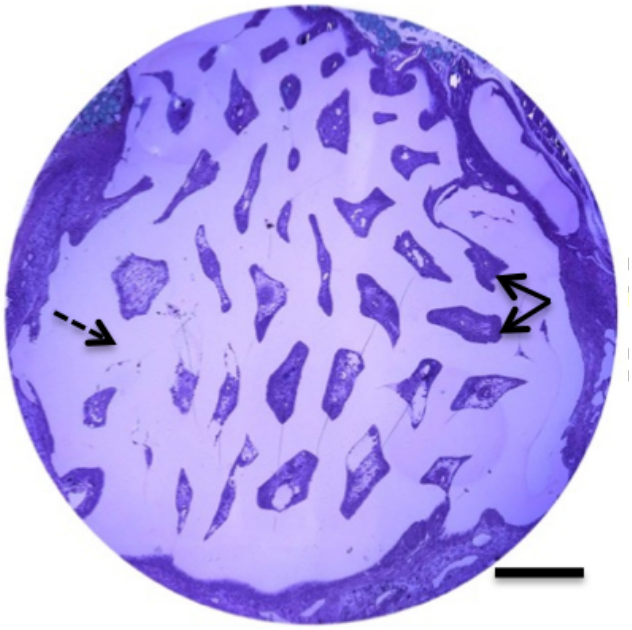

Figure 5.5: PEGDA continues swelling in the spinal cord after initial *in vitro* swelling. A cross-sectional image of PEGDA scaffold 4 weeks post-implantation in the T3 spinal cord of a rat stained with toluidine blue is shown. The lumen volume of the scaffold is 13.8%. Solids arrows point to the open channels and dashed arrow point to the scaffold wall. The scale bar is 0.3 mm.

degradable agarose scaffolds [55, 65, 158]. Thus, the PEGDA *in vivo* results provide encouraging data for a degradable scaffold that maintains its linear channels for a month-long period and can linearly guide axons through the transected spinal cords in rats.

5.4.4 LbL BDNF release

To functionalize the PEGDA/RGD scaffolds with a local sustained protein release, a HLbL drug delivery system was used. BDNF was chosen as the growth factor since it was previously shown that its presence significantly increased axon density in transected spinal cords in rats [55, 158]. As shown in Fig. 5.6, a high dosage of BDNF was released on day 1 (6000 ng/ml of microchannel volume) and reduced by more than a factor on day 2. The BDNF concentration remained above the required value of 50 ng/ml of microchannel volume for nerve regeneration for 6 more days. Studies on the pH-controlled LbL assembly on agarose hydrogel have shown the release of lysozyme (a BDNF analog for the LbL system) for at least 30 days [116]. In addition, BDNF was released from templated agarose scaffolds for at least 14 days and its bioactivity was confirmed [105]. Hence, LbL drug release shows significant potential for integration with nerve implants. This work confirms the compatibility of the HLbL drug delivery system to PEGDA hydrogels.

Providing linear guidance for growing axons and promoting their growth are two important criteria for nerve repair [12]. Previous works confirmed the efficacy of linear microchannel scaffolds in guiding axons in the gaps of spinal cord in rats [55, 65, 158]. However, the degradation rate of the scaffolds needed to be optimized. In addition, it was ideal to functionalize the microchannel scaffolds with an acellular drug delivery system that continuously releases a nerve growth factor to promote nerve regeneration. Leveraging the experience in 1) microchannel scaffolds [55, 65, 158] and 2) LbL drug delivery systems [104, 105, 115, 116], a new generation of dual-

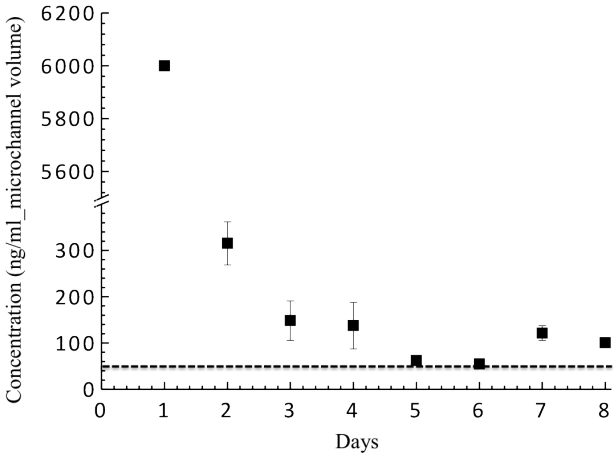

Figure 5.6: BDNF LbL release profile from PEGDA scaffolds. The concentration of BDNF released from a BDNF/LbL-coated PEGDA scaffold shows BDNF release for 8 days. The dashed line indicated the minimum BDNF required for nerve regeneration (50 ng/ml). Relatively high dosages of BDNF is released on days 1 and 2, while the release plateaus thereafter.

purpose scaffolds is introduced. First, degradable PEGDA microchannel scaffolds were tested for their efficacy in linearly guiding axons in the transected rat spinal cord. Second, the scaffolds were functionalized with the acellular LbL drug delivery system to continuously release BDNF above the required dosage for nerve regeneration for 8 days. Future work will involve increasing the lumen volume of the PEGDA scaffold and implanting BDNF/LbL-incorporated PEGDA scaffolds in the transected rat spinal cord to assess the performance of the functionalized scaffolds in linearly guiding high density of axons through the nerve gap.

5.5 Conclusion

The elastic modulus of PEGDA increased from 2.6 kPa to 130.1 kPa as the hydrogel $wt.\%$ increased from 5 $wt.\%$ to 20 $wt.\%$. However, the uv crosslinking time minimally affected the stiffness of the material. Next, PEGDA was modified with RGD peptides to improve its biocompatibility. PEGDA/RGD microchannel scaffolds

were fabricated using a fiber templating technique. The scaffolds were inserted in 2 *mm*-long transected spinal cords of rats and linear axon growth through the channels was observed 28 days post-implantation. Moreover, PEGDA scaffolds swelled by over 50% in 28 days *in vivo*. PEGDA was also modified with an HLbL drug delivery system and the release of BDNF *in vitro* was confirmed for 8 days. Overall, PEGDA/RGD scaffolds are effective in linearly guiding axons but modifications are necessary to increase their open volume.

CHAPTER VI

Hydrogel Peripheral Nerve Microchannel Scaffolds Mechanically Supported by poly caprolactone (PCL) Conduits

6.1 Abstract

Nerve repair in *cm*-long nerve gaps often requires interventional technology. Microchannel scaffolds have proven effective for bridging nerve gaps and guiding axons in the peripheral nervous system (PNS). Nonetheless, fabricating *cm*-long microchannel scaffolds remains a challenge. In this work, a computer aided microdrilling technique was used to fabricate *cm*-scale agarose scaffolds consisting of 0.3 *mm* diameter microchannels and 0.085 *mm* thick walls. The agarose scaffolds alone, however, did not exhibit adequate stiffness and integrity to withstand the mechanical stresses during implantation and suturing. To provide mechanical support and enable suturing, poly caprolactone (PCL) conduits were developed. A modified salt-leaching technique was developed to introduce interconnected porosity in PCL to allow for tuning of the mechanical properties such as elastic modulus and strain to failure. Over 10 *mm* long kink resistant conduits were fabricated. In *in vivo* testing, it was shown that the PCL conduits were effective in stabilizing the agarose scaffolds in sciatic nerve gaps in rats for at least 8 weeks. Robust axon ingress and Schwann cell integration with axons

were observed within the microchannel scaffolds without the use of growth factors.

6.2 Introduction

Peripheral nerve injury (PNI) occurs in 3% of all trauma cases and 30% of combat injuries [4, 11, 85]. This results in approximately 600,000 surgical procedures for PNI annually [15]. Although spontaneous nerve regeneration can occur, functional restoration is often limited and depends on the severity of the injury. Interventional technology may be required to repair *cm*-long injuries after acute nerve trauma. Autologous grafts are the current "gold standard" approach to treat PNI, but have practical limitations such as donor site morbidity and can result in painful neuromas [11, 95, 175]. Bioengineered grafts are under development as an alternative therapy. The goal of this approach was to circumvent issues related to donor availability while guiding axons in *cm*-long peripheral nerve gaps. Several types of bioengineered conduits such as Neurotube®[79], Surgisis®[68, 71, 157], NeuroMatrix®[79], Neuroflex®[96] and NeuraGen®[4, 85] are currently approved by the USA FDA for PNI repair. All of these devices, consist of single-lumen or open channel tubes. An alternative implant design entails the use of linear, multi-lumen microchannels that can organize or group axons into fascicles [175] and guide them toward distal targets. Examples involve the design, fabrication, and testing of multi-lumen microchannel scaffolds consisting of $<$ 0.3 *mm* inner diameter channels [55, 65, 130, 151, 159]. Compared to single-lumen conduits, multi-lumen microchannels confine axons into discrete bundles, thus providing physical guidance toward distal targets. For example, multi-lumen agarose scaffolds were effective in linearly guiding axons in transected spinal cords [55, 65, 159]. The agarose scaffolds were fabricated using ordered arrays of polystyrene fibers as a template to pattern 2 *mm* long, hexagonally-packed linear channels.

In this work, a subtractive mechanical technique (microdrilling) was used as an alternative approach to make 10 *mm*-long microchannels in agarose hydrogel. The

drilling process was controlled by a computer numerical control (CNC) machine to pattern hexagonally-arranged microchannels to achieve $\sim 40\%$ lumen volume, which is comparable to that of the fiber templating process previously used. For use in a rat sciatic nerve model, 10 mm-long, 1.4 mm-outer diameter agarose scaffolds were prepared consisting of 0.3 mm-diameter microchannels separated by 0.085 mm-thick walls. However, agarose hydrogel does not have adequate mechanical integrity to allow its suturing to nerve stumps.

To mechanically stabilize the agarose scaffold, a novel outer nerve guidance conduit was fabricated to secure the agarose microchannel scaffolds to the nerve stumps. The conduits consisted of poly caprolactone (PCL). PCL was selected as the conduit material because: 1) it is FDA-approved for applications such as sutures, 2) it is known to be biocompatible with nerve tissue [24, 34], and 3) it can be made porous [87, 97, 141] to control its mechanical properties [183]. Porosity was introduced into the PCL using a salt-leaching technique to enable suturing to the nerve stumps by reducing the elastic modulus (stiffness) and increasing its strain to failure. In addition, a casting process was used to prepare relatively thin-wall PCL conduits (0.06 mm) to minimize the conduit/scaffold construct volume.

The purpose of this work was to fabricate and test the *in vivo* efficacy of an agarose microchannel scaffold that is mechanically supported by a porous PCL nerve guidance conduit. In this study, agarose scaffolds were fabricated using micromachining, consisting of 0.3 mm-diameter 10 mm-long microchannels with 0.085 mm-thick spacing. PCL conduits enabled suturing of the microchannel agarose scaffolds to the nerve stump. By introducing porosity into the PCL using a modified salt-leaching technique, strain to failure was increased from 17% to over 100%. Moreover, the porous PCL conduit was kink-free for up to 58° of bending; an important criterion to consider when implanted in regions where muscle tissue undergoes significant displacement [30, 79, 96, 114]. When sutured to a rat sciatic nerve stump, the scaffold/conduit

construct remained mechanically stable with negligible inflammation after 8 weeks *in vivo* and some axon and Schwann cell penetration into the proximal site of the scaffold was observed. This work demonstrates the efficacy of a hybrid nerve guidance scaffold approach whereby a hydrogel microchannel scaffold (agarose) physically guides axons toward distal targets while a robust outer conduit provides mechanical integrity and enables suturing to nerve stumps. It is thought that the hybrid design can allow for the integration of myriad scaffold material types and configurations to produce viable alternatives to autologous nerve implants.

6.3 Experimental

6.3.1 Agarose scaffold fabrication

Agarose hydrogel was prepared by heating agarose powder (3 $wt.\%$, Sigma Aldrich; St. Louis, MO) in reverse osmosis (RO) water at $\sim 100°C$ to form a monomer solution. To eliminate air bubbles, the agarose solution was centrifuged at 1500 rotations per minute (rpm) for 30 s. The solution was poured into a 12 well-plate (VWR; Radnor, PA) and cooled to room temperature to form a hydrogel. After gelation, the cylindrically-shaped hydrogel cylinders were extracted from the well plate and machined to produce 10.0 mm-tall cylinders. A computer numerical control (CNC) machine (US Digital, Vancouver, WA) was used to machine the hydrogel cylinder height using a 3.0 mm drill bit (McMaster, Aurora, IL) and create cylinders with parallel faces.

The scaffold microdrilling process is illustrated in Fig. 6.1. A 3 x 8 mm piece of polystyrene (PS) (VWR) was attached to the top corner of a well of a 12-well plate. To ensure the channels extended through the 10 mm-tall cylinder, a sacrificial layer (7 mm-thick) of agarose hydrogel was prepared similar to the 10 mm-tall cylinder and was placed at the bottom of the well plate. The 10 mm-tall agarose cylinder

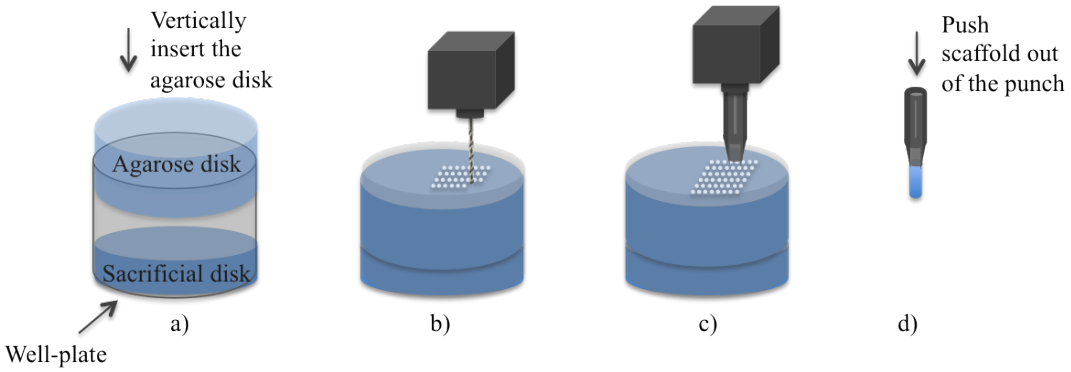

Figure 6.1: Steps in microdrilling agarose scaffolds. (a) A sacrificial agarose disk is placed at the bottom of the well of a well-plate. An agarose disk with a height equivalent to the desired height of the scaffold (10 mm in the present study) was placed over the sacrificial layer with a PS piece anchoring the disk in place. (b) A CNC-controlled microdrill patterned linear channels in the agarose disk. (c) A titanium tube was sharpened to a knife-edge and was used to cut scaffolds. (d) The scaffolds are extracted from the sharpened punch.

was placed over the sacrificial agarose with the PS piece anchoring the cylinder and preventing it from spinning/moving during microdrilling. A 0.300 mm (McMaster) microdrill bit was used to drill the agarose cylinder in a hexagonal arrangement with spacing of 0.1 mm using the CNC and a patterning program (Artsoft Software Inc.; Livermore Falls, ME). A feed rate of 25.4 mm/min was used to microdrill channels. After each 0.25 mm of drilling, the bit was extracted from the agarose hydrogel disk to remove swarf (also known as peck drilling). Feed rates and peck drilling depths above and below the mentioned values did not result in linear channels or symmetric hexagonal patterning. A total depth of 11.6 mm was drilled (thus drilling into the sacrificial cylinder) to ensure the channels extended the entire length of the scaffold. A few ml of water was maintained above the hydrogel cylinder during drilling to prevent dehydration and help remove swarf from the channels and microdrill bit. The agarose cylinder was drilled for at least 1.4 x 1.4 mm-wide surface to fabricate a scaffold with a diameter of 1.4 mm.

A customized sharpened punch with an inner diameter of 1.4 mm was used to

extract agarose scaffold from the drilled cylinder. The punch was inserted perpendicular to the surface of the cylinder at a speed of 25.4 mm/min for a depth of 14 mm and retracted above the surface. The agarose scaffold was pushed out of the punch by inserting a 1 mm-wide metal rod inside the punch. Air was gently blown into the scaffold to remove any residual agarose and clear the channels. The channel linearity and agarose scaffold dimensions were characterized using optical microscopy (Leica EZ4D; Buffalo Grove, IL). The scaffolds were stored in RO water with 5% ethanol (Alfa Aesar; Ward Hill, MA) until implantation.

6.3.2 Nerve guidance conduit fabrication and scaffold assembly

Porosity was introduced using sodium chloride (NaCl) particles as a porogen. NaCl (Columbus Chemical Industries, INC.; Columbus, WI) was ground using a planetary ball-mill (Retsch PM 100; Haan, Germany) in a 250 ml agate jar with 12 agate balls for 1 hr at 400 rpm with 5 min rest every 5 min. ϵ-caprolactone (MW: 114.14) (Sigma; St. Lois, MO) was dissolved in chloroform (Sigma) (3 $wt.\%$) and added to the ball-milled NaCl to produce a 30:70 vol % of PCL:NaCl mixture. The mixture was ball-milled for 20 min at 400 rpm with 5 min rest every 5 min. The rest period prevented over-heating of the jar. To fabricate porous PCL conduits, a steel rod with an outer diameter of 1.4 mm was placed in the PCL/NaCl mixture and air-dried. After the chloroform evaporated ($\sim$2 min), the PCL-coated rod was immersed in methanol (Sigma) for $\sim$1 min. The PCL tubes were removed from the rod and cut into 12 mm-long tubes using a razor. The tubes were then placed in RO water to leach out NaCl. The PCL conduit was bent around fingertips and optical images were taken (iPhone 5, Apple Inc.; Cupertino, CA).

Assembling the scaffolds entailed the insertion of the agarose scaffolds into the tubes. Agarose scaffolds (fabricated in section 6.3.1) were partially dehydrated to temporarily cause radial contraction and facilitate insertion into the tubes. Dehy-

drated scaffolds were inserted and centered in the 12 mm-long PCL tubes with 1 mm overhangs at each end. Agarose scaffolds returned to the original dimensions after rehydration in RO water. By dehydrating, inserting, and re-hydrating, the outer diameter of the agarose scaffolds matched the inner diameter of the PCL tube, which immobilized the scaffold inside the PCL tubes. The scaffolds were sterilized and stored in 10 $vol\%$ ethanol in RO water.

6.3.3 Characterizing the mechanical properties and porosity of PCL

Non-porous and porous PCL films were fabricated to characterize the mechanical properties of PCL. The 3 $wt.\%$ PCL dissolved in chloroform and the PCL/NaCl mixture (described in section 6.3.2) were poured on copper foil (McMaster) secured to an automated tape casting coater using vacuum (MTI Corporation; Richmond, CA). A doctorblade (Tape Casting Warehouse, Inc.; Morrisville, PA) with a height of 0.050 mm was used to evenly spread the solutions. The PCL films were air-dried. To delaminate the films from the copper foil, methanol (Sigma) was poured on top of the films. The film with NaCl was then placed in water for at least 12 hr to remove NaCl. PCL rectangular pieces (25 x 6 mm) were cut using a razor, and tensile testing was performed with a 1.5 N/min loading rate ($n = 5$) (Instron; Norwood, MA). To characterize porosity, the salt-leached PCL tubes described in 6.3.2. were fractured after immersion in liquid N_2 followed by sputter coating with gold for 120 s (3 nm-thick coating) (SPI Supplies; West Chester, PA). The fracture surfaces were imaged using scanning electron microscopy (SEM) (FEI Nova NanoLabTM 600 DualBeam; Columbus, OH). A needle was passed through a salt-leached PCL tube *in vitro* to evaluate suture-ability. The punctured PCL was gold-coated similar to the PCL tube and characterized in the SEM.

6.3.4 *In vivo* testing

Animals were housed 2-3 per cage with free access to food and water in a vivarium approved by the American Association for the Accreditation of Laboratory Animal Care. All animal studies were carried out according to protocols approved by the Institutional Animal Care and Use Committee of the VA Healthcare System, San Diego and following the IASP Guidelines for Use of Animals in Research. Adult male Sprague-Dawley rats (150-200 g) underwent surgery under anesthesia using ketamine (25 mg/ml), xylazine (1300 mg/ml) and acepromazine (0.25 mg/ml). A total of 7 animals were used. The hindquarters were shaved and sterilized with ethanol (Sigma). Skin was incised parallel to the femur, and the sciatic nerve was exposed via a gluteal muscle-splitting approach. A 5-mm segment of sciatic nerve, 5 mm proximal to the sciatic trifurcation, was cut. A sterilized 10 mm-long agarose scaffold inside a 12 mm-long PCL conduit (described in sections 6.3.1 and 6.3.2) was inserted in each rat nerve gap and the PCL conduit was sutured to the ends of nerve stumps with two interrupted 9-0 nylon microsutures. Muscle was sutured with 5-0 polyglactin (Vicryl Ethicon Suture; Somerville, NJ), and the skin was stapled. Following surgery, rats received banamine (1 mg/kg) and ampicillin (0.2 mg/kg) in lactated Ringers for three days.

Paraformaldehyde (PFA) (4%) was used to perfuse the animals eight weeks after implantation. The site of surgery was cut and the scaffold and the nerve were transferred to sucrose:1xDPBS solution (30:70 $wt.$ ratio) prior to dissection and sectioning. For evaluation of the scaffold site, 0.020 mm-thick longitudinal tissue sections were cryosectioned. The slides were treated with proteinase K:antigen retrieval (1:20) (Millipore; Darmstadt, Germany) for 20 min. Subsequent washes were followed by using 50% methanol for 10 min, 100% methanol for 20 min and 50% methanol for 5 min. Later the slides were placed in 5% of goat serum and Tris-buffered saline (TBS) for 20 min. Mouse-anti-Neurofilament 200 (1:500) (Millipore) and rabbit-anti-S100 pro-

tein (1:500) (Dako; Carpinteria, CA) were used to label neurofilaments and Schwann cells, respectively. Slides were washed with TBS and labeled with Goat-anti-mouse Alexa-Fluor 488 and Goat-anti-rabbit 594 (Life Technologies, Carlsbad, CA). Slides are visualized using an Olympus BX 53 microscope. Fluorescent images were taken with a mounted camera (Q imaging Retina 2000R) and CellSens Digital Imaging computer software.

6.4 Results and Discussion

6.4.1 Agarose scaffold and PCL conduit characterization

The agarose scaffold PCL nerve guidance conduits constructs were characterized using optical microscopy (Fig. 6.2). The agarose scaffolds were 10.0 mm in length and 1.4 mm in outer diameter. Each microchannel diameter was 0.3 ± 0.01 mm with spacing of 0.085 ± 0.005 mm (Fig. 6.2(a)). The spacing between the channels (specified as 0.1 mm on the CNC) was the smallest spacing that resulted in linear channels when microdrilling the agarose and was therefore used to maximize the lumen volume of the scaffold. Attempts in reducing the wall thickness to increase the lumen volume resulted in scaffolds with inadequate mechanical integrity to withstand implantation and suturing. To ensure microchannel linearity, longitudinal images were analyzed (Fig. 6.2(b)). The linear features in Fig. 6.2(b) represent the microchannels, which appear continuous and regular along the entire scaffold length. The optical analysis confirms that the microdrilling process was successful in fabricating microchannel agarose scaffolds with relatively thin walls (0.085 ± 0.005 mm) and high aspect ratio channels (33:1), but using a mechanical rather than a chemical removal process.

The agarose microchannel scaffolds did not have sufficient mechanical properties to allow for their suturing to nerve stumps. Thus, PCL conduits were developed to mechanically reinforce the agarose scaffolds (Fig. 6.2(c)). The PCL mechanical

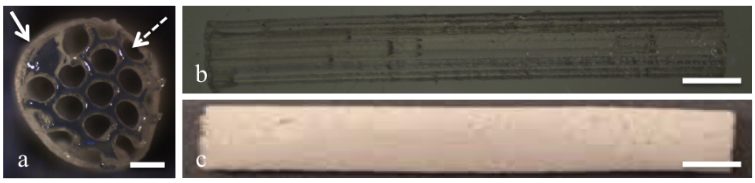

Figure 6.2: Agarose microchannel scaffold with PCL nerve guidance conduit. (a) Cross-section showing an array of 0.3 mm inner diameter channels and 0.085 mm thick walls, (b) longitudinal view shows 10 mm long linear channels, and agarose scaffold is inserted in (c) a PCL conduit with an overhang of 1 mm from each end. The solid arrow points to the PCL conduit around the agarose scaffold and the dashed arrow highlights the additional channels created by the conduit around the scaffold. The scale bar in (a) is 0.3 mm and the scale bars in (b) and (c) are 10 mm.

property characterization is separated into two separate sections below.

6.4.2 Correlating PCL mechanical properties with porosity

A dramatic reduction in elastic modulus was observed by introducing porosity. PCL films without porosity had an elastic modulus of 182 MPa while 70 $vol\%$ porous PCL films had an elastic modulus of 2.1 MPa (Fig. 6.3). To assess handle-ability and suture-ability, the degree of deformation was measured by obtaining the strain to failure. Strain to failure is the strain% (($length_{final}$ - $length_{initial}$)/$length_{initial}$))x100 before rupture. Strain to failure increased with increasing porosity from 17% in non-porous films to 100% in 70 $vol\%$ porous films (Fig. 6.3). By increasing the strain to failure by introducing porosity, the PCL conduits could withstand puncturing with a suturing needle without rupture (Fig. 6.4). Without the porosity, dense PCL of comparable thickness cracks rather than punctures, thus demonstrating the need to increase the strain to failure to allow for suturing. Representative SEM cross-sectional images of the salt-leached porous PCL (70 $vol\%$) conduit consisted of interconnected porosity with a diameter of 17 μm (Fig. 6.5). In addition to reducing the elastic modulus and increasing the strain to failure, the interconnected porosity may also facilitate wetting and transport of nutrients, oxygen, and waste products within the

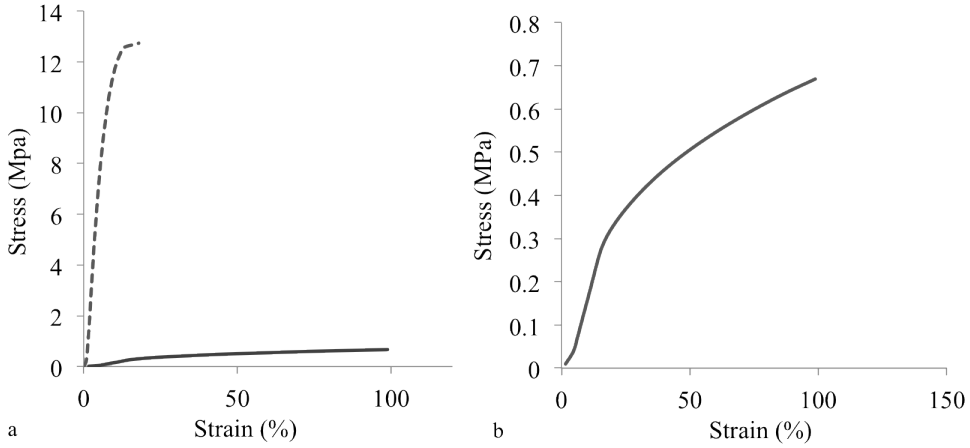

Figure 6.3: Stress-strain curves of non-porous and porous PCL. (a) Dashed line demonstrates 100% non-porous PCL and solid line indicates 70 $vol\%$ porosity PCL. The elastic modulus of PCL reduces from 182 MPa to 2.1 MPa while the strain to failure increases from 17% to 100% when 70 $vol\%$ porosity is introduced. (b) is the stress-strain curve of 70 $vol\%$ porosity PCL and highlights the elastic behavior to about 17% strain and plastic behavior thereafter

implant.

6.4.3 PCL conduit flexibility

The PCL conduits were fabricated in lengths > 100 mm and exhibited flexibility comparable to state-of-the-art nerve guidance conduits [30, 79, 96, 114]. PCL conduit flexibility was demonstrated by measuring the maximum bend angle before a kink occurred. As demonstrated in Fig. 6.6, the tubes were kink-resistant up to a bend angle of 58°. Based on their flexibility and kink-resistance, the PCL conduit properties are comparable to state-of-the-art, FDA-approved conduits.

6.4.4 Scaffold nerve stump integration

Microchannel agarose scaffolds integrated into PCL conduits were implanted in 10 mm long rat sciatic nerve gaps. The agarose scaffolds were 10 mm long and inserted into 12 mm long PCL conduits. The additional PCL conduit length created

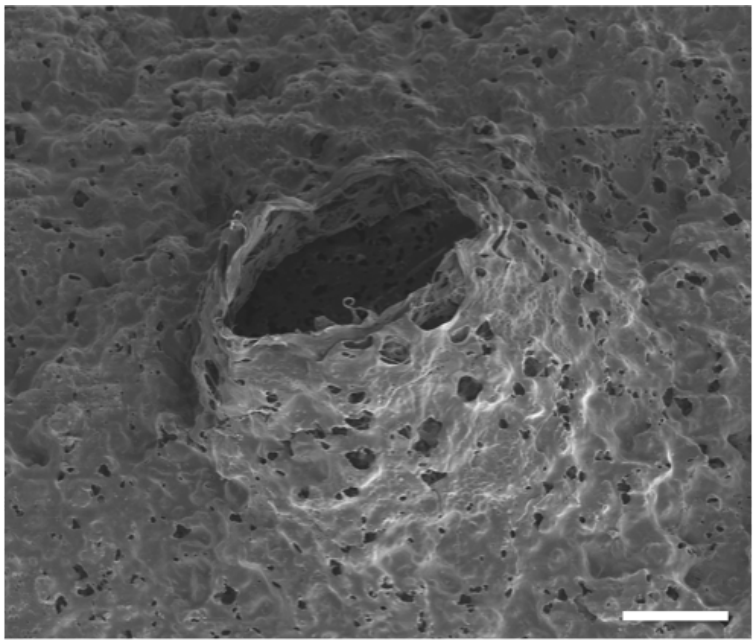

Figure 6.4: An SEM image of a PCL conduit after a simulated suturing test. The scale bar is 0.1 mm.

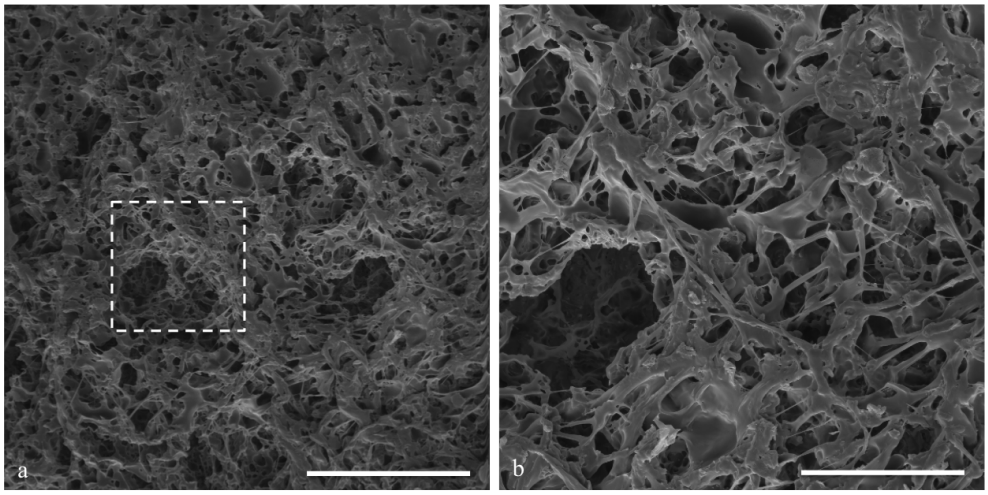

Figure 6.5: Interconnected pores are observed in the salt-leached PCL nerve guidance conduit. (b) is a higher magnification of the box in (a). The scale bars in (a) and (b) are 50 μm and 20 μm, respectively.

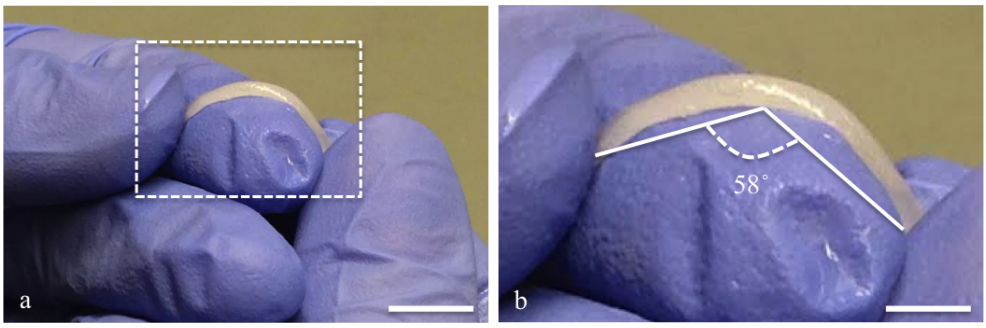

Figure 6.6: PCL conduit is kink-resistant up to 58°. No kink is present when the conduit is bent around fingertips. (b) is a magnified image of the box in (a) and demonstrates no kink is present for at least 58° of bending. The scale bar in (a) is 10 *mm* and in (b) is 0.5 *mm*.

1 *mm* overhangs (cuff) on each end of the implant. The overhangs enabled suturing of the scaffolds to the ends of the nerve stump. After 8 weeks of *in vivo*, the scaffold remained integrated with the nerve, demonstrating the efficacy of the PCL tube in stabilizing a scaffold in the highly mobile region of sciatic nerve (Fig. 6.7(a),(b)). In addition, the PCL tubes and agarose scaffolds maintained their mechanical integrity and no signs of degradation were observed. The overhangs allowed for suturing of the nerve stumps to the scaffold, which was also previously demonstrated; for example, PGA Neurotube^{TM} conduits with 3 *mm* long overhangs were sutured to the nerve stumps of 10 *mm*-long rat sciatic nerve gaps using 4 sutures on each side [73]. The conduits remained stable for at least 16 weeks confirming the advantages of overhangs in stabilizing scaffolds to nerve stumps.

6.4.5 *In vivo* characterization

Agarose microchannel scaffolds integrated into PCL conduits were implanted in 10 *mm*-long sciatic nerve gaps. Animals were perfused 8 weeks post implantation and the scaffolds were sectioned at the proximal, middle, and distal ends. The longitudinal view of the proximal end confirmed a high density of axons and Schwann cells were present in the scaffold channels (Fig. 6.8). In addition, the neural orientation was

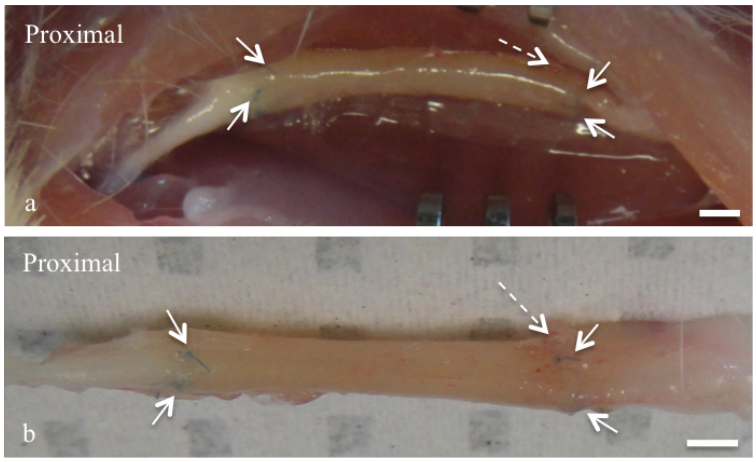

Figure 6.7: The PCL nerve guidance conduit stabilized the agarose scaffold in the nerve gap. The agarose scaffold with PCL conduit 8 weeks post-implantation (a) in the nerve tissue *in vivo* and (b) dissected from the nerve tissue shows the scaffold remains intact and integrated with the nerve. The conduit was sutured to the host nerve using two sutures at each end as shown with solid arrows. Some capillary formation was observed at the distal end as indicated by the dashed arrow. The scale bars are 10 mm.

linear and parallel to the scaffold channels. To further assess the stability of the scaffolds and the presence of axons/Schwann cells, cross-sectional images in the middle of the scaffold were taken (Fig. 6.9). The microchannels of the scaffold remained intact and in the original hexagonal pattern. Some of the channels contained axons and Schwann cells, but were mostly observed around the periphery of the scaffold in close proximity to inner walls of the PCL conduit. Nevertheless, Fig. 6.9 demonstrates the partial channels that occupy the space between the periphery of the agarose scaffold and the inner wall of the PCL conduit can also linearly guide axons toward distal targets. This observation may also suggest that since axons and Schwann cells recruitment were most pronounced along the inner wall of the PCL conduit, that PCL may be a more favorable surface for cell attachment compared to agarose.

A microchannel construct provides a structure that, compared to hollow conduits, is more effective in linearly guiding axons through the nerve gap and maintaining their organization. The present agarose microchannel scaffold/PCL constructs provided

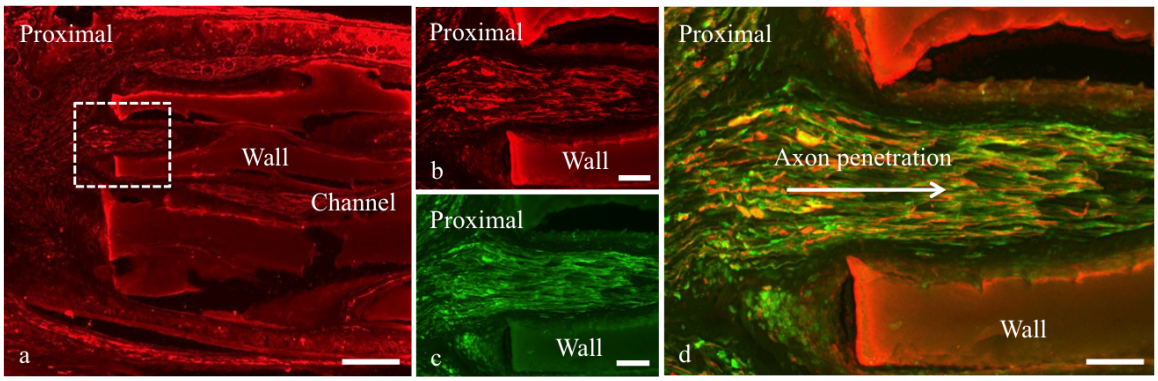

Figure 6.8: Axon and Schwann cell penetration into scaffold channels. (a) The proximal side of an agarose scaffold in a PCL conduit in a 10 mm long rat sciatic nerve gap 8 weeks post-implantation. Neurofilament (red) immunoreactivity highlights axon penetration into the agarose scaffold channels. The boxed region in (a) is magnified in (b), (c), and (d). (b) Axon immunoreactivity with NF200 (red) and (b) Schwann cells (SC) immunoreactivity with S100 (green) inside scaffold channels. The axon (red) and SC (green) labeling is superimposed in (c), which indicates their integration. The scale bar in (a) is 400 μm; all the other scale bars are 100 μm.

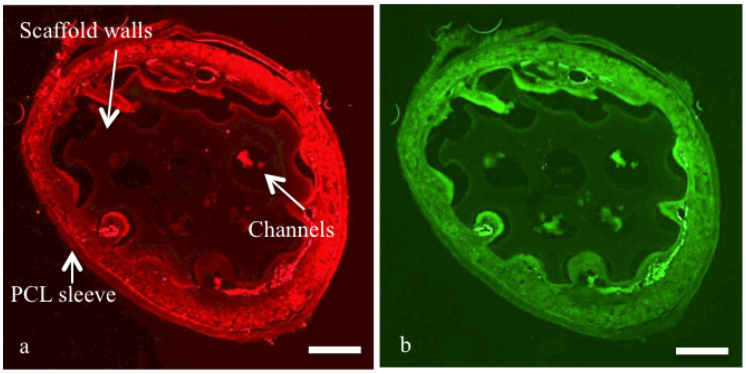

Figure 6.9: Axons and Schwann cells are located inside some channels and around the periphery of the scaffold. Cross-section of an agarose scaffold inside a PCL conduit stained with (a) NF200 for axons (red) and (b) S100 for Schwann cells (green). Axons and Schwann cells grew through some of the channels and in the interstitial space between the scaffold periphery and the inner wall of the PCL conduit. Scale bars are 400 μm.

linear ingress of axons and peneteration of Schwann cells into the scaffolds after 8 weeks of implantation. It is believed that the axon and Schwann cell density and degree of axon growth could be significantly augmented if growth factors for axons and Schwann cells were present. Future work will involve filling scaffolds with growth factors in efforts to improve nerve regeneration and recapitulation.

6.5 Conclusions

A computer-controlled microdrill was used to fabricate agarose hydrogel scaffolds consisting of 10 mm-long microchannels. To provide mechanical support, robust PCL outer conduit technology reinforced the agarose microchannel scaffolds and enabled suturing of the PCL conduits to peripheral nerve stumps. *In vivo* testing in the sciatic nerve model demonstrated that the agarose microchannel scaffold/PCL nerve guidance implants were effective in linearly guiding and organizing axons and Schwann cells. Overall, this investigation demonstrated that the combination of synthetic microchannel scaffolds and outer protective conduits could be a viable alternative to autologous nerve implants.

CHAPTER VII

A Novel Technique to Synthesize and Fabricate High Lumen Volume poly caprolactone (PCL) Microchannel Scaffolds for Spinal Cord Repair

7.1 Abstract

Microchannel scaffolds can linearly guide growing axons in the lesion of the spinal cord. However, the volume occupied by the scaffold walls must be reduced to maximize the volume available for regeneration. In this work, nerve guidance scaffolds with significantly higher open volume were developed by reducing the thickness of the walls of the scaffolds. Poly caprolactone (PCL) was selected as the scaffold material based on its biocompatibility and month-long degradation. However, dense PCL does not exhibit suitable properties such as porosity, stiffness, strength and cell adhesion for nerve regeneration. To address these issues, PCL was processed using a modified salt-leaching technique whereby sodium chloride (NaCl) particles were planetary ball-milling (PBM) to reduce the average particle size ($\sim$0.017 mm). By controlling porosity, the tensile elastic modulus was controlled between 182.1-2.09 MPa. The porosity also enhanced cell attachment and proliferation. Salt-leached PCL microtubes were fabricated and translated into scaffolds with 60 lumen $vol\%$. The scaffolds were tested in a rat spinal cord injury model and linear axon growth

into the scaffold was observed. Overall, a new materials processing and scaffold fabrication technique is presented that generates scaffolds with significantly higher lumen volume than state-of-the-art scaffolds for spinal cord repair.

7.2 Introduction

One approach to regenerate axons is to provide physical cues to guide regenerating tissue across the lesion site. Examples include electrospun fibers [25, 74, 117, 178], conduits [181, 182, 185] and multilumen scaffolds [50, 55, 67, 116, 130, 137, 158, 172, 176]. While linear guidance of axons toward distal targets was demonstrated using several of these approaches, the ability to achieve native axon densities comparable to native nerve tracts requires further technological refinement. Specifically, in approaches employing synthetic nerve regeneration scaffolds, the volume fraction of scaffold occupying the lesion site must be reduced to maximize the open volume available for guidance and nerve tissue regeneration. For example, scaffolds consisting of close packed arrays of microchannels (honeycomb structure), can achieve over 40% lumen volume using a fiber templating process to pattern hydrogels [158]. In practice, fiber templating can achieve $> 60\%$ lumen volume [103]; however, the strength and strain to failure of typical hydrogels is not likely to be sufficient to fabricate high lumen volume, thin-wall scaffolds that can survive the rigors of fabrication and/or surgical implantation [103]. Hence, there is a need to develop new materials and materials processing technology to enable the fabrication of nerve guidance scaffolds comprised of microchannels with relatively high lumen volume.

In this study, an approach was developed to create scaffolds consisting of microtubes with walls < 0.060 mm-thick that are porous to 1) reduce stiffness and 2) enhance cell attachment. Poly caprolactone (PCL) was selected as a representative synthetic polymer based on its known biocompatibility with the nerve tissue [24, 34], month-long degradation rate [24, 34] and strength. However, some properties of PCL

need to be modified. First, interconnected porosity is required for the transport of nutrition, oxygen and waste in the nerve tissue. Second, the elastic modulus and strain to failure of PCL needs to be optimized to be suitable as a nerve guidance scaffold. Third, PCL does not allow cell attachment [136, 147] and it may be beneficial to improve its cell adhesion properties to improve nerve growth. Several techniques have been previously studied to introduce porosity to tune the mechanical properties of PCL. For example, techniques such as photo cross-linking of a modified PCL [42] and a customized patterning technique [153] were developed to pattern porous PCL nerve guidance scaffolds. However, in these studies, the porosity was > 0.450 mm in diameter, which can allow the axons to cross between scaffold walls and lose directionality along the lesion cavity. Selective laser sintering is also a patterning technology used to create pores in PCL [44, 183, 184, 187]. Although the pore size distribution was precisely controlled, the pores were > 0.030 mm, which may again allow axonal growth between scaffold walls. Solvent casting is another technique to fabricate porous PCL by mixing a porogen with the monomer solution or melted polymer, forming a solid polymer and selectively etching the porogen with a solvent. Porogens such as poly propylene glycol [24], poly ethylene glycol (PEG) [97], sodium chloride (NaCl) [87] and a mixture of PEG and NaCl [141] were used to create pores within PCL. Although there are examples that demonstrate the ability to create interconnected porosity [97, 141], control of pore size can be difficult. Moreover, the NaCl porogen particles that have been reported are generally > 0.150 mm in diameter [87]. When the porogen size was reduced using a vortex, the distribution of the particle size was relatively large (from 0.020 to 0.50 mm) [141]. Because the goal of this work is to reduce the scaffold wall thickness to < 0.060 mm, the state-of-the-art porogen size would create line-of-site voids that axons could penetrate. In addition, these relatively large discontinuities compared to the targeted scaffold wall thickness compromise the mechanical integrity of the scaffold. By reducing the porogen dimen-

sions, synthetic polymer scaffold walls consisting of numerous interconnected pores can be created. The reduction in pore size can also prevent axons from growing between microchannels.

A modified salt-leaching process was developed to introduce and control porosity in the PCL scaffold walls. A technique commonly used in ceramic material processing (high energy planetary ball-milling) was used to reduce the porogen (NaCl) particle size, thus reducing the porogen size to unprecedented length scales. Using the salt-leaching technique, the volume fraction of porogen in PCL monomer solution was varied between 0 and 70% to control the porosity and therefore the elastic modulus. An optimum volume fraction of resulting porosity was determined to obtain interconnected porosity and reduced stiffness. The porogen size was reduced from 0.350 mm (as received) to $\sim$ 0.017 mm while producing a more uniform size distribution. The formation of pores in PCL was characterized by changing the porogen size and concentration. It is also demonstrated that by increasing porosity in PCL, the strain to failure is improved from 17% to 100% and the stiffness of the films was reduced from 182.1 MPa to 2.09 MPa. In addition, porous PCL improved cell attachment, which may promote axon survival and growth. The modified PCL salt-leaching process was integrated into a modified fabrication process [67] to produce microtubes (0.060 mm wall thickness and 0.260 mm inner diameter). The microtubes were assembled into packed arrays to achieve 60 vol % lumen scaffolds and implanted into rats with complete transections of the spinal cord at thoracic level 3 (T3). The primary purpose of this study was to determine if the high lumen volume scaffolds had adequate strength to withstand fabrication, implantation, and were durable enough to maintain integrity and provide linear axon growth for four weeks *in vivo*. In addition, because no growth factor or cells were integrated in this study, high-density axon growth and functional recovery were not predicted. Nonetheless, favorable integration with host tissue and linear axonal growth were observed.

7.3 Experimental

7.3.1 Porogen size reduction

Sodium Chloride (NaCl) was purchased from Columbus Chemical Industries, INC. (Columbus, WI). NaCl (5 g) was placed in a 250 ml agate vial with twelve 9.1 mm-diameter agate balls. A planetary ball-mill (Retsch PM 100; Haan, Germany) was used to reduce NaCl particle size (Fig. 7.1, step (1a)). To study the effects of ball-milling time and vial rotational speeds on particle size distribution, 100 and 400 revolutions per minute (rpm) and ball-milling times of 1, 5, 10, 30, 60 and 90 min were used. An alternating sequence of 5 min of ball-milling followed by 5 min rest was used to minimize media heating. In addition, the ball-milling direction was reversed after each 5 min rest to reduce NaCl particle agglomeration. The ball-milled NaCl particle morphology and size were characterized and measured using scanning electron microscopy (SEM) images (FEI Nova NanoLabTM 600 DualBeam; Columbus, OH). Owing to favorable particle size distributions, the NaCl ball-milled at 400 rpm for 60 min was used for all the polymer fabrication processes unless otherwise is mentioned.

7.3.2 PCL/NaCl mixture preparation

ϵ-caprolactone (MW: 114.14) (Sigma; St. Lois, MO) was dissolved in chloroform (3 $wt.\%$) and mixed with 0-80 volume % (vol%) of the NaCl ball-milled at 400 rpm for 60 min. The mixture (20-30 g) was ball-milled for 20 min at 400 rpm with 5 min rests every 5 min to enhance the dispersion of the NaCl (Fig. 7.1, step (1b)). The $vol\%$ of the NaCl in the PCL mixture corresponds to the intended $vol\%$ of porosity after solvent evaporation and salt-leaching. To characterize the effect of porogen size on pore formation in PCL, 70 $vol\%$ of NaCl ball-milled at 400 rpm for 1 min was vortexed (Mini vortexer- VWR; Radnor, PA) with the PCL solution for 1 min. Mixing with a vortex was chosen over ball-milling to prevent altering the NaCl particle size.

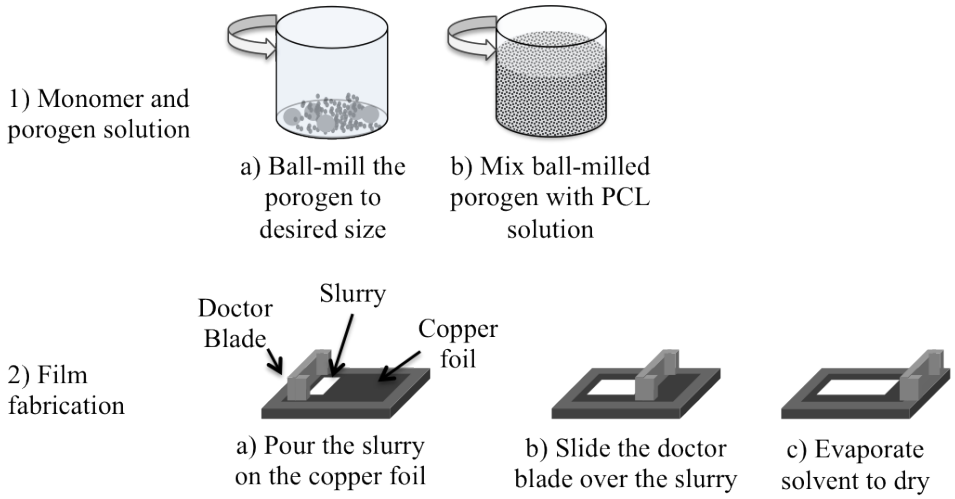

Figure 7.1: Porogen preparation and film fabrication. (1) Synthesizing a uniform solution of PCL and NaCl and (2) fabricating porous PCL films. (1): (a) NaCl is ball-milled to the desired diameter and (b) the NaCl from (1a) is ball-milled with a PCL:chloroform solution to uniformly disperse the NaCl. The slurry from (1b) is used on an automated tape casting apparatus as shown in (2) to produce porous films for tensile testing.

7.3.3 PCL film fabrication and characterization

PCL films consisting of 0-70 $vol\%$ porosity were fabricated for mechanical testing and SEM imaging. To fabricate films, the ball-milled PCL/NaCl mixtures were cast using an automated tape casting coater (Fig. 7.1, step (2)) (MTI Corporation; Richmond, CA). Copper foil (McMaster; Aurora, OH) was placed on the tape casting coater and the slurry was poured on the foil. A doctor blade (set at 0.050 mm clearance between the copper foil and bottom of the blade) was passed over the slurry, spreading it uniformly at 0.05 s/mm. The film was air-dried after casting. To delaminate the PCL films from the copper foil, the films were moistened with methanol (Sigma). The NaCl was removed from the PCL films by placing the films in 2 l of tap water for 18 hr.

To perform uniaxial tensile testing, films were cut to rectangular pieces of about 30 x 8 mm using a razor blade. A uniaxial tension test was performed on the films (Instron; Norwood, MA) under a constant extension rate of 0.2 mm/min and the

elastic moduli were measured. To characterize the porosity of the films, PCL films were fractured in liquid N_2 before and after salt-leaching, gold-sputtered for 120 s and their cross-sectional images were taken using SEM. Films with 100% PCL remained ductile in liquid nitrogen and could not be fractured for SEM cross-sectional imaging. Therefore, the 100% PCL films were mounted in epoxy (Leco Corporation; St. Joseph, MI) and polished using 600, 1200 and 1500 grit sand paper (McMaster). The cross-section was further polished with 0.012 mm and 0.006 mm diamond paste (Leco Corporation). The 100% PCL film was then coated with gold for SEM analysis.

7.3.4 Cell attachment characterization

PCL films (100% and 30 $vol\%$ porosity) were fabricated as explained in section 7.3.3 and were cut to the diameter of the wells of a tissue culture-treated 24 well-plate (Fisher Scientific; Pittsburg, PA). The films were sterilized in ethanol (Decon Labs, Inc.; King of Prussia, PA) for 10 min, washed 3 times with sterile 1xDPBS (ThermoFisher Scientific; Grand Island, NY) and placed under uv (280 nm) for 30 min. PCL films were then placed in the wells of a 24 well-plate. Three different surfaces were studied: 1) control well-plate surface, 2) 100% PCL film and 3) 30 $vol\%$ porous PCl film ($n = 3$ for each group) with and without fibronectin (Sigma) pre-coated (1 mg/ml) for 18 hr and then washed with 1xDPBS. NIH 3T3 fibroblast cells were plated at a seeding density of 5 x 10^4 $cells/well$. After 72 hr of incubation, the cells were washed with warm 1xDPBS and fixed with 4% formaldehyde (ThermoFisher) for 10 min followed by 3 washes with 1xDPBS. To stain for actin, Alexa Fluor 488 Phalloidin (ThermoFisher) was used. Briefly, the fixed cells were incubated with 1% bovine serum albumin (BSA) (Sigma) in 1xDPBS solution for 20 min at room temperature, washed with 1xDPBS and stained with Phalloidin for 20 min at room temperature and washed with 1xDPBS. The nuclei of the cells were stained with DAPI and subsequently washed with 1xDPBS. Fluorescent images were

taken (fluorescent microscope- Olympus BX53; Center Valley, PA).

7.3.5 Scaffold fabrication

The tube and scaffold fabrication process is illustrated in Fig. 7.2(a) and 7.2(b). A copper wire (99% purity) (McMaster) with a diameter of 0.200 mm and a stainless steel rod (grade 304) (McMaster) with a diameter of 1.60 mm were used to fabricate inner and outer tubes, respectively. The metal wires and rods (referred here as fibers) were placed in a PCL:NaCl mixture with 30:70 $vol\%$ and were removed after 5 s of immersion and spun manually while holding horizontally to uniformly evaporate the solvent. To facilitate delamination, the PCL coated metal rods, were immersed in methanol for about 30 s. The tubes were removed, dried in a fume hood and cut into 2 mm-long tubes using a razor blade.

To fabricate scaffolds, eleven inner tubes (0.260 mm inner diameter, 2 mm long) were inserted into an outer tube (1.6 mm inner diameter, 2 mm long). Optical microscope (Leica EZ4D; Buffalo Grove, IL) was used to image the scaffolds. The scaffold lumen volume percentage was calculated according to the following equation:

$$Lumen\ Volume = \frac{Outer\ Tube\ Open\ Volume - Volume\ of\ Inner\ tube\ walls}{Outer\ Tube\ Open\ Volume} \text{ x } 100$$

The scaffolds were placed in water for at least 18 hr to remove the NaCl. Sterilization was done in ethanol for 1 hr following scaffold-coating with 1 mg/ml of fibronectin (Sigma) for 1 hr prior to implantation.

7.3.6 Surgical procedures and *in vivo* characterization

Adult female Fischer 344 rats (150-200 g) were handled according to the NIH laboratory protocol for animal care and safety. Animal preparation, scaffold implantation and tissue fixation was performed as described previously [81, 158]. Briefly, animals were anesthetized using a mixture of ketamine (25 mg/ml), xylazine (1.3 mg/ml) and acepromazine (0.25 mg/ml). Laminectomy was performed at spinal level T3 and

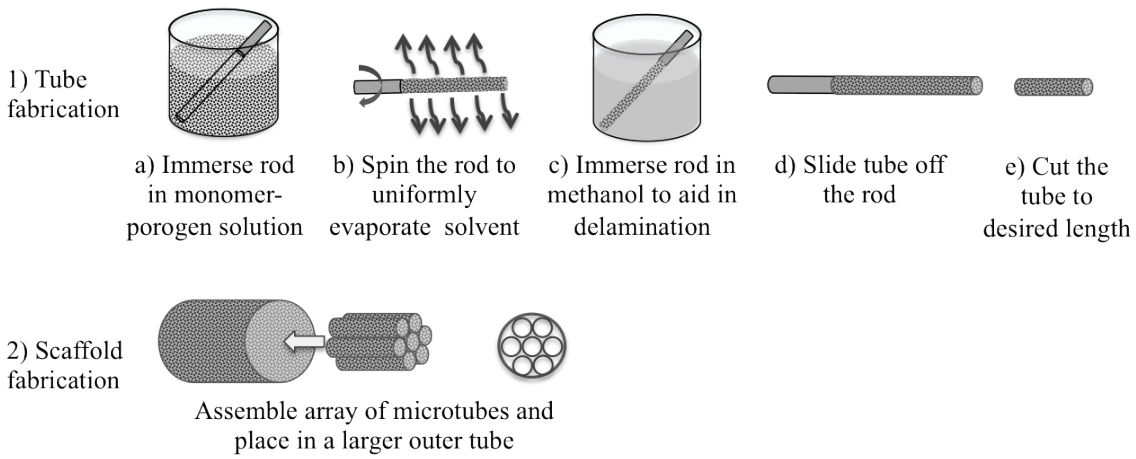

Figure 7.2: Steps in fabricating (1) PCL tubes and (2) PCL scaffolds.

2 mm of the spinal cord was removed by scissors, cut and micro-aspirated.

Sterilized PCL scaffolds (described in section 7.3.5) were surgically placed in the transected spinal cord ($n = 8$). Four weeks after implantation, animals were perfused with 4% paraformaldehyde (PFA) ($4°C$) and spinal cords were stored in sucrose:1xDPBS solution (30:70 weight ratio) for 48 shr. Longitudinal sections (0.030 mm-thick) were obtained through cryosectioning. Slides were placed in proteinase K:antigen retrieval (1:20) (Millipore; Darmstadt, Germany) for 20 min, washed in methanol for 5 min, and were blocked with 5% of goat serum and Tris-buffered saline (TBS) for 1 hr. Axons were identified by a mouse-anti-neurofilament 200 (1:500) (Millipore). Sections were washed with TBS. Slides were labeled with Goat-anti-mouse 647 (1:250) (Life Technologies; Carlsbad, CA) as a secondary antibody for 1 hr and washed with TBS. Prior to fluorescent imaging (Olympus BX53; Center Valley, PA), slides were labeled with Fluoromount G (Southern Biotechnology Associates, Inc.; Birmingham, Alabama).

7.4 Results and Discussion

7.4.1 NaCl porogen size reduction via planetary ball-milling

Planetary ball-milling was used to reduce the NaCl porogen particle size. After PBM at 100 *rpm*, regardless of time ranging from 1 *min* to 90 *min*, a negligible reduction in NaCl particle size was observed. It was likely the kinetic energy was not sufficient to fracture particles [59]. To improve the kinetic energy, a rotation speed of 400 *rpm* was used to correlate PBM time with NaCl particle size. To determine the particle size and characterize the surface morphology, SEM was conducted (Fig. 7.3). The as-received NaCl consisted of particles with relatively smooth surfaces and an average diameter of 0.360 ± 0.115 *mm* (Fig. 7.3(a)). The NaCl particle size was reduced to 0.191 ± 0.070 *mm* with 1 *min* of PMB at 400 *rpm* (Fig. 7.3(b)). After 5 and 30 *min* of PMB at 400 *rpm*, the particle size was reduced to 0.043 ± 0.012 *mm* and 0.017 ± 0.010 *mm*, respectively (Fig. 7.3(c),(d)). Compared to the as-received NaCl, the PBM particle surfaces and geometries were irregular, which is common when using a mechanical comminution process [59]. No significant change in particle size was observed after PMB at 400 *rpm* for more than 30 *min*, indicating that increasing time would not further significantly reduce particle size. In mechanical comminution, it is common for the particle size to approach an asymptotic limit governed by the kinetic energy of a particular process [59]. Assuming the kinetic energy of each ball collision is fixed (by the rotational speed of the PBM in this case), it is known that the impact energy required to fracture particles is inversely proportional to the square root of the diameter of the particles. Thus, when the NaCl particles reached $\sim$0.017 *mm* (at 400 *rpm*), increasing the PBM time did not further reduce the particle size. Nevertheless, the goal of this activity was to produce NaCl particles that were smaller (2-4X) than the scaffold walls (aimed to be 0.03-0.06 *mm*) to prevent line-of site gaps between microchannels that would allow axons to lose directionality as they extend

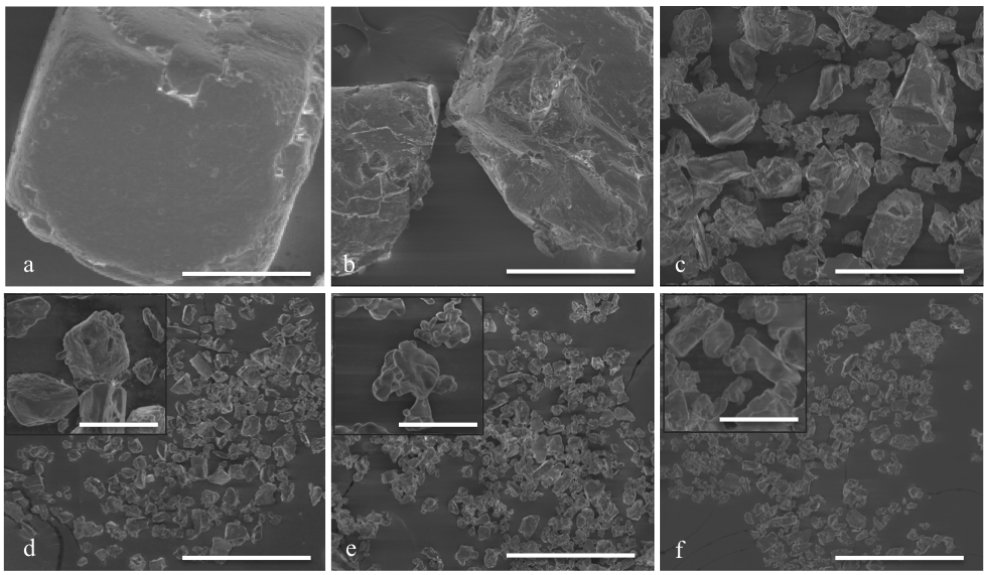

Figure 7.3: Increasing the planetary ball-milling time reduces the particle size and size distribution. SEM images of NaCl (a) as-received, and NaCl ball-milled at 400 *rpm* for: (b) 1 *min*, (c) 5 *min*, (d) 30 *min*, (e) 60 *min* and (f) 90 *min*. The inset scale bars are 0.025 *mm*; all other scale bars are 0.20 *mm*.

toward distal targets. Thus, 0.017 *mm* diameter NaCl particles were sufficiently small to produce PCL tubes for scaffold fabrication.

7.4.2 Salt-leached PCL microstructural analysis

As described in the previous section, 0.017 *mm* NaCl was selected as the porogen size to introduce porosity in PCL. The volume fraction of 0.017 *mm* NaCl porogen was varied between 0 and 70 *vol*% to form PCL films. Above 70 *vol*% NaCl, the samples were fragile and difficult to handle and therefore not characterized. SEM was used to assess the pore morphology and to determine if the NaCl was uniformly distributed. The fracture surface of a 100% solvent cast PCL exhibited no porosity (Fig. 7.4), which was in agreement with previous reports [97, 147]. Though it may be assumed that the absence of NaCl porogen would produce dense films, bubbles, voids, or other defects may have formed; however, image in Fig. 7.4 confirms that the PCL was 100% dense. Because one of the goals of this work was to reduce the PCL elastic modulus,

the highest *vol*% porosity (70%) was the focus and therefore this composition is used hereafter unless otherwise specified. SEM analysis was conducted on PCL before and after removal of the 0.017 *mm* NaCl porogen (NaCl ball-milled at 400 *rpm* for 60 *min*) (Fig. 7.5). Prior to salt-leaching, the NaCl particles (Fig. 7.5(a),(c)) consisted of cuboidal or faceted NaCl particles embedded in PCL. After salt-leaching and removal of NaCl, pores with sizes and geometries similar to the NaCl particles were generated (Fig. 7.5(b),(d)). Additional observations were made. First, the cuboidal or faceted NaCl particles in Figs. 7.5(a) and 7.5(c) did not resemble the irregular NaCl particle surfaces observed after 60 *min* of PBM at 400 *rpm* (Fig. 7.3(e)). It is possible that the NaCl/PCL monomer solution partially etched the NaCl particles resulting in a change in morphology from irregular before casting to cuboidal after casting. To investigate this, NaCl particles were exposed to chloroform and methanol with no PCL monomer present. The NaCl particles maintained their irregular shape in both cases (data not shown); thus, the presence of PCL monomer is believed to cause partial etching resulting in smooth and faceted surfaces. Further work is required to better understand this phenomenon. Second, in addition to the porosity created by the NaCl particles, a second smaller scale of porosity was apparent (Fig. 7.5). Because the smaller pores were apparent before salt-leaching (Fig. 7.5(a),(c)), they are considered intrinsic; to be distinguished from salt-leached porosity. Lin *et al.* [97] also observed similar intrinsic porosity when PEG was used as a porogen. The intrinsic porosity increases the *vol*% porosity and likely reduces the elastic modulus and perhaps enhances cell attachment as discussed below. We believe the intrinsic porosity is a combination of both the volume fraction of porogen (70%) and relatively small porogen particles (0.017 *mm*) that modulates the PCL polymerization process. To support the latter aspect, PCL salt-leached with 0.191 *mm* NaCl was prepared and observed using SEM (Fig. 7.6). The only porosity observed when using 0.191 *mm* NaCl was the porosity introduced using the salt-leaching process. Overall, hi-

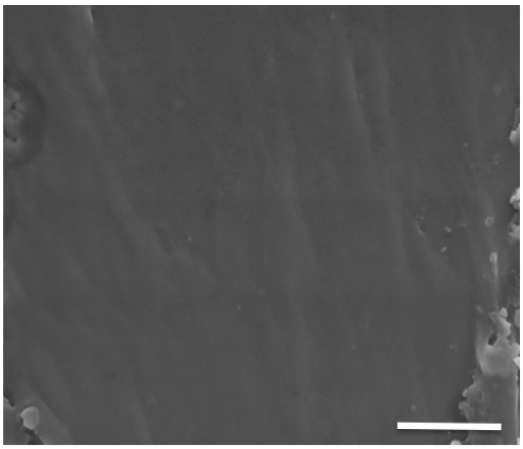

Figure 7.4: SEM analysis of 100% PCL (no porosity). The scale bar is 3 μm.

erarchical porosity was generated; relatively large ∼0.017 mm pores were created by salt-leaching while relatively small intrinsic pores were formed as a byproduct of the modified salt-leaching process described in this work.

7.4.3 Correlating porosity with mechanical properties

Tensile testing was used to measure the elastic modulus and strain to failure. Since the goal was to reduce the elastic modulus of PCL and improve the strain to failure, porosity was introduced using NaCl as a porogen. To characterize the change in the elastic modulus as a function of porosity, PCL films with different densities were used for tensile testing. The elastic moduli of PCL films decreased from 182.1 to 2.09 MPa when the porosity was increased from 0 to 70 $vol\%$ (Fig. 7.7) demonstrating the ability to control the stiffness of PCL by introducing porosity. Eshraghi *et al.* reported an average elastic modulus of 354.1 MPa for 100% solvent cast PCL [44]. However, the study used a higher PCL MW, which likely explains the higher elastic modulus exhibited by the 100% PCL. Another study [141] used a porogen (0.02-0.5 mm porogen sizes) and correlated the compressive modulus of PCL to porosity. The reported modulus of 80 $vol\%$ porous PCL is comparable to the present study. Because one of the goals of this work was to reduce the PCL elastic modulus, the modified salt-

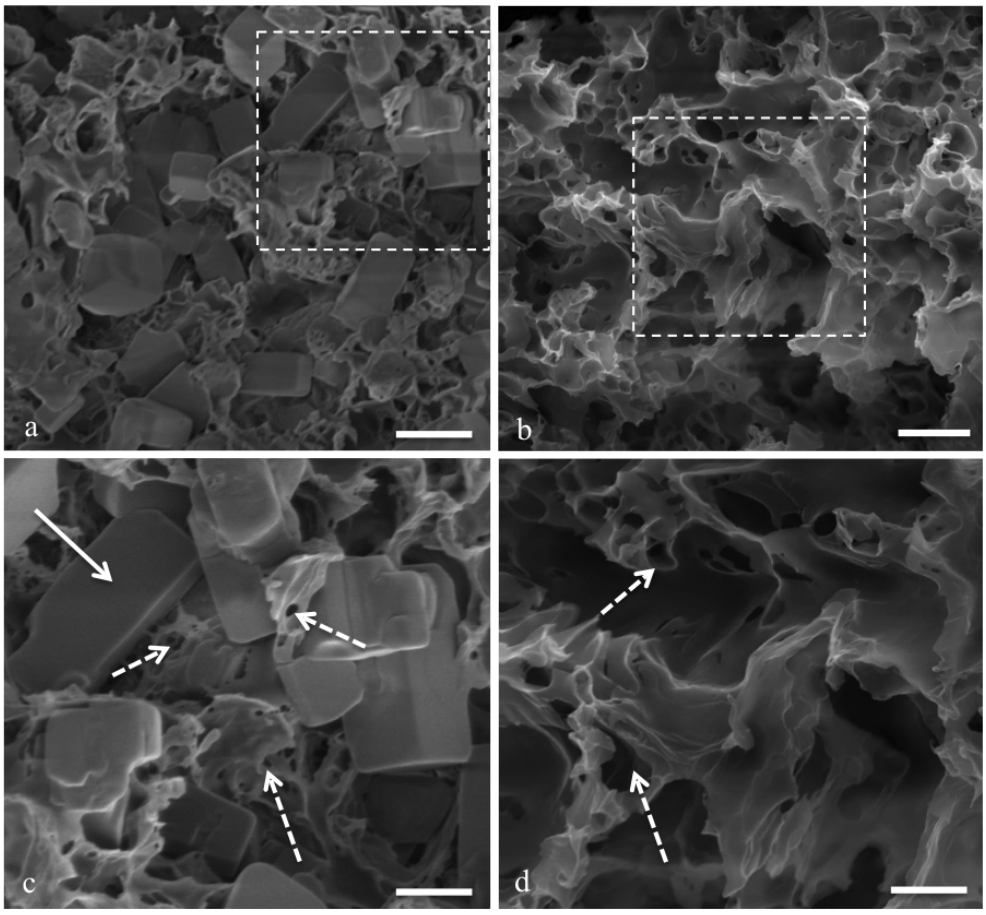

Figure 7.5: SEM analysis before and after salt leaching. A 70 $vol\%$ porosity PCL film fabricated using 17 μm (avg. diameter) NaCl particles (a) prior to and (b) after salt-leaching. (c) and (d) are higher magnification images of the dashed-boxes shown in (a) and (b), respectively. The solid arrow in (c) points to a NaCl particle and the dashed arrows point to PCL. Scale bars in (a) and (b) are 10 μm and in (c) and (d) are 5 μm.

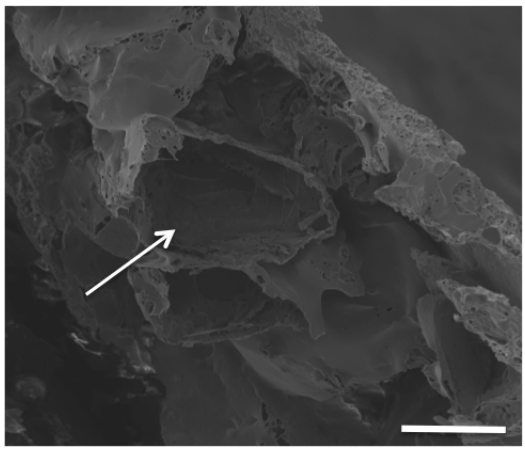

Figure 7.6: SEM analysis of PCL salt leached with 0.191 *mm* NaCl. Cross-sectional SEM image of a 70 *vol*% porosity PCL film fabricated using 0.191 *mm* (avg. diameter) NaCl particles. The black arrow points to a salt-leached pore. The scale bar is 0.1 *mm*.

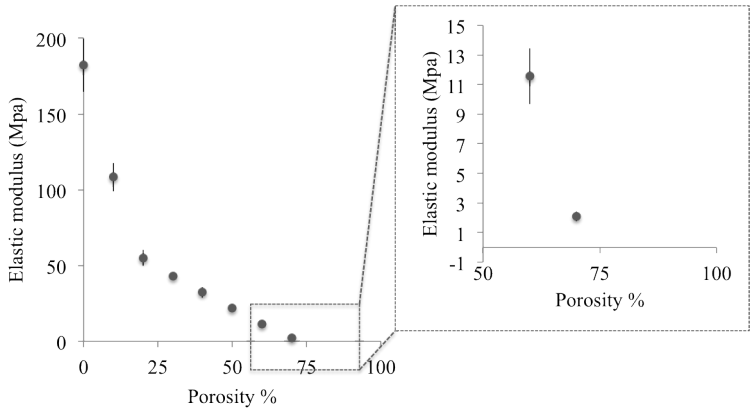

Figure 7.7: The elastic modulus PCL vs. porosity% created by 0.017 *mm* NaCl particles.

leaching process described herein introduces sufficient porosity to reduce the elastic modulus by nearly two orders of magnitude.

7.4.4 Cell attachment

NIH 3T3 fibroblast cells did not attach or survive well on non-porous PCL, but attached to and proliferated on porous PCL (Fig. 7.8). The observed differences are believed to be a result of the increase in surface roughness (as shown in Fig. 7.8(c),(f)) as well as improved wettability. The presence of interconnected porosity

improved the water permeability of the films and likely translated to improved cell attachment and survival. To our knowledge, this is the first report that enhances cell attachment on PCL by optimizing its physical properties. Previous reports have used chemical modifications to enhance cell attachment. For example, a composition of PCL and proteins such as collagen and hyaluronic acid (HA) improved cell attachment [149, 184]. Similarly, when PCL was coated with fibronectin, regardless of its porosity and physical properties, cell attachment and proliferation was observed (Fig. 7.8(e),(h)). However, the improved cell attachment with fibronectin-coating is predicted to be temporary due to the lack of affinity of fibronectin for PCL, while the physical modification of PCL is only effected through its degradation. Overall, it is demonstrated that enhancing surface roughness provided robust cell attachment and proliferation on PCL.

7.4.5 Scaffold characterization

The scaffolds consisted of close-packed arrays of microtubes in which inner channels were separately fabricated and inserted into a larger outer tube as illustrated in Fig. 7.2. Both the inner and outer tubes consisted of 70 $vol\%$ porous salt-leached PCL. This composition was chosen because it had interconnected porosity and the lowest elastic modulus while maintaining mechanical integrity for scaffold fabrication. A representative cross-sectional image of a 2 mm-long PCL scaffold is shown in Fig. 7.9. The inner tubes of the scaffold had a wall thickness of 0.060 ± 0.015 mm and an average inner diameter (ID) of 0.260 mm. The outer tube ID was 1.62 mm with a wall thickness of 0.090 mm occupying an outer diameter (OD) of 1.80 mm. The ID of the inner tubes was selected as 0.20-0.30 mm since linear axon growth was previously demonstrated in micro-channel scaffolds with 0.20 mm-diameter channels [55, 65, 158]. In addition, the PCL scaffold was designed to have an OD of 1.8 mm to fit in the T3 rat spinal column. The scaffolds had 60% open volume as compared

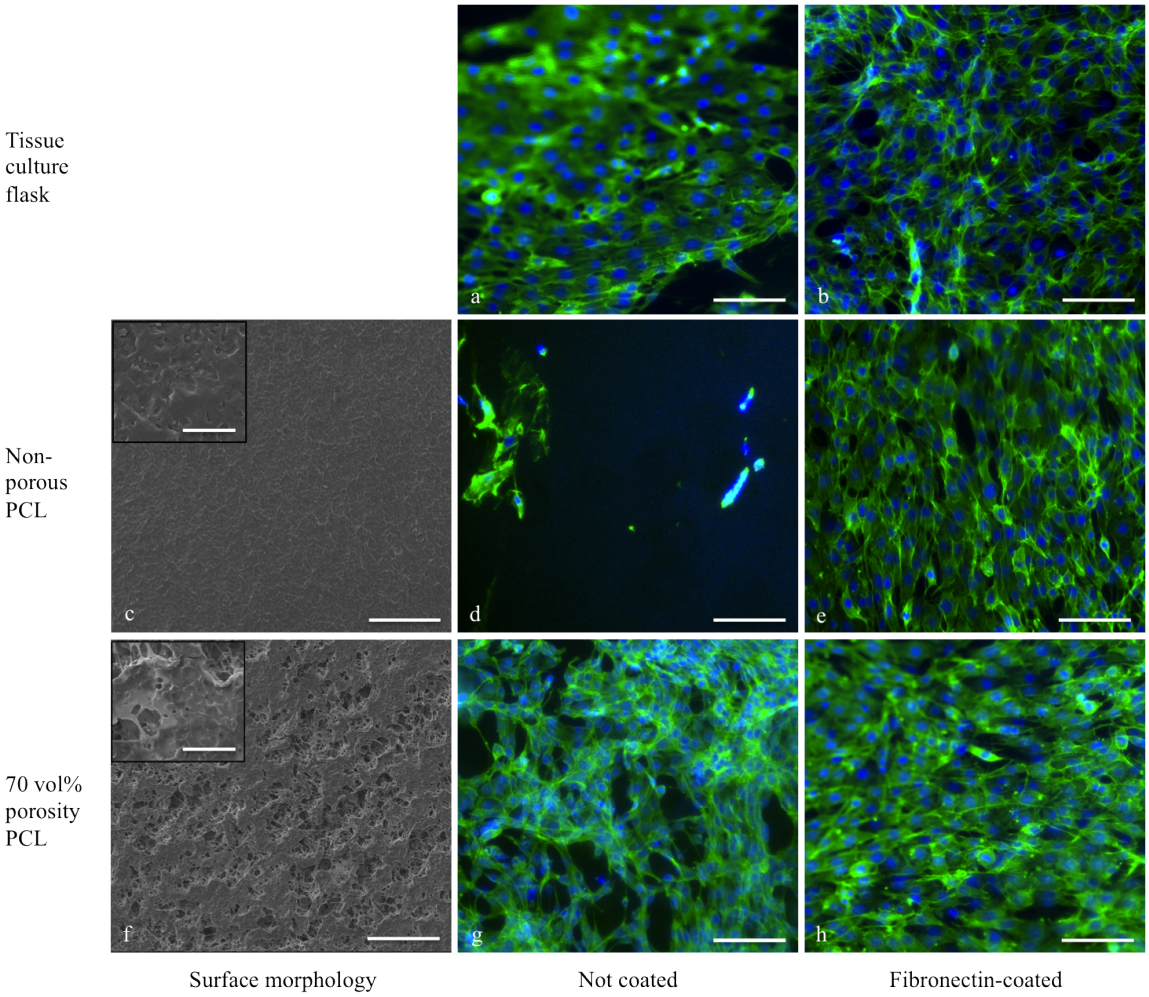

Figure 7.8: Cell attachment and proliferation on PCL is improved by introducing porosity and by fibronectin-coating. NIH 3T3 fibroblasts were cultured on (a) uncoated and (b) coated tissue-culture treated flask as controls, (d) uncoated non-porous PCL film, (e) fibronectin coated non-porous PCL film, (g) uncoated 30 $vol\%$ porous PCL film, and (h) fibronectin-coated 70 $vol\%$ porosity PCL film. Cells were fixed after 72 hr and stained for actin (green) and nuclei (blue). Unlike non-porous PCL, 70 $vol\%$ porosity PCL films provided cell attachment and proliferation comparable to the positive control. Both groups exhibited cell attachment and proliferation after fibronectin coating. SEM images of the top surface of (c) non-porous PCL film and (f) 70 $vol\%$ porosity PCL with corresponding magnified images demonstrate an increased surface roughness in porous PCL. Scale bars in the magnified boxes in (c) and (f) are 0.01 mm. All other scale bars are 0.1 mm.

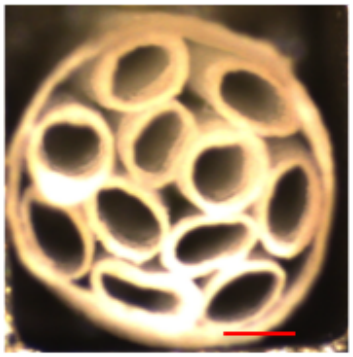

Figure 7.9: Optical image of a PCL scaffold. Microtube inner diameter is 0.260 mm, salt-leached (0.017 mm NaCl), 70 $vol\%$ porosity PCL walls were 0.060 mm thick. Scale bar is 0.2 mm..

to $< 45\%$ open volume provided by state-of-the-art scaffolds.

To characterize the porosity of the tubes and to confirm interconnected porosity, SEM images of the inner surface, cross-section and outer surface of the inner PCL tubes were taken (Fig. 7.10). Interconnected porosity with average pore size of 0.017 mm was observed. The interconnected porosity could allow the transport of nutrients, oxygen and waste in the nerve tissue and may be important for nerve growth. In addition, the scale of the porosity is believed to be sufficiently small to prevent axonal growth orthogonal to the microtubes. Few studies successfully fabricated micro-channel scaffolds with ideal wall porosity; nevertheless, the scaffolds had less than 45% open volume [55, 116, 130, 137, 158, 172]. The scaffolds described in this work have more than 60% open volume and do not allow the axons to cross through the scaffold walls of the scaffold. In addition, since the NaCl particles used during scaffold fabrication were 0.017 mm in diameter, tubes with a wall thickness of about 0.020 mm were fabricated. Therefore, using the microtubes with a wall thickness of 0.020 mm can produce scaffolds with 85% open volume, which is a significant improvement compared to previously described nerve guidance scaffolds.

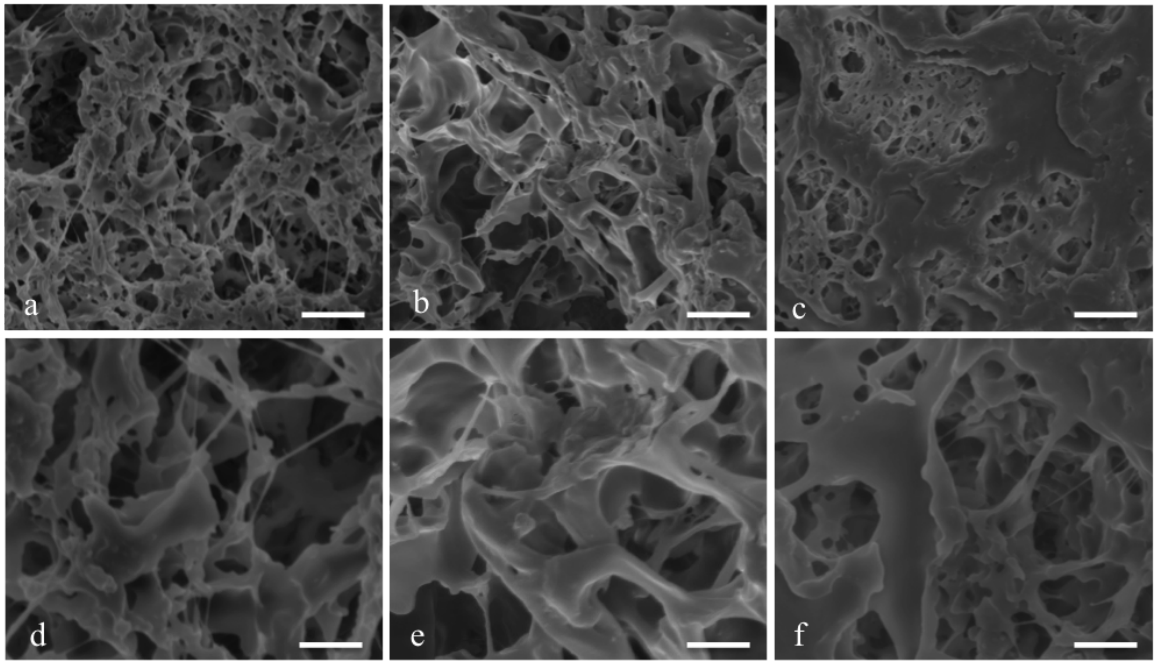

Figure 7.10: Interconnected porosity is maintained through the wall of the tubes. (a) shows the inner surface (b) the cross-section and (c) the outer surface of a PCL tube. Images in (d), (e) and (f) are the x2 magnifications of (a), (b) and (c), respectively. Scale bars in (a), (b), (c) are 5 μm and in (d), (e) and (f) are 2.5 μm.

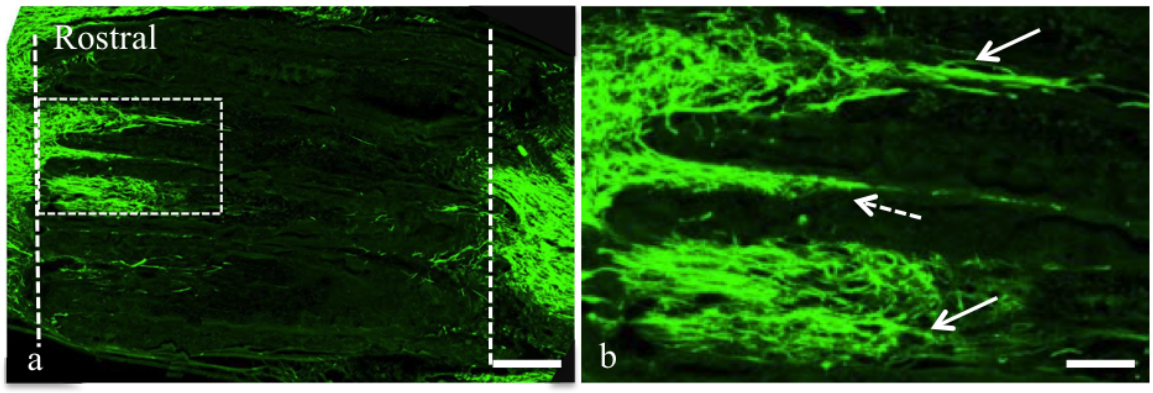

Figure 7.11: Axons grow into PCL scaffolds after implantation in T3 complete transection. PCL scaffold is shown 4 weeks post-implantation by immunolabeling neurofilaments (green). (a) Scaffold interfaces with host are indicated by dashed lines. (b) Higher magnification of boxed region in (a) demonstrate axonal growth into scaffold and linear growth pattern. Solid arrows in (b) demonstrate the axons grow linearly inside the microtubes while the dashed arrow indicate some axons grow linearly in between the microtubes. The scale bar in (a) is 0.3 *mm* and in (b) is 0.1 *mm*.

7.4.6 *In vivo* characterization

PCL scaffolds (2 *mm* long) were implanted in the T3 rat transected spinal cords for 4 weeks and analyzed by histology. Sections parallel to the longitudinal axis of the spinal cord were sliced and immunostained for neurofilaments. Since no growth factor was introduced in the lesion, high density axon growth was not expected [158]. Nonetheless, neurofilament-labeled axons grew into the scaffold and extended linearly through the scaffold for distances up to 0.7 *mm* (Fig. 7.11). In addition, axons grew both inside and between the inner tubes (Fig. 7.11(b)) demonstrating that the entire open volume of the scaffold (including the space between the inner tubes) is effectively available for nerve growth. The scaffold was present after 4 weeks of *in vivo* and had not yet degraded.

Microchannel scaffolds are a promising approach to treat spinal cord injuries. However, existing scaffold technologies require further refinement to establish clini-

cal relevance. In this study, novel materials processing and scaffold fabrication approaches were investigated to develop nerve guidance scaffolds exhibiting an unprecedented combination of features. First, this study leverages previous efforts to develop microchannel scaffolds, but with an emphasis on increasing lumen volume compared to state-of-the-art technology. Herein, a process was developed to fabricate scaffolds with a unique architecture to enable high lumen volume. Rather than fabricate arrays of microchannels in one step, this process entails the fabrication of individual thin wall tubes that were assembled into close-packed arrays (Fig. 7.2). This fabrication approach created additional interstitial volume between the microtubes that is equally capable of linearly guiding axons toward distal targets. Second, the novel scaffold manufacturing process provided the impetus to develop alternative materials to enable the fabrication of individual, thin-wall tubes. Hydrogels in general, do not exhibit adequate mechanical properties and are not compatible with this process. Hence, PCL was selected owing to its higher stiffness and strength. In annealed (melting and cooling) form, however, PCL was too brittle during implantation. To improve the handling of PCL and increase its strain to failure, PCL was solvent-cast. Porosity was also introduced via a modified salt-leaching process to allow the transport of nutrition, waste and oxygen through the walls. By controlling the mechanical properties, individual 0.060 mm thick PCL microtubes with few centimeter lengths could be fabricated, cut to desired lengths and integrated into 60% open volume scaffolds (Fig. 7.9). Third, the porosity that was introduced in PCL enhanced cell attachment. Achieving cell attachment demonstrates another significant benefit of salt-leached PCL over most hydrogel-based scaffolds that do not inherently allow cell attachment.

When characterized *in vivo* for 4 weeks, the microtube PCL scaffolds maintained integrity and demonstrated the ability to linearly guide axons. It is expected that, in the presence of growth factors, the axon growth rate and density will be much

higher. Overall, this work presents a degradable biocompatible scaffold with 60% lumen volume that linearly guides axons in the transected rat spinal cords. Future work will focus on incorporating growth factors and characterizing biocompatibility and degradation.

7.5 Conclusion

The pore size and pore size distribution of PCL is controlled by using a modified salt-leaching technique and optimizing the porogen size and distribution using planetary ball-milling. By increasing the volume fraction of porosity, the elastic modulus of PCL was reduced from 182.1 to 2.09 MPa and the strain to failure was improved from 17% to 100%. In addition, porous PCL exhibited a significant improvement in cell attachment and cell proliferation compared to non-porous PCL, perhaps due to enhanced surface roughness and wettability. To create nerve guidance scaffolds, porous PCL microchannel scaffolds were fabricated consisting of 0.06 mm wall thickness, 0.260 mm inner diameter microtubes and 60% open volume. In addition, the scaffold length could be increased from the mm-scale to clinically-relevant cm-long scaffolds. The scaffold *in vivo* performance was studied in a rat T3 full-transection spinal cord model. Linear growth of axons was observed through both the microtubes interior as well as in the interstitial space in between the microtubes, demonstrating that the entire 60% open volume of the scaffold can be effectively used for nerve growth and linear guidance. Also the scaffold was not degraded after 4 weeks, which can be beneficial for clinically relevant cm-long nerve gaps that require slower degradation rates. Overall, this work presents a modified salt-leaching process combined with a novel scaffold preparation technique to fabricate high open volume nerve regeneration scaffolds for linear axon growth.

CHAPTER VIII

Further Research and Outlook

8.1 Advancing the scaffold fabrication technology

8.1.1 Translating PCL synthesis and scaffold fabrication technology to other polymers

The purpose of this work was to test and confirm the viability of translating the materials synthesis and scaffold fabrication technique introduced in Chapter VII to other FDA-approved synthetic polymers. Poly lactic-co-glycolic acid (PLGA) is selected as the experimental material owing to 1) its common use in tissue engineering [62, 121, 167, 169, 172], and 2) its higher degradation rate compared to poly caprolactone (PCL) [21, 143]. With modifications to the methods described in Chapter VII, PLGA films with porosity% between 0-90% were fabricated. Scanning electron microscopy (SEM) images of the PLGA fracture surfaces showed the consistent increase in the porosity as the PLGA porosity $vol\%$ was increased. Interconnected porosity was observed at and below 30 $vol\%$ porosity. In addition, similar to PCL films, the elastic modulus of PLGA films decreased by increasing porosity. Cell attachment studies using primary rat Schwann cells indicated that PLGA provided cell attachment when porous and fibronectin-coated. Finally PLGA tubes with inner diameters of $300 \pm 10\ \mu m$ were produced and fabricated into microchannel scaffolds.

The SEM images of PLGA films fractured in liquid N_2 with different porosity $vol\%$ are shown in Fig. 8.1. As expected, a consistent increase with porosity was observed by decreasing PLGA $vol\%$. In addition, interconnected porosity is observed when the porosity $vol\%$ is less than or equal to 30%. Consequently, increasing porosity $vol\%$ was expected to reduce the elastic modulus of the films. Indeed, the PLGA elastic modulus decreased from 465.7 MPa to 14.8 MPa when the porosity increased from 0% to 70 $vol\%$ (Fig. 8.2).

To understand the cell adhesion properties of PLGA, primary rat Schwann cells were cultured on 1) tissue culture-treated well-plate coated with poly-D-lysine (PDL) as positive control (a surface that allows Schwann cell attachment), 2) 70 $vol\%$ porosity PLGA and 3) non-porous PLGA (Fig. 8.3). The affect of laminin or fibronectin coating was also studied by coating the substrates with 1 mg/ml of the protein for 18 hr. It was observed that fibronectin coating provided more cell attachment compared to laminin-coating for both control and porous PLGA. Non-porous PLGA, regardless of coating, exhibited no cell survival or attachment. It was concluded that PLGA allowed Schwann cell attachment when both porous and fibronectin-coated.

PLGA inner tubes (70 $vol\%$ porosity) with inner diameters of 300 $\pm$ 10 μm were used to fabricate tubes. The PLGA tubes were inserted into a 70 $vol\%$ PCL outer tube (described in Chapter VII) with an inner diameter of 1.60 mm (Fig. 8.4). PCL was used as the outer tube instead of PLGA owing to its slower degradation rate relative to PLGA [21, 143]. A slower degrading outer tube was desired since the outer tube stabilizes the structure of the scaffold. Therefore, the PCL outer tube is predicted to degrade after PLGA inner tubes *in vivo* thus securing the PLGA tubes in the tissue until they degrade.

PLGA scaffolds were implanted in the transected spinal cords of rats for 1 month. Preliminary data confirmed the biocompatibility of the scaffolds and some axon penetration into the scaffold. However, the scaffold design should be optimized to increase

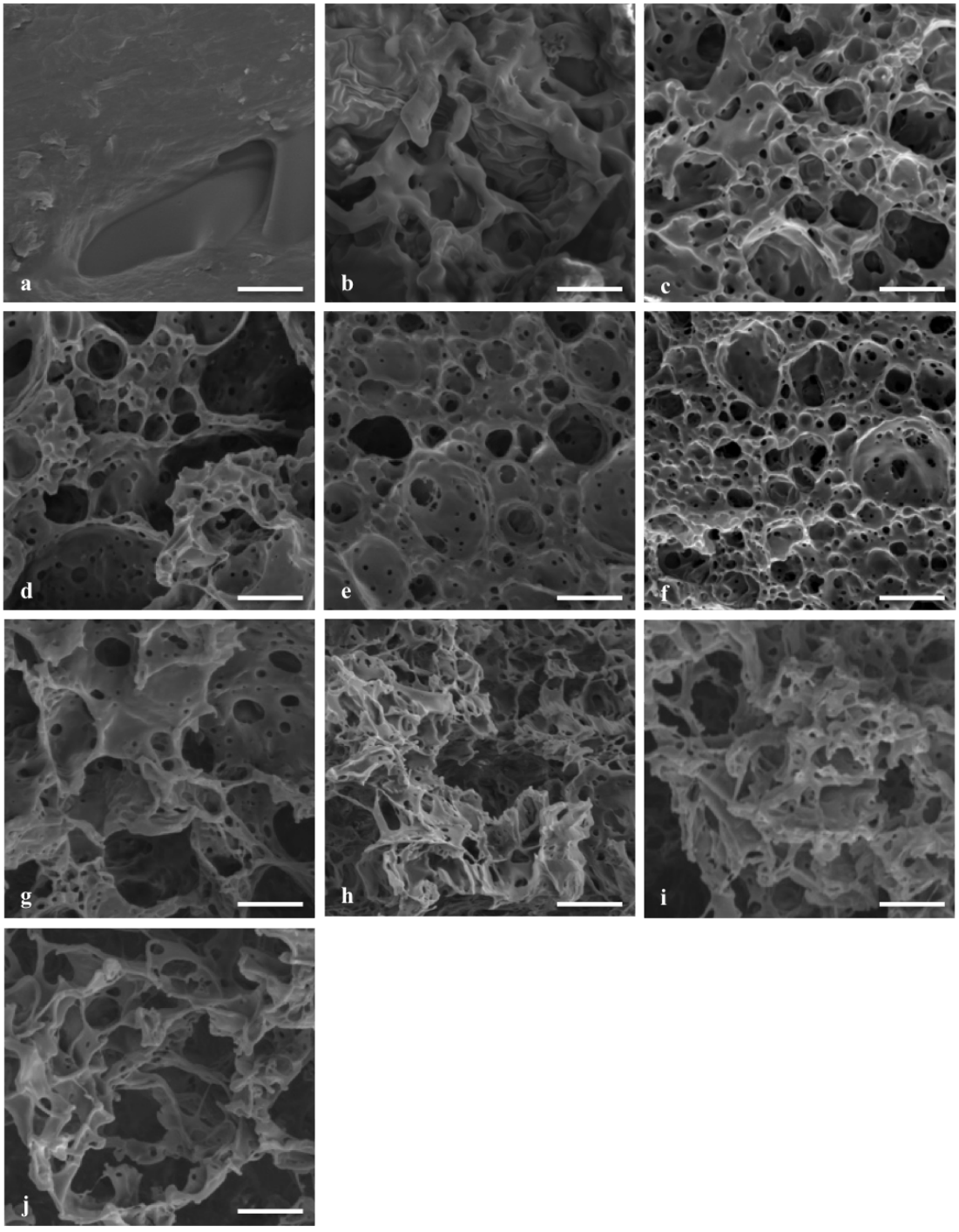

Figure 8.1: SEM images of PLGA fracture surface with porosity% of 0%, 10%, 20% to 90% are shown in (a), (b), (c) through (j), respectively. By reducing the PLGA $vol\%$ (thus increasing porosity $vol\%$), the morphology changes from a non-porous structure (0% porosity shown in (a)) to porous structures. Scale bars are 5 μm.

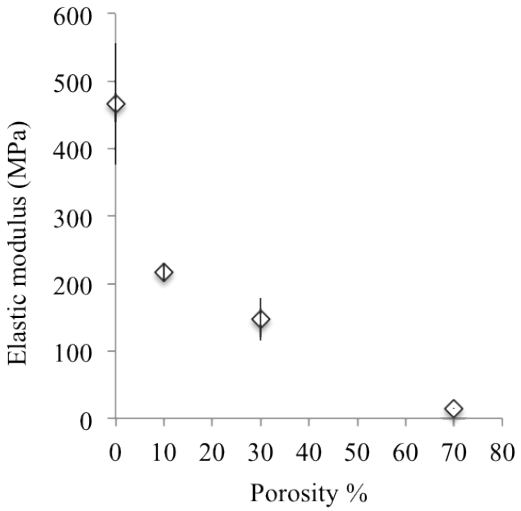

Figure 8.2: The elastic modulus of PLGA decreases by increasing porosity.

the number of inner tubes and avoid their movement *in vivo*. In addition, further *in vivo* characterization is necessary before conclusions can be drawn. For example, the degradation of the scaffolds can be assessed by implanting the scaffolds for a longer time period such as 4 months.

8.1.2 Microchannel scaffold technology for clinical translation

To translate the microchannel scaffold technology to clinical translation, it is essential to develop scaffolds with clinically-relevant dimensions. More specifically, few mm-wide scaffolds are desired since a human spinal cord diameter varies from 15 mm to 6.2 mm while continuously decreasing from cervical to lumbar region [41], and the length of the injury is 1-2 vertebra (> 10 mm). In addition, prior to human clinical trials, it is advantageous to test the nerve guidance scaffolds (NGS) in a large animal model (relative to rodents) such as a minipig. The goal of this study, therefore, was to confirm that few mm-long and wide PCL microchannel scaffolds can be manufactured. The PCL technology introduced in Chapter VII was advanced to scaffolds with sizes matching the sciatic nerve of a minipig and tested *in vivo*.

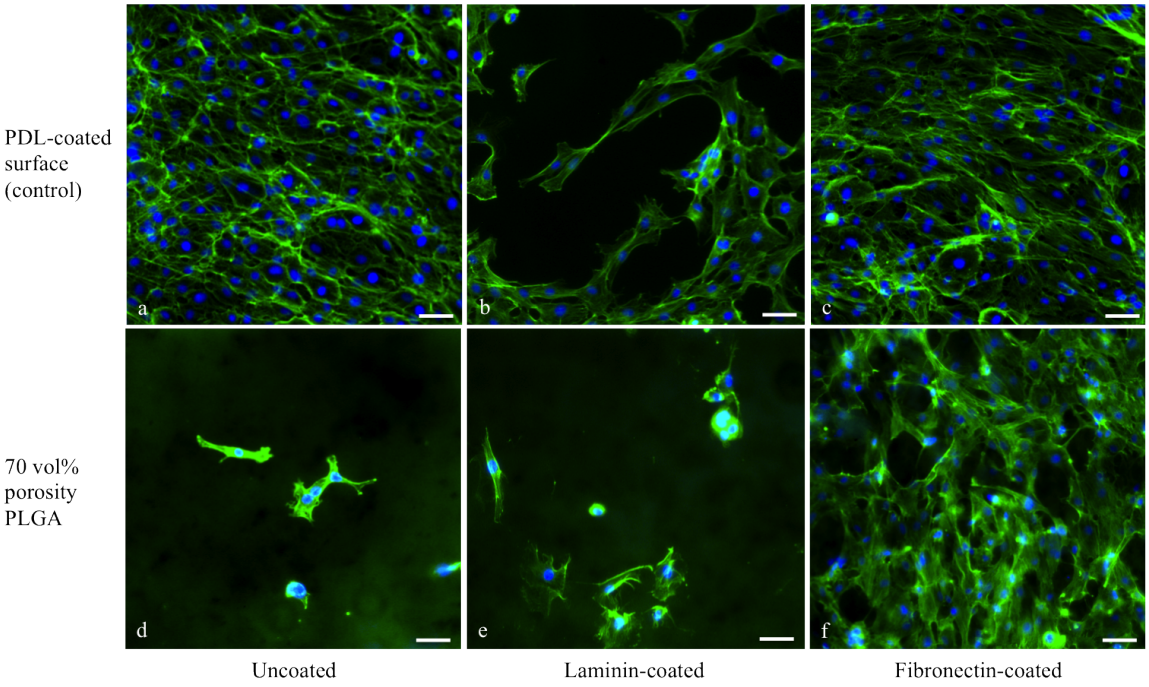

Figure 8.3: Cell attachment and proliferation on PLGA is improved when 1) porous and 2) fibronectin-coated. Primary rat Schwann cells were cultured on (a) uncoated, (b) laminin-coated and (c) fibronectin-coated PDL-coated surfaces as controls. Cells were also cultured on (d) uncoated, (e) laminin-coated and (f) fibronectin-coated 70 $vol\%$ porous PLGA, and also on non-porous PLGA (data not shown). Cells were fixed after 48 hr and stained for actin (green) and nuclei (blue). Porous PLGA film provided cell attachment and proliferation comparable to the positive control when coated with fibronectin while non-porous PLGA exhibited no cell survival or attachment regardless of the coating substance. Scale bars 50 μm.

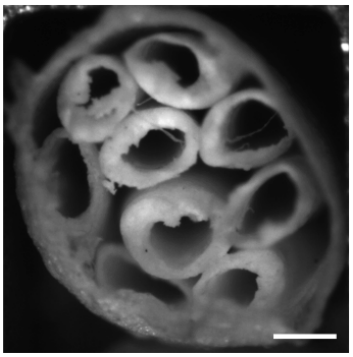

Figure 8.4: A cross-sectional image of a PLGA scaffold with PLGA inner tubes inserted inside a PCL outer tube. The scale bar is 300 μm.

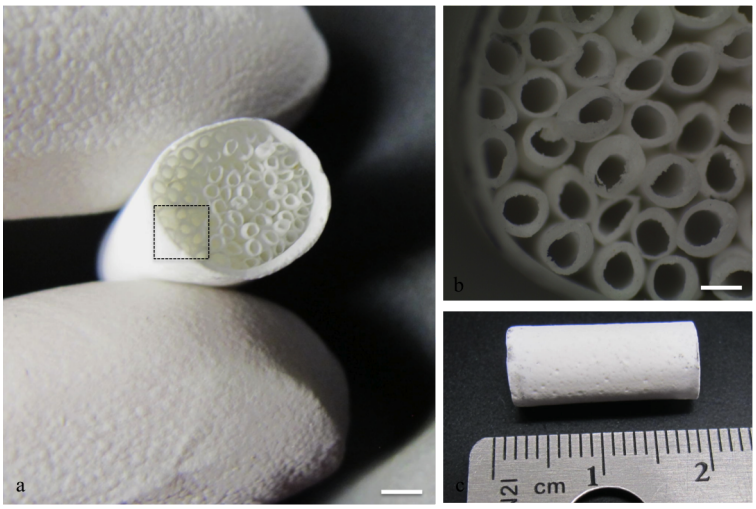

Figure 8.5: PCL microchannel scaffold. The boxed region in (a) is magnified in (b), and shows the scaffold microchannel architecture. (b) is the longitudinal view of the scaffold. The scale bar in (a) is 2 *mm* and in (b) is 0.5 *mm*.

A total of 79 PCL inner tubes with an average inner diameter of 0.47 *mm* were inserted inside a PCL conduit with an inner diameter of 7.6 *mm* and an outer diameter of 8.0 *mm* (Fig. 8.5). The inner tubes were 10 *mm* in length and the outer conduit had 1 *mm*-long overhangs on each end to allow suturing to the nerve stumps. The scaffold was implanted in the sciatic nerve gap of a minipig for 4 months and preliminary sensory functional recovery was observed. The developed PCL microchannel scaffold is therefore a promising approach for advancing nerve guidance scaffold technology to human translation.

8.2 Criteria for a microchannel scaffold

The goal of this doctoral work was to select and synthesize a material and fabricate it into a scaffold that could linearly guide axons through nerve gaps. Throughout the work, several criteria and materials/scaffold properties proved to be of particular significance when developing a scaffold and are divided into three tasks: 1) materials processing and optimization, 2) scaffold design and fabrication, and 3) *in vivo* efficacy. Each task is discussed below.

8.2.1 Material selection and synthesis

When selecting and synthesizing a material for nerve regeneration, the main properties that needed to be characterized and optimized are thought to be biocompatibility, degradation, porosity, stiffness, strength, and cell attachment properties. Most of these properties should be first evaluated *in vitro* and then *in vivo*. First, a material biocompatible to the nerve tissue has to be selected/synthesized. Initial experiments include *in vitro* cytotoxicity assays followed by *in vivo* characterization explained in section 8.2.3. Second, the scaffold material would be selected/synthesized to degrade after the axons have bridged the nerve gap. Moreover, depending on the degradation mechanism, nerve repair may be more affective if the implant degrades over time and not all at once. As an example, since the byproducts of PLGA are acidic and can be detrimental to the nerve tissue [60], a gradual degradation can reduce pH change and lower its negative effects on the tissue. Next, fabricating a porous scaffold is important to allow the transfer of nutrients, oxygen and waste but prohibit the penetration of axons in between channel walls. In addition, the mechanical properties of the material are of particular importance and interest and are discussed in length in section 8.3. Lastly, it may be beneficial for the material to provide cell attachment. Neuron cell survival and proliferation may be improved upon attachment to the scaffold; however, the material may also become a suitable substrate for inflammatory cells such as fibroblasts to migrate on and form scar tissues. Thus, it is ideal to control cell attachment on the scaffold material and understand its effect on nerve repair.

8.2.2 Scaffold design and fabrication

A nerve guidance scaffold should consist of linear channels to effectively guide growing axons through the lesion gap while maintaining their organization. In addition, since axons generally grow in bundles, the channel diameter should be large enough for a nerve bundle to grow into but it should be small enough to avoid the

turning of the axons. Unpublished work has demonstrated that axons generally deviate from a linear path and no longer grow toward the distal end of the nerve gap when the channel diameter of a scaffold is more than 300 μm. Subsequently, a channel diameter of 200-300 μm was targeted in this work. Lastly, for the translational application of the scaffolds, clinically-relevant cm-wide and cm-long scaffolds should be fabricated.

8.2.3 *In vivo* evaluation

Although *in vitro* characterization provides a valuable understanding of a material and a scaffold, *in vivo* characterization can suggest the efficacy of scaffolds for nerve repair. For example, once cytotoxicity assays eliminate materials with high toxicity, *in vivo* evaluations such as nissl staining and immunolabeling for inflammatory cells provide a better understanding of the biocompatibility of the material. Similar to biocompatibility, the degradation of a material can be significantly different from *in vitro* to *in vivo* as demonstrated in Chapter III. Axon growth, supporting neural cell presence and capillary formation are important steps in evaluating the *in vivo* efficacy of the material. More *in vivo* characterization methods are suggested in section 8.5.

8.3 The dogma of "softer is better"

In tissue engineering, it is often believed that an ideal implant should match the stiffness of the tissue. However, there is no concrete evidence to support that softer substrates are more effective for spinal cord repair. This work is the first study that compared the *in vivo* performance of microchannel scaffolds fabricated from multiple soft hydrogels versus rigid polymers in transected spinal cords. It was observed that the growth of axons toward and in close proximity to a nerve guidance scaffold was significantly enhanced in rats transected spinal cords when the scaffold substrate changed from soft hydrogels to rigid polymers. This doctoral work is, therefore, the

first report that suggests against the dogma of "softer is better", in the context of spinal cord repair.

Previous studies have focused on the *in vitro* understanding of axon growth with the change in substrate stiffness. For example, multiple reports studied the change in the rate of neurite extension of soft hydrogels with elastic moduli varying from 0.5-2.1 kPa and discovered that the softest gel provided a higher rate of neurite extension while negligable attachment was observed on stiffer materials [6, 58, 88, 99]. In addition, when substrates with elastic modulus of 0.1-40 kPa were tested, only substrates with 0.1-1 kPa elastic modulus provided the differentiation of stem cells to neurons [43]. Lastly, when the adhesion of cortical neuronal cells did not significantly differ on substrates with stiffnesses of 0.25-2.1 kPa, the observation was reported as a "surprise" [58]. Overall, *in vitro* works on understanding the relationship between substrate stiffness and axon growth reinforce the belief that "softer is better" while *in vivo* evidence is missing from the literature.

In this work, the effect of substrate stiffness on axon growth *in vivo* was tested by comparing axon penetration and growth on materials with different stiffness in spinal cords of rats. Nerve guidance scaffolds were fabricated from multiple soft hydrogels and rigid polymers. Experimented hydrogels included agarose, alginate, chitosan and PEGDA and rigid polymers were PCL and PLGA. The elastic moduli varied from 30.6 kPa to 14800 kPa as summarized in Table 8.1. The materials were fabricated into microchannel scaffolds and implanted in rats transected spinal cords. Fig. 8.6 shows the comparison of axon behavior with each scaffold. A reactive cell layer generally separated axons from soft hydrogels and axons did not grow toward or in close proximity to the material (Fig. 8.6(a)-(d)). However, no scar tissue was detected between axons and rigid polymers and, unlike what has been observed *in vitro*, axons grew on the these rigid substrates *in vivo* (Fig. 8.6(e),(f)). These results suggest that the formation of a reactive cell layer is significantly reduced from hydrogels to rigid

polymers while axon attachment occurs on rigid materials *in vivo*.

Substrate	Elastic modulus (kPa)
Agarose hydrogel (3 $wt.\%$)	310
Alginate hydrogel (3 $wt.\%$)	*388
Dense chitosan	*603
PEGDA hydrogel (10 $wt.\%$)	30.6
PCL (70 $vol\%$ porosity)	2,100
PLGA (70 $vol\%$ porosity)	14,800

Table 8.1: The table summarizes the elastic modulus of the scaffold materials used through the dissertation. The elastic modulus of alginate is calculated from its shear modulus of 155.3 kPa obtained in Chapter III assuming a poisson's value of 0.25. *Alginate and chitosan degrade within weeks in the spinal cord, which effectively results in lower stiffness than what is shown.

It is acknowledged that the present study is not a side-by-side comparison of the affect of stiffness on *in vivo* axon behavior since the modulus is not the only variable that changes between each material. Indeed, it may be challenging to synthesize substrates with all properties, except for the stiffness, the same. For example, when the stiffness changes, properties such as chemical structure, morphology, pH, degradation, strain to failure and/or swelling may change. The purpose of this study was to test how *in vivo* axon growth changes from a soft hydrogel to a rigid material. Unlike the common belief, however, it was discovered that rigid materials were more effective for axon growth and induced less reactive cell layer formation.

Much research solely focuses on natural biomaterials for the prime reason of using soft substrates to better match the stiffness of the tissue. The results of this dissertation suggest that a softer substrate may *not* necessarily provide more effective spinal cord repair. It is therefore encouraged to expand the pool of materials choice to all level of stiffness to not miss on valuable opportunities for better understanding axon behavior and ultimately finding a cure for spinal cord and peripheral nerve injuries.

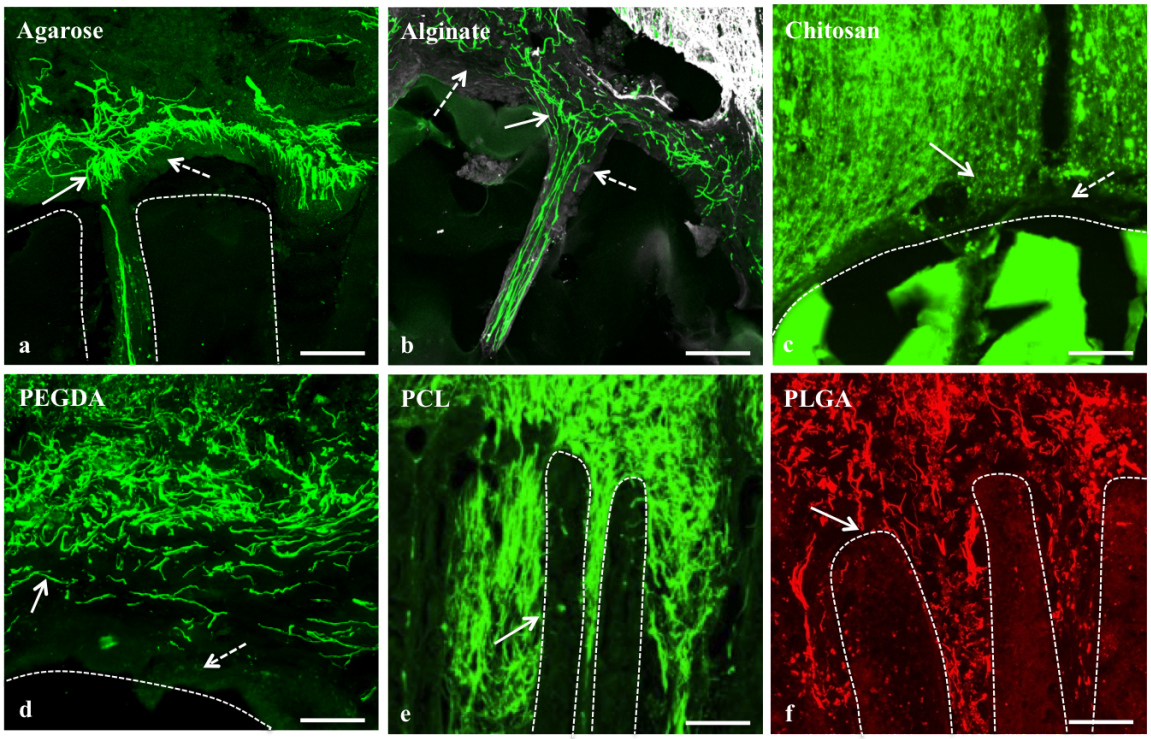

Figure 8.6: *In vivo* evidence averse to the dogma of "softer is better" for spinal cord repair. Microchannel scaffolds fabricated from (a) agarose, (b) alginate, (c) chitosan, (d) PEGDA, (e) PCL and (f) PLGA implanted in transected spinal cords of rats and stained for neurofilaments after 2 weeks for alginate and 4 weeks for all the other scaffolds. Axons are shown in green from (a)-(e) and red in (f) pointed to by solid arrows. The dashed lines indicate the boundary of the scaffold walls. Since alginate scaffold had degraded when sectioning was performed, it was difficult to point to its original location; thus, a dashed line is not shown. As images (a)-(d) demonstrate, the axons do not grow in close proximity to the foreign substrate and a reactive cell layer (pointed to by dashed arrows) often forms between the axons and the hydrogel scaffolds walls. However, axons grew toward and in close proximity to PCL and PLGA. The scale bars in (a) and (b) are 100 μm, in (c) 120 μm, in (d) and (e) are 80 μm and in (f) is 100 μm.

8.4 Conclusions

An interventional approach to linearly guide axons through lesion gaps can significantly help develop a cure for traumatic large-lesion nerve injuries. In this work, materials with different stiffness ranging from 30 kPa to 14800 kPa were synthesized, characterized and developed into microchannel scaffolds and their *in vivo* efficacy was investigated in transected central and peripheral nerves of animals. Among these materials, rigid polymers such as PCL appeared to be the most effective for axon guidance, penetration and integration. A novel technique was investigated to synthesize PCL with optimized porosity, stiffness and cell adhesion properties. Next, using the synthesized PCL as the scaffold material, a unique microchannel scaffold design and fabrication technique was introduced which increased the open volume available by the scaffold by 3 fold compared to state-of-the-art scaffolds. In addition, PCL tubes were kink-resistant and could be sutured to the nerve stumps, which is beneficial for peripheral nerve repair. This dissertation, therefore, introduces a viable nerve guidance scaffold for central and peripheral nerve repair.

8.5 Future work

The microtube scaffold fabrication technique can be optimized to maximize the scaffolds open volume. PCL tubes as thin as 20 μm were produced, which would result in over 85% open volume scaffolds. However, the tube fabrication process was cumbersome, which makes manufacturing scaffolds impractical. Methods to automatize tube fabrication and scaffold assembly can significantly develop the introduced technology. In addition, functionalizing the scaffolds with a drug delivery technique can further stimulate axonal growth. Techniques such as incorporating drug-eluting nanofibers into the scaffold channels may be considered.

Further *in vivo* characterization studies can provide a better understanding of

biocompatibility, degradation and axon regeneration. Immunolabeling for inflammatory cells and/or implanting scaffolds for a longer period can help understand the long-term biocompatibility of the material as well as its degradation behavior. In addition, to confirm axon regeneration (as opposed to the sprouting of intact axons), the source, pathway and termination point of an axon can be confirmed by labeling it with genetically-modified fluorescent markers [173]. Double retrograde tracing can also be used by for example injecting a retrograde tracer into a section of the spinal cord, injuring the section and introducing a different retrograde tracer into the original injection site after sufficient time is given for axon regeneration [102]. Any axon inside or passed the lesion site that exhibits both tracers is a regenerated axon. Finally, studies such as electrophysiology can verify the synapse formation between newly-grown axons and host axons and confirm the efficacy of the scaffolds for axon regeneration and recapitulation. Motor and sensory functional recovery can provide valuable information assuming encouraging immunolabeling and electrophysiology results are observed.

Finally, in this study, a full-transection nerve model was tested, which is considered the most severe case of traumatic nerve injury. Though, a clinically-relevant SCI is generally less severe than a full transection model. Indeed, most human nerve injuries involve the contusion and/or the crush of the nerve in which, unlike in a full transection model, the sprouting of undamaged axons through the lesion is possible [173]. In addition, a fully transected nerve retracts, which enlarges the size of the nerve gap and exacerbates the injury. Therefore, providing axon regeneration in a full transection model is a promising step for clinical translation. It is, however, noted before microchannel scaffolds can be used in partially damaged nerves, the scaffold outer dimension has to match the lesion cavity. A combination of imaging techniques to measure the shape and the dimensions of the injury as well as modifications to the scaffold fabrication technique such as using 3-D printing to fabricate scaffolds with

precise dimensions to mimic the shape of the injury may be necessary.

APPENDICES

APPENDIX A

Chitosan Microchannel Scaffolds for Nerve Repair

A.1 Dense chitosan microchannel scaffolds teste in the rat spinal cords

A.1.1 Overview

In this work, the efficacy of chitosan microchannels for spinal cord repair is assessed. Chitosan was investigated as the scaffold material owing to reported nerve growth *in vivo* [3, 52, 132, 176, 178]. Herein, to reduce the degradation rate of chitosan hydrogel, its porosity was significantly reduced. Dense chitosan films and later scaffolds were produced by expanding the technique introduced in Chapter IV. Briefly, chitosan disks were fabricated by the subsequent drying of chitosan/sodium chloride (NaOH) solution until chitosan disk with a desired height was obtained. The disk was then cross-linked with acetic acid and microdrilled to form microchannel scaffolds. The *in vivo* efficacy of chitosan scaffolds was tested in T3 transected rats spinal cords. The scaffolds fragmented into debris and caused an inflammatory response within 4 weeks of implantation. An alternative technique was therefore needed to improve the biocompatibility of chitosan and reduce its degradation rate.

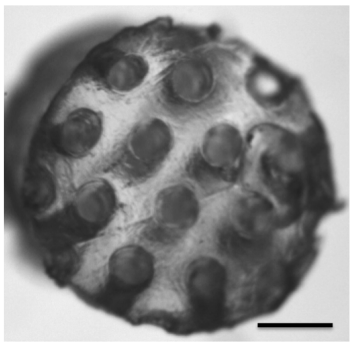

Figure A.1: Image of a dense chitosan microchannel scaffold. The scale bar is 0.5 mm.

A.1.2 Experimental and results

Dense chitosan disks (2 mm-long) were fabricated and microdrilled to produce 1.8 mm-diameter scaffolds with linear channels (Fig. A.1). The channel diameter was 0.20 mm and channel spacing was 0.30 mm. The scaffolds were implanted in the transected T3 rat spinal cords (2 mm-long) and immunolabeled after 4 weeks. Neurofilament staining of the longitudinal section showed the scaffold had fragmented into debris (Fig. A.2). In addition, axons did not penetrate into the lesion possibly due to reactive cell layer (RCL) formation around the scaffold. Moreover, necrosis (unnatural cell death) was observed in the host spinal cord. Overall, 1) the scaffolds degraded too quickly, 2) did not provide appreciable amount of axon growth, and 3) caused inflammatory response. The introduced chitosan scaffolds are therefore not effective for nerve regeneration and modification are needed to address the unfavorable *in vivo* observations.

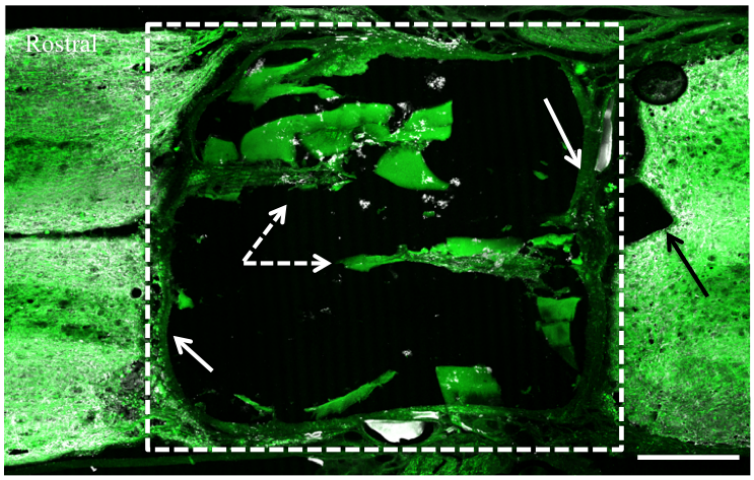

Figure A.2: The longitudinal view of a dense chitosan microchannel scaffold implanted in a T3 transected rat spinal cord stained for neurofilaments (green) 4 weeks post-implantation. The dashed box demonstrates the transected section of the spinal cord. Debris from the scaffold were observed (shown with dashed white arrows). In addition, reactive cell layer is formed around the lesion cavity as pointed by solid white arrows. The necrosis of host spinal cord shown by a solid black arrow was also observed. The scale bar is 0.25 mm.

A.2 Microdrilled agarose scaffolds with chitosan supporting conduits implanted in a pig sciatic nerve

A.2.1 Overview

The goal of this work was to study the efficacy of using supporting conduits around microchannel scaffolds for peripheral nerve repair. Agarose was investigated as the scaffold material since previous reports have demonstrated the efficacy of agarose microchannels in linearly guiding axons [55, 65, 158]. Because the scaffold had to be stabilized in the highly mobile region of sciatic nerve, a supporting conduit was used around the scaffold to be sutured to the nerve stump. Chitosan was selected as the conduit material owing to its common use in tissue engineering [3, 52, 132, 176, 178], flexibility and suture-ability. The scaffolds were tested in a 1 cm-long transected nerve gap in a minipig. Sectioning and immunolabeling 6 weeks post-implantation showed high degree of inflammation and limited axon growth. The agarose/chitosan

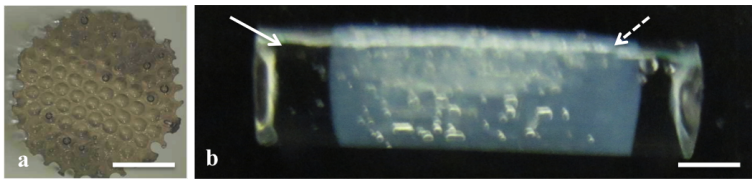

Figure A.3: (a) Cross-section and (b) longitudinal image of a microdrilled agarose scaffold is demonstrated. In (b) the scaffold (pointed to by the dashed arrow) is inserted into a chitosan tube (indicated by a solid arrow). The scale bars are 150 μm in (a) and 200 μm in (b).

hybrid scaffolds were, therefore, determined to be ineffective for nerve repair unless further modifications are made.

A.2.2 Experimental and results

Agarose scaffolds were microdrilled using a technique described in Chapter VI. The scaffolds were 10 mm-long and 4 mm in diameter with an average channel diameter of 0.30 mm and an average channel spacing of 0.085 mm (Fig. A.3). Since agarose tears if sutured, a supporting conduit was needed to secure the scaffold to the nerve stump. Chitosan was investigated for its efficacy as the outer conduit.

To quantify the change in the stiffness of chitosan with the change in its composition, chitosan films with different $mass/surface\ area$ were fabricated and their elastic moduli were measured. Briefly, 4 $wt.\%$ chitosan (MW 140,000-220,000. Sigma; St. Louis, MO) was dissolved in 100 mM NaOH, dehydrated into films overnight and cross-linked with 100 mM acetic acid for 4 hr. The elastic modulus of the films were characterized based on the change in their $mass/surface\ area$. Fig. A.4 shows the elastic modulus increases from 508.1 kPa to 1320.6 kPa for chitosan films with concentrations of 5 g/cm^2 to 15 g/cm^2 ($n = 5$).

Upon characterizing the mechanical properties of chitosan films, chitosan conduits were fabricated. A 4 mm-diameter steel rod was dipped inside the 4 $wt.\%$ chitosan/NaOH solution and dried overnight while spinning horizontally on a rotisserie device. The process was repeated 3 times. The rod was then placed in 100 mM

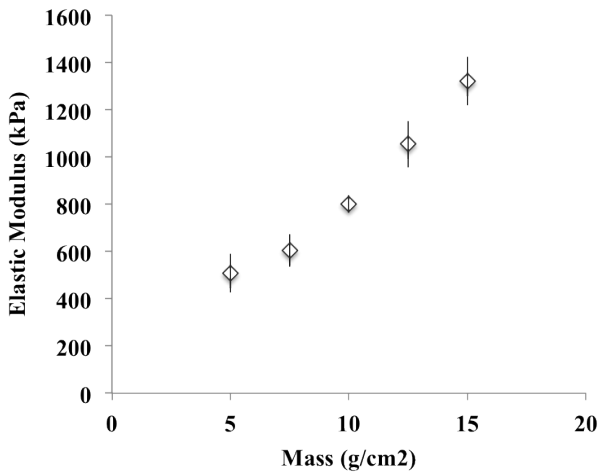

Figure A.4: The elastic modulus of dense chitosan film increases as its $mass/surface\ area$ increases.

acetic acid for 4 hr. Chitosan conduits were removed from the rods, soaked in 2 l of reverse osmosis (RO) water overnight and cut in length to 12 mm using a razor blade.

Agarose scaffolds were inserted into the chitosan conduits (Fig. A.3(b)). Two 4 mm-diameter scaffolds were implanted adjacent to each other in the 8 mm diameter sciatic nerve of a minipig. Due to visible inflammation of the implantation site in the animal and the loss of a toe, the study was pre-maturely terminated 6 weeks post-implantation and the animal was perfused. Sectioning and immunostaining indicated a high degree of scar tissue formation around the scaffold (Fig. A.5). Moreover, immunostaining for neurofilaments did not show any axon penetration. The scaffold design was therefore determined ineffective for nerve repair unless further modifications are made.

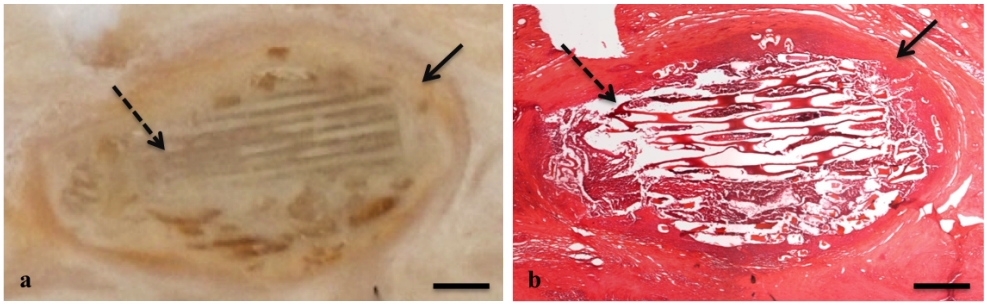

Figure A.5: (a) Optical image and (b) electron microscopy image of the longitudinal view of an agarose scaffold inside a chitosan tube in a 10 mm-long sciatic nerve gap in a minipig. The scaffold (pointed to by the dashed arrows) is surrounded by a scar tissue as indicated by the solid arrows. The scale bars are 0.3 mm.

BIBLIOGRAPHY

BIBLIOGRAPHY

[1] Olivier Alluin, Catherine Wittmann, Tanguy Marqueste, Jean-François Chabas, Stéphane Garcia, Marie-Noëlle Lavaut, Didier Guinard, François Feron, and Patrick Decherchi. Functional recovery after peripheral nerve injury and implantation of a collagen guide. *Biomaterials*, 30(3):363–373, January 2009.

[2] Laura Taylor Alto, Leif A Havton, James M Conner, Edmund R Hollis, II, Armin Blesch, and Mark H Tuszynski. Chemotropic guidance facilitates axonal regeneration and synapse formation after spinal cord injury. *Nature Neuroscience*, 12(9):1106–1113, August 2009.

[3] Q Ao, CK Fung, A Yat-Ping Tsui, S Cai, and HC Zuo. The regeneration of transected sciatic nerves of adult rats using chitosan nerve conduits seeded with bone marrow stromal cell-derived Schwann cells 10.1016/j.biomaterials.2010.09.046 : Biomaterials — ScienceDirect.com. *Biomaterials*, 2011.

[4] S J Archibald, J Shefner, C Krarup, and R D Madison. Monkey median nerve repaired by nerve graft or collagen nerve guide tube. *The Journal of . . .*, 1995.

[5] D Arslantunali, T Dursun, D Yucel, and N Hasirci. Peripheral nerve conduits: technology update. *Medical . . .*, 2014.

[6] AP Balgude, X Yu, A Szymanski, and RV Bellamkonda. Agarose gel stiffness determines rate of DRG neurite extension in 3D cultures. *Biomaterials*, 22(10):1077–1084, 2001.

[7] Lisa M Barrangou, Christopher R Daubert, and E Allen Foegeding. Textural properties of agarose gels. I. Rheological and fracture properties. *Food Hydrocolloids*, 20(2-3):184–195, March 2006.

[8] D M Basso and M S Beattie. A sensitive and reliable locomotor rating scale for open field testing in rats. *Journal of . . .*, 1995.

[9] T N Behar, MM Dugich Djordjevic, and Y X Li. Neurotrophins stimulate chemotaxis of embryonic cortical neurons. *European Journal of Neuroscience*, 9(12):2561–2570, 1997.

[10] R. Bellamkonda. Peripheral nerve regeneration: An opinion on channels, scaffolds and anisotropy. *Biomaterials*, March 2006.

[11] Michael J Beltran, Travis C Burns, Tobin T Eckel, Benjamin K Potter, Joseph C Wenke, and Joseph R Hsu. Fate of Combat Nerve Injury. *Journal of Orthopaedic Trauma*, 26(11):e198–e203, November 2012.

[12] A Blesch and M.H. Tuszynski. Spinal cord injury: plasticity, regeneration and the challenge of translational drug development. *Trends in neurosciences*, 32(1):41–47, 2009.

[13] B Blomback and L A Hanson. Blombäck: Plasma proteins - Google Scholar. New York: John Wiley and Sons, 1979.

[14] D Bouhassira, N Attal, J Fermanian, and H Alchaar. Development and validation of the neuropathic pain symptom inventory. *Pain*, 2004.

[15] K Brattain. ANALYSIS OF THE PERIPHERAL NERVE REPAIR MARKET IN THE UNITED STATES. *content.stockpr.com*, March 2012.

[16] M B Browning, S N Cereceres, P T Luong, and E M Cosgriff-Hernandez. Determination of the in vivo degradation mechanism of PEGDA hydrogels. *Journal of Biomedical Materials Research Part A*, pages n/a–n/a, February 2014.

[17] Stephanie J Bryant, Ryan J Bender, Kevin L Durand, and Kristi S Anseth. Encapsulating chondrocytes in degrading PEG hydrogels with high modulus: Engineering gel structural changes to facilitate cartilaginous tissue production. *Biotechnology and Bioengineering*, 86(7):747–755, 2004.

[18] Ramon Y Cajal. Degeneration and regeneration of the nervous system. London: Oxford University Press, 1928.

[19] X Cao and M.S. Shoichet. Delivering neuroactive molecules from biodegradable microspheres for application in central nervous system disorders. *Biomaterials*, 20(4):329–340, 1999.

[20] Chen-Jung Chang, Shan-hui Hsu, Hung-Jen Yen, Han Chang, and Shih-Kuang Hsu. Effects of unidirectional permeability in asymmetric poly(DL-lactic acid-co-glycolic acid) conduits on peripheral nerve regeneration: Anin vitro andin vivo study. *Journal of Biomedical Materials Research Part A*, 83B(1):206–215, 2007.

[21] Hoi-Yan Cheung, Kin-Tak Lau, Tung-Po Lu, and David Hui. A critical review on polymer-based bioengineered materials for scaffold development. *Composites Part B: Engineering*, 38(3):291–300, April 2007.

[22] J H Cheung, W B Stockton, and M F Rubner. Molecular-Level Processing of Conjugated Polymers. 3. Layer-by-Layer Manipulation of Polyaniline via Electrostatic Interactions. *Macromolecules*, 30(9):2712–2716, May 1997.

[23] SY Chew, R Mi, and A Hoke. ScienceDirect.com - Biomaterials - The effect of the alignment of electrospun fibrous scaffolds on Schwann cell maturation. *Biomaterials*, 2008.

[24] Hou-Yu Chiang, Hsiung-Fei Chien, Hsin-Hsin Shen, Jean-Dean Yang, Yu-Hua Chen, Jui-Hsiang Chen, and Sung-Tsang Hsieh. Reinnervation of Muscular Targets by Nerve Regeneration through Guidance Conduits. *Journal of Neuropathology & Experimental Neurology*, 64(7):576, July 2005.

[25] Woon N Chow, David G Simpson, John W Bigbee, and Raymond J Colello. Evaluating neuronal and glial growth on electrospun polarized matrices: bridging the gap in percussive spinal cord injuries. *Neuron Glia Biology*, 3(02):119, August 2007.

[26] Christopher Reeve Paralysis Foundation. *One degree of separation: Paralysis and spinal cord injury in the United States*. Christopher and Dana Reeve Foundation, 2009.

[27] Palma Ciaramitaro, Mauro Mondelli, Francesco Logullo, Serena Grimaldi, Bruno Battiston, Arman Sard, Cecilia Scarinzi, Giuseppe Migliaretti, Giuliano Faccani, Dario Cocito, and on behalf of the Italian Network for Traumatic Neuropathies. Traumatic peripheral nerve injuries: epidemiological findings, neuropathic pain and quality of life in 158 patients. *Journal of the Peripheral Nervous System*, 15(2):120–127, June 2010.

[28] P.D. Dalton, L Flynn, and M.S. Shoichet. Manufacture of poly (2-hydroxyethyl methacrylate-co-methyl methacrylate) hydrogel tubes for use as nerve guidance channels. *Biomaterials*, 23(18):3843–3851, 2002.

[29] Luis de Medinaceli, Richard Jed Wyatt, and William J Freed. Peripheral nerve reconnection: mechanical, thermal, and ionic conditions that promote the return of function. *Experimental neurology*, 81(2):469–487, August 1983.

[30] Godard C W de Ruiter, Martijn J A Malessy, Michael J Yaszemski, Anthony J Windebank, and Robert J Spinner. Designing ideal conduits for peripheral nerve repair. *Neurosurgical FOCUS*, 26(2):E5, February 2009.

[31] G Decher. Fuzzy nanoassemblies: toward layered polymeric multicomposites. *Science*, 277(5330):1232, 1997.

[32] Gero Decher, Jong-Dal Hong, and J. Schmitt. Buildup of ultrathin multilayer films by a self-assembly process, 1 consecutive adsorption of anionic and cationic bipolar amphiphiles on charged surfaces. *Makromolekulare Chemie. Macromolecular Symposia*, 46(1):321–327, 1991.

[33] Solitaire A DeLong, James J Moon, and Jennifer L West. Covalently immobilized gradients of bFGF on hydrogel scaffolds for directed cell migration. *Biomaterials*, 26(16):3227–3234, June 2005.

[34] W F A den Dunnen, P H Robinson, R van Wessel, A J Pennings, M B M van Leeuwen, and J M Schakenraad. Long-term evaluation of degradation and foreign-body reaction of subcutaneously implanted poly(DL-lactide-?-caprolactone). *Journal of biomedical materials research*, 36(3):337–346, September 1997.

[35] M DeVivo, Y Chen, and S Mennemeyer. Costs of care following spinal cord injury. *Topics in Spinal Cord ...*, 16(4):1–9, 2011.

[36] N.O. Dhoot, C.A. Tobias, I Fischer, and M.A. Wheatley. Peptidemodified alginate surfaces as a growth permissive substrate for neurite outgrowth. *Journal of Biomedical Materials Research Part A*, 71(2):191–200, 2004.

[37] Beibei Ding, Jie Cai, Junchao Huang, Lina Zhang, Yun Chen, Xiaowen Shi, Yumin Du, and Shigenori Kuga. Facile preparation of robust and biocompatible chitin aerogels. *Journal of Materials Chemistry*, 22(12):5801–5809, 2012.

[38] Dustin J Donnelly and Phillip G Popovich. Inflammation and its role in neuroprotection, axonal regeneration and functional recovery after spinal cord injury. *Experimental neurology*, 209(2):378–388, February 2008.

[39] Xiaodong Duan, Christopher McLaughlin, May Griffith, and Heather Sheardown. Biofunctionalization of collagen for improved biological response: Scaffolds for corneal tissue engineering. *Biomaterials*, 28(1):78–88, January 2007.

[40] TB Ducker. Experimental improvements in the use of Silastic... [J Neurosurg. 1968] - PubMed - NCBI. *Journal of neurosurgery*, 1968.

[41] H Chandler Elliott. Crosssectional diameters and areas of the human spinal cord. *The Anatomical Record*, 1945.

[42] Laura Elomaa, Sandra Teixeira, Risto Hakala, Harri Korhonen, Dirk W Grijpma, and Jukka V Seppälä. Preparation of poly(ε-caprolactone)-based tissue engineering scaffolds by stereolithography. *Acta biomaterialia*, 7(11):3850–3856, November 2011.

[43] Adam Engler, Shamik Sen, Lee Sweeney, and Dennis E Discher. Matrix Elasticity Directs Stem Cell Lineage Specification . *Cell*, 126:677, 2006.

[44] Shaun Eshraghi and Suman Das. Mechanical and microstructural properties of polycaprolactone scaffolds with one-dimensional, two-dimensional, and three-dimensional orthogonally oriented porous architectures produced by selective laser sintering. *Acta biomaterialia*, 6(7):2467–2476, July 2010.

[45] J R Fann, C H Bombardier, J S Richards, and D G Tate. Depression after spinal cord injury: comorbidities, mental health service use, and adequacy of treatment. *Archives of physical ...*, 92(3):352–360, 2011.

[46] J W Fawcett and R J Keynes. Peripheral nerve regeneration. *Annual Review of Neuroscience*, 13:43–60, 1990.

[47] M G Fehlings, LHS Sekhon, and C Tator. The role and timing of decompression in acute spinal cord injury: what do we know? What should we do? *Spine*, 91(1):1–11, 2001.

[48] KJL Fernandes and W Tetzlaff. *Gene expression in axotomized neurons: identifying the intrinsic determinants of axonal growth.* Axonal Regeneration in the Central Nervous System, 2002.

[49] M T Fitch and J Silver. Glial cell extracellular matrix: boundaries for axon growth in development and regeneration. *Cell and tissue research*, 290(2):379–384, 1997.

[50] Lauren Flynn, Paul D Dalton, and Molly S Shoichet. Fiber templating of poly (2-hydroxyethyl methacrylate) for neural tissue engineering. *Biomaterials*, 24(23):4265–4272, 2003.

[51] Scott Freeman, Kim Quillin, and Lizabeth Allison. *Biological Science: Pearson New International Edition.* Pearson Higher Ed, August 2013.

[52] T Freier, H.S. Koh, K Kazazian, and M.S. Shoichet. Controlling cell adhesion and degradation of chitosan films by N-acetylation. *Biomaterials*, 26(29):5872–5878, 2005.

[53] B Fritzsch, I Silos-Santiago, and L M Bianchi. The role of neurotrophic factors in regulating the development of inner ear innervation. *Trends in neurosciences*, 20(20):159–164, 1997.

[54] H L Gabelnick. Biodegradable implants: alternative approaches. *Advanced in human fertility and reproductive endocrinology: vol. 2: Long acting steroid contraception. New York: Raven Press*, pages 149–173, 1983.

[55] Mingyong Gao, Paul Lu, Bridget Bednark, Dan Lynam, James M Conner, Jeff Sakamoto, and Mark H Tuszynski. Templated agarose scaffolds for the support of motor axon regeneration into sites of complete spinal cord transection. *Biomaterials*, 34(5):1529–1536, February 2013.

[56] RW Garrity. The use of plastic and rubber tubing in the manag... [Surg Forum. 1956] - PubMed - NCBI. *Surgical forum*, 1956.

[57] N Genes. Effect of substrate mechanics on chondrocyte adhesion to modified alginate surfaces. *Archives of Biochemistry and Biophysics*, 422(2):161–167, February 2004.

[58] Penelope C Georges, William J Miller, David F Meaney, Evelyn S Sawyer, and Paul A Janmey. Matrices with Compliance Comparable to that of Brain Tissue Select Neuronal over Glial Growth in Mixed Cortical Cultures. *Biophysical Journal*, 90(8):3012–3018, April 2006.

[59] Randall M German. *Powder Metallurgy Science*. Metal Powder Industry, 1994.

[60] D K Gilding. *Biodegradable Polymers. Biocompatibility of Clinical Implant Materials. Vol II*, volume 2. Williams DF, ed. CRC Press, Boca Raton, FL, 1981.

[61] N Gomez and C.E. Schmidt. Nerve growth factorimmobilized polypyrrole: Bioactive electrically conducting polymer for enhanced neurite extension. *Journal of Biomedical Materials Research Part A*, 81(1):135–149, 2007.

[62] Alex Goraltchouk, Vanessa Scanga, Cindi M Morshead, and Molly S Shoichet. Incorporation of protein-eluting microspheres into biodegradable nerve guidance channels for controlled release. *Journal of Controlled Release*, 110(2):400–407, January 2006.

[63] PR Gordon-Weeks. Neuronal Growth Cones. Cambridge University Press, 2005.

[64] Eiko Goto, Masahiro Mukozawa, Hideki Mori, and Masayuki Hara. A rolled sheet of collagen gel with cultured Schwann cells: Model of nerve conduit to enhance neurite growth. *Journal of Bioscience and Bioengineering*, 109(5):512–518, May 2010.

[65] T Gros, J.S. Sakamoto, A Blesch, L.A. Havton, and M.H. Tuszynski. Regeneration of long-tract axons through sites of spinal cord injury using templated agarose scaffolds. *Biomaterials*, 31(26):6719–6729, 2010.

[66] Jonathan W Gunn, Suzanne D Turner, and Brenda K Mann. Adhesive and mechanical properties of hydrogels influence neurite extension. *Journal of biomedical materials research*, 72A(1):91–97, 2004.

[67] Tessa Hadlock, Jennifer Elisseeff, Robert Langer, Joseph Vacanti, and Mack Cheney. A Tissue-Engineered Conduit for Peripheral Nerve Repair. *Archives of Otolaryngology–Head & Neck Surgery*, 124(10):1081–1086, 1998.

[68] Tessa A Hadlock, Cathryn A Sundback, Daniel A Hunter, Joseph P Vacanti, and Mack L Cheney. A new artificial nerve graft containing rolled Schwann cell monolayers. *Microsurgery*, 21(3):96–101, 2001.

[69] T Hashimoto, Y Suzuki, M Kitada, K Kataoka, S Wu, K Suzuki, K Endo, Y Nishimura, and C Ide. Peripheral nerve regeneration through alginate gel: analysis of early outgrowth and late increase in diameter of regenerating axons. *Experimental Brain Research*, 146(3):356–368, August 2002.

[70] J Hermans and J McDonagh. *Fibrin: structure and interactions.*, volume 8. Seminars in thrombosis and hemostasis, 1982.

[71] Michael Hiles and Jason Hodde. Tissue engineering a clinically useful extracellular matrix biomaterial. *International Urogynecology Journal*, 17(S1):39–43, April 2006.

[72] K W Horch and P R Burgess. *Functional specificity and somatotopic organization during peripheral nerve regeneration.* Nerve Repair and Regeneration, 1980.

[73] Jason H Huang, D Kacy Cullen, Kevin D Browne, Robert Groff, Jun Zhang, Bryan J Pfister, Eric L Zager, and Douglas H Smith. Long-Term Survival and Integration of Transplanted Engineered Nervous Tissue Constructs Promotes Peripheral Nerve Regeneration. *dx.doi.org*, 2009.

[74] Andres Hurtado, Jared M Cregg, Han B Wang, Dane F Wendell, Martin Oudega, Ryan J Gilbert, and John W McDonald. Robust CNS regeneration after complete spinal cord transection using aligned poly-L-lactic acid microfibers. *Biomaterials*, 32(26):6068–6079, 2011.

[75] Satoshi Ichihara, Yuji Inada, and Tatsuo Nakamura. Artificial nerve tubes and their application for repair of peripheral nerve injury: an update of current concepts. *Injury*, 39:29–39, October 2008.

[76] C B Jenq and R E Coggeshall. Sciatic nerve regeneration after autologous sural nerve transplantation in the rat. *Brain Research*, 406:52–61, 1987.

[77] L L Jones, R U Margolis, and M.H. Tuszynski. The chondroitin sulfate proteoglycans neurocan, brevican, phosphacan, and versican are differentially regulated following spinal cord injury. *Experimental neurology*, 182(2):399–411, 2003.

[78] T.A. Kapur and M.S. Shoichet. Chemically-bound nerve growth factor for neural tissue engineering applications. *Journal of Biomaterials Science, Polymer Edition*, 14(4):383–394, 2003.

[79] S Kehoe, X F Zhang, and D Boyd. FDA approved guidance conduits and wraps for peripheral nerve injury: A review of materials and efficacy. *Injury*, 43(5):553–572, May 2012.

[80] Ji Hye Kim, Sang Bong Lee, Seon Jeong Kim, and Young Moo Lee. Rapid temperature/pH response of porous alginate-g-poly(N-isopropylacrylamide) hydrogels. *Polymer*, 43(26):7549–7558, December 2002.

[81] Jacob Koffler, Ramsey F Samara, and Ephron S Rosenzweig. Using Templated Agarose Scaffolds to Promote Axon Regeneration Through Sites of Spinal Cord Injury. In *Axon Growth and Regeneration*, pages 157–165. Springer New York, New York, NY, April 2014.

[82] R Kohn. Ion binding on polyuronates - alginate and pectin. *Pure and Applied Chemistry*, 42(3):371–397, 1975.

[83] Bryan Kolb and Ian Whishaw. An introduction to brain and behaviour. Worth Pub, 2001.

[84] H J Kong, E Alsberg, D Kaigler, K Y Lee, and D J Mooney. Controlling Degradation of Hydrogels via the Size of Crosslinked Junctions. *Advanced Materials*, 16(21):1917–1921, November 2004.

[85] Christian Krarup, Simon J Archibald, and Roger D Madison. Factors that influence peripheral nerve regeneration: An electrophysiological study of the monkey median nerve. *Annals of Neurology*, 51(1):69–81, January 2002.

[86] C.K. Kuo and P.X. Ma. Ionically crosslinked alginate hydrogels as scaffolds for tissue engineering: Part 1. Structure, gelation rate and mechanical properties. *Biomaterials*, 22(6):511–521, 2001.

[87] H Y Kweon, M K Yoo, I K Park, T H Kim, H C Lee, and H S Lee. A novel degradable polycaprolactone networks for tissue engineering. *Biomaterials*, 2003.

[88] Kyle J Lampe, Alexander L Antaris, and Sarah C Heilshorn. Design of three-dimensional engineered protein hydrogels for tailored control of neurite growth. *Acta biomaterialia*, 9(3):5590–5599, March 2013.

[89] C W Lee, E A Vitriol, S Shim, A L Wise, and R P Velayutham. Dynamic localization of G-actin during membrane protrusion in neuronal motility. *Current Biology*, 2013.

[90] Jungwoo Lee, Meghan J Cuddihy, and Nicholas A Kotov. Three-Dimensional Cell Culture Matrices: State of the Art. *Tissue Engineering Part B: Reviews*, 14(1):61–86, March 2008.

[91] Kuen Yong Lee and David J Mooney. Alginate: Properties and biomedical applications. *Progress in Polymer Science*, 37(1):106–126, January 2012.

[92] S K Lee and S W Wolfe. Peripheral nerve injury and repair. *Journal of the American Academy of . . .*, 8(4):243–252, 2000.

[93] M A LeRoux, F Guilak, and L A Setton. Compressive and shear properties of alginate gel: effects of sodium ions and alginate concentration. *Journal of Biomedical . . .*, 1999.

[94] J M Levine, R Reynolds, and J W Fawcett. The oligodendrocyte precursor cell in health and disease. *Trends in neurosciences*, 24(1):39–47, 2001.

[95] Ruijun Li, Zhigang Liu, Yuemei Pan, Lei Chen, Zhixin Zhang, and Laijin Lu. Peripheral Nerve Injuries Treatment: a Systematic Review. *Cell Biochemistry and Biophysics*, 68(3):449–454, September 2013.

[96] Shu-Tung Li and Debbie Yuen. Implant devices for nerve repair. *US Patent*, 2004.

[97] Wen-Jen Lin and Chia-Hui Lu. Characterization and permeation of microporous poly(ε-caprolactone) films. *Journal of Membrane Science*, 198(1):109–118, March 2002.

[98] M Lind. Growth factors: Possible new clinical tools: A review. *Acta Orthopaedica*, 1996.

[99] Yo-El Ju Beatrice Marg Miriam Osterfield Paul A Janmey Lisa A Flanagan. Neurite branching on deformable substrates. *Neuroreport*, 13(18):2411, December 2002.

[100] Xinxing Liu, Liying Qian, Tan Shu, and Zhen Tong. Rheology characterization of sol–gel transition in aqueous alginate solutions induced by calcium cations through in situ release. *Polymer*, 44(2):407–412, January 2003.

[101] Laura Anne Lowery and David Van Vactor. The trip of the tip: understanding the growth cone machinery. *Nature Reviews Molecular Cell Biology*, 10(5):332–343, April 2009.

[102] Paul Lu, Armin Blesch, Lori Graham, Yaozhi Wang, Ramsey Samara, Karla Banos, Verena Haringer, Leif Havton, Nina Weishaupt, David Bennett, Karim Fouad, and Mark H Tuszynski. Motor Axonal Regeneration after Partial and Complete Spinal Cord Transection. *The Journal of ...*, 2012.

[103] D. Lynam, B. Bednark, C. Peterson, D Welker, M Gao, and J.S. Sakamoto. Precision microchannel scaffolds for central and peripheral nervous system repair. *Journal of Materials Science: Materials in Medicine*, 22:1–12, 2011.

[104] Daniel Lynam, Chelsea Peterson, Ryan Maloney, Dena Shahriari, Alexa Garrison, Sara Saleh, Sumit Mehrotra, Christina Chan, and Jeff Sakamoto. Augmenting protein release from layer-by-layer functionalized agarose hydrogels. *Carbohydrate Polymers*, 103:377–384, March 2014.

[105] Daniel A Lynam, Dena Shahriari, Kayla J Wolf, Phillip A Angart, Jacob Koffler, Mark H Tuszynski, Christina Chan, Patrick Walton, and Jeffrey Sakamoto. Brain derived neurotrophic factor release from layer-by-layer coated agarose nerve guidance scaffolds. *Acta biomaterialia*, 18:128–131, May 2015.

[106] Aaron D Lynn, Themis R Kyriakides, and Stephanie J Bryant. Characterization of the in vitromacrophage response and in vivohost response to poly(ethylene glycol)-based hydrogels. *Journal of Biomedical Materials Research Part A*, 9999A:NA–NA, 2009.

[107] B L MacInnis. Retrograde Support of Neuronal Survival Without Retrograde Transport of Nerve Growth Factor. *Science*, 295(5559):1536–1539, January 2002.

[108] J Mai, L Fok, H Gao, X Zhang, and M m Poo. Axon Initiation and Growth Cone Turning on Bound Protein Gradients. *Journal of Neuroscience*, 29(23):7450–7458, June 2009.

[109] J F Mano, R A Sousa, L F Boesel, and N M Neves. Bioinert, biodegradable and injectable polymeric matrix composites for hard tissue replacement: state of the art and recent developments. *Composites Science and . . .*, 2004.

[110] R Marchand, S Woerly, L Bertrand, and N Valdes. Evaluation of two cross-linked collagen gels implanted in the transected spinal cord. *Brain Research Bulletin*, 30(3-4):415–422, January 1993.

[111] Marina Matyash, Florian Despang, Chrysanthy Ikonomidou, and Michael Gelinsky. Swelling and mechanical properties of alginate hydrogels with respect to promotion of neural growth. *Tissue Engineering Part C: Methods*, 20(5):401–411, May 2014.

[112] Marina Matyash, Florian Despang, Rakesh Mandal, Diccon Fiore, Michael Gelinsky, and Chrysanthy Ikonomidou. Novel soft alginate hydrogel strongly supports neurite growth and protects neurons against oxidative stress. *Tissue Engineering Part A*, 18(1-2):55–66, January 2012.

[113] Christopher A McKay, Rebecca D Pomrenke, Joshua S McLane, Nicholas J Schaub, Elise K DeSimone, Lee A Ligon, and Ryan J Gilbert. An Injectable, Calcium Responsive Composite Hydrogel for the Treatment of Acute Spinal Cord Injury. *Acs Applied Materials & Interfaces*, 6(3):1424–1438, 2014.

[114] M F Meek and J H Coert. US Food and Drug Administration/Conformit Europe-Approved Absorbable Nerve Conduits for Clinical Repair of Peripheral and Cranial Nerves. *Annals of Plastic Surgery*, 60(1):110–116, January 2008.

[115] S. Mehrotra, D. Lynam, R. Maloney, K.M. Pawelec, M.H. Tuszynski, I Lee, C Chan, and J Sakamoto. Time Controlled Protein Release from LayerbyLayer Assembled Multilayer Functionalized Agarose Hydrogels. *Advanced Functional Materials*, 20(2):247–258, 2010.

[116] Sumit Mehrotra, Daniel Lynam, Chun Liu, Dena Shahriari, Ilsoon Lee, Mark Tuszynski, Jeffrey Sakamoto, and Christina Chan. Time Controlled Release of Arabinofuranosylcytosine (Ara-C) from Agarose Hydrogels using Layer-by-Layer Assembly: An In Vitro Study. *Journal of Biomaterials Science, Polymer Edition*, 23(1-4):439–463, January 2012.

[117] Sally Meiners, Ijaz Ahmed, Abdul S Ponery, Nathan Amor, Suzan L Harris, Virginia Ayres, Yuan Fan, Qian Chen, Roberto Delgado-Rivera, and Ashwin N Babu. Engineering electrospun nanofibrillar surfaces for spinal cord repair: a discussion. *Polymer International*, 56(11):1340–1348, 2007.

[118] TKL Meyvis, S C De Smedt, Jo Demeester, and W E Hennink. Rheological monitoring of long-term degrading polymer hydrogels. *Journal of rheology*, 43(4):933–950, 1999.

[119] Tom KL Meyvis, Barbara G Stubbe, Mies J Van Steenbergen, Wim E Hennink, Stefaan C De Smedt, and Joseph Demeester. A comparison between the use of dynamic mechanical analysis and oscillatory shear rheometry for the characterisation of hydrogels. *International journal of pharmaceutics*, 244(1):163–168, 2002.

[120] H Millesi. *Nerve grafting*. Reconstructive Plastic Surgery, 1977.

[121] Kathryn Moore, Margaret MacSween, and Molly Shoichet. Immobilized concentration gradients of neurotrophic factors guide neurite outgrowth of primary neurons in macroporous scaffolds. *Tissue Engineering*, 12(2):267–278, February 2006.

[122] A Mosahebi, M Wiberg, and G Terenghi. Addition of fibronectin to alginate matrix improves peripheral nerve regeneration in tissue-engineered conduits. *Tissue Engineering*, 9(2):209–218, 2003.

[123] National Spinal Cord Injury Statistical Center. Spinal Cord Injury (SCI) Facts and Figures at a Glance. *National Spinal Cord Injury Statistical Center*, October 2014.

[124] M E Nimni, D Cheung, B Strates, M Kodama, and K Sheikh. Chemically modified collagen: A natural biomaterial for tissue replacement. *Journal of biomedical materials research*, 21(6):741–771, June 1987.

[125] J Noble, C A Munro, and VSSV Prasad. Analysis of upper and lower extremity peripheral nerve injuries in a population of patients with multiple injuries. *Journal of Trauma and ...*, 1998.

[126] A Nussinovitch, M Peleg, and Normand M D. A Modified Maxwell and a Nonexponential Model for Characterization of the Stress Relaxation of Agar and Alginate Gels. *Journal of food science*, 54(4):1013–1016, July 1989.

[127] G Orive, S Ponce, R M Hernandez, A R Gascon, M Igartua, and J L Pedraz. Biocompatibility of microcapsules for cell immobilization elaborated with different type of alginates. *Biomaterials*, 23(18):3825–3831, September 2002.

[128] M Oudega. Axonal regeneration into Schwann cell grafts within resorbable poly(α-hydroxyacid) guidance channels in the adult rat spinal cord. *Biomaterials*, 22(10):1125–1136, May 2001.

[129] M Oudega, S Varon, and T Hagg. Regeneration of adult rat sensory axons into intraspinal nerve grafts: promoting effects of conditioning lesion and graft predegeneration. *Experimental neurology*, 129(2):194–206, 1994.

[130] Kiran Pawar, Brian J Cummings, Aline Thomas, Lonnie D Shea, Ariel Levine, Sam Pfaff, and Aileen J Anderson. Biomaterial bridges enable regeneration and re-entry of corticospinal tract axons into the caudal spinal cord after SCI: Association with recovery of forelimb function. *Biomaterials*, 65:1–12, June 2015.

[131] Kiran Pawar, Rainer Mueller, Massimiliano Caioni, Peter Prang, Ulrich Bogdahn, Werner Kunz, and Norbert Weidner. Increasing capillary diameter and the incorporation of gelatin enhance axon outgrowth in alginate-based anisotropic hydrogels. *Acta biomaterialia*, 7(7):2826–2834, July 2011.

[132] Lukas A Pfister, Eva Alther, Michaël Papaloïzos, Hans P Merkle, and Bruno Gander. Controlled nerve growth factor release from multi-ply alginate/chitosan-based nerve conduits. *European Journal of Pharmaceutics and Biopharmaceutics*, 69(2):563–572, June 2008.

[133] A Piattelli and A Scarano. Clinical and histologic aspects of biphasic calcium phosphate ceramic (BCP) used in connection with implant placement. *Biomaterials*, 1996.

[134] Elsie S Place, Luis Rojo, Eileen Gentleman, José P Sardinha, and Molly M Stevens. Strontium- and Zinc-Alginate Hydrogels for Bone Tissue Engineering. *Tissue Engineering Part A*, 17(21-22):2713–2722, November 2011.

[135] Phillip G Popovich and WILLIAM F HICKEY. Bone Marrow Chimeric Rats Reveal the Unique Distribution of Resident and Recruited Macrophages in the Contused Rat Spinal Cord. *Journal of Neuropathology & Experimental Neurology*, 60(7):676, July 2001.

[136] Molamma P Prabhakaran, J Venugopal, Casey K Chan, and S Ramakrishna. Surface modified electrospun nanofibrous scaffolds for nerve tissue engineering. *Nanotechnology*, 19(45):455102, October 2008.

[137] P Prang, R Muller, A Eljaouhari, K Heckmann, W. Kunz, T. Weber, C. Faber, M. Vroemen, U. Bogdahn, and N. Weidner. The promotion of oriented axonal regrowth in the injured spinal cord by alginate-based anisotropic capillary hydrogels. *Biomaterials*, 27(19):3560–3569, 2006.

[138] R M Quencer and R P Bunge. The injured spinal cord: imaging, histopathologic, clinical correlates, and basic science approaches to enhancing neural function after spinal cord injury. *Spine*, 21(18):2064, 1996.

[139] Françoise Quignard, Romain Valentin, and Francesco Di Renzo. Aerogel materials from marine polysaccharides. *New Journal of Chemistry*, 32(8):1300, 2008.

[140] Branden Reid, Matthew Gibson, Anirudha Singh, Janis Taube, Cecilia Furlong, Melissa Murcia, and Jennifer Elisseeff. PEG hydrogel degradation and the

role of the surrounding tissue environment. *Journal of Tissue Engineering and Regenerative Medicine*, pages n/a–n/a, March 2013.

[141] Joël Reignier and Michel A Huneault. Preparation of interconnected poly(ε-caprolactone) porous scaffolds by a combination of polymer and salt particulate leaching. *Polymer*, 47(13):4703–4717, June 2006.

[142] Dongwen Ren, Hongfu Yi, Wei Wang, and Xiaojun Ma. The enzymatic degradation and swelling properties of chitosan matrices with different degrees of N-acetylation. *Carbohydrate Research*, 340(15):2403–2410, October 2005.

[143] K Rezwan, Q Z Chen, J J Blaker, and A R Boccaccini. Biodegradable and bioactive porous polymer/inorganic composite scaffolds for bone tissue engineering. *Biomaterials*, 27(18):3413–3431, June 2006.

[144] K E Rhodes and J W Fawcett. Chondroitin sulphate proteoglycans: preventing plasticity or protecting the CNS? *Journal of anatomy*, 204(1):33–48, 2004.

[145] M Samii and R Wallenborn. Tierexperimentelle Untersuchungen über den Einfluß der Spannung auf den Regenerationserfolg nach Nervennaht. *Acta Neurochirurgica*, 27(2):87–110, 1972.

[146] Dan H Sanes, Thomas A Reh, and William A Harris. *Development of the Nervous System*. Academic Press, January 2011.

[147] Lizzie Y Santiago, Richard W Nowak, J Peter Rubin, and Kacey G Marra. Peptide-surface modification of poly(caprolactone) with laminin-derived sequences for adipose-derived stem cell applications. *Biomaterials*, 27(15):2962–2969, May 2006.

[148] C.E. Schmidt and J B Leach. Neural tissue engineering: strategies for repair and regeneration. *... review of biomedical engineering*, 5(2):293–347, 2003.

[149] E Schnell, K Klinkhammer, S Balzer, G Brook, D. Klee, P. Dalton, and J. Mey. Guidance of glial cell migration and axonal growth on electrospun nanofibers of poly- ε-caprolactone and a collagen/poly- ε-caprolactone blend. *Biomaterials*, 28(19):3012–3025, 2007.

[150] M E Schwab and D Bartholdi. Degeneration and regeneration of axons in the lesioned spinal cord. *Physiological reviews*, 76(2):319–370, April 1996.

[151] Dena Shahriari, Jacob Koffler, Daniel A Lynam, Mark H Tuszynski, and Jeffrey S Sakamoto. Characterizing the degradation of alginate hydrogel for use in multilumen scaffolds for spinal cord repair. *Journal of Biomedical Materials Research Part A*, 104(3):611–619, November 2015.

[152] JL Sharon. Immobilization of glycoproteins, such as VEGF, on biodegradable substrates . *Acta biomaterialia*, 2008.

[153] Lauren Shor, Selçuk Güçeri, Xuejun Wen, Milind Gandhi, and Wei Sun. Fabrication of three-dimensional polycaprolactone/hydroxyapatite tissue scaffolds and osteoblast-scaffold interactions in vitro. *Biomaterials*, 28(35):5291–5297, December 2007.

[154] D J Short, W S El Masry, and P W Jones. High dose methylprednisolone in the management of acute spinal cord injury–a systematic review from a clinical perspective. *Spinal Cord*, 38(5):273–286, 2000.

[155] D H Sierra. Fibrin Sealant Adhesive Systems: A Review of Their Chemistry, Material Properties and Clinical Applications. *Journal of Biomaterials Applications*, 7(4):309–352, January 1993.

[156] Lisa A Simpson, Janice J Eng, Jane T C Hsieh, Wolfe, and Dalton L the Spinal Cord Injury Re. The Health and Life Priorities of Individuals with Spinal Cord Injury: A Systematic Review. *Journal of Neurotrauma*, 29(8):1548–1555, May 2012.

[157] Ryan M Smith, Christina Wiedl, Paul Chubb, and Charlotte H Greene. Role of Small Intestine Submucosa (SIS) as a Nerve Conduit: Preliminary Report. *Journal of Investigative Surgery*, 17(6):339–344, January 2004.

[158] Shula Stokols, Jeff Sakamoto, Chris Breckon, Todd Holt, James Weiss, and Mark H Tuszynski. Templated Agarose Scaffolds Support Linear Axonal Regeneration. *Tissue Engineering*, 12(10):2777–2787, October 2006.

[159] Shula Stokols and Mark H Tuszynski. Freeze-dried agarose scaffolds with uniaxial channels stimulate and guide linear axonal growth following spinal cord injury. *Biomaterials*, 27(3):443–451, January 2006.

[160] Svetlana A Sukhishvili and Steve Granick. Layered, erasable, ultrathin polymer films. *... -AMERICAN CHEMICAL SOCIETY*, 2000.

[161] Svetlana A Sukhishvili and Steve Granick. Layered, Erasable Polymer Multilayers Formed by Hydrogen-Bonded Sequential Self-Assembly. *Macromolecules*, 35(1):301–310, January 2002.

[162] DR Sumner, TM Turner, and AF Purchio. Enhancement of bone ingrowth by transforming growth factor-beta. *The Journal of bone ...*, 1995.

[163] S Sunderland. *Disturbances of the brachial plexus origin associated with unusual anatomical arrangements in the cervico-brachial region: The thoracic outlet syndrome*. Nerves and Nerve Injuries. Edinburgh: Churchill Living- stone., 2nd edition, 1978.

[164] D M Suter and P Forscher. Substrate-cytoskeletal coupling as a mechanism for the regulation of growth cone motility and guidance. *Journal of neurobiology*, 2000.

[165] Y Suzuki, M Kitaura, S Wu, K Kataoka, K Suzuki, K Endo, Y Nishimura, and C Ide. Electrophysiological and horseradish peroxidase-tracing studies of nerve regeneration through alginate-filled gap in adult rat spinal cord. *Neuroscience letters*, 318(3):121–124, 2002.

[166] C.H. Tator. Update on the pathophysiology and pathology of acute spinal cord injury. *Brain Pathology*, 5(4):407–413, 1995.

[167] Y.D. Teng, E.B. Lavik, X. Qu, K.I. Park, J. Ourednik, D. Zurakowski, R. Langer, and E.Y. Snyder. Functional recovery following traumatic spinal cord injury mediated by a unique polymer scaffold seeded with neural stem cells. *Proceedings of the National Academy of Sciences*, 99(5):3024, 2002.

[168] J K Terzis. *Patterns of cutaneous innervation and reinnervation follwoing nerve transection.* Posttraumatic Peripheral Nerve Regeneration, 1981.

[169] Aline M Thomas, Matthew B Kubilius, Samantha J Holland, Stephanie K Seidlits, Ryan M Boehler, Aileen J Anderson, Brian J Cummings, and Lonnie D Shea. Channel density and porosity of degradable bridging scaffolds on axon growth after spinal injury. *Biomaterials*, 34(9):2213–2220, March 2013.

[170] R D Treede, T S Jensen, J N Campbell, and G Cruccu. Neuropathic pain redefinition and a grading system for clinical and research purposes. *Neurology*, 2008.

[171] K L Tucker, M Meyer, and Y A Barde. Neurotrophins are required for nerve growth during development. *Nature Neuroscience*, 4:29–37, 2001.

[172] Hannah M Tuinstra, Misael O Aviles, Seungjin Shin, Samantha J Holland, Marina L Zelivyanskaya, Alan G Fast, Sarah Y Ko, Daniel J Margul, Anne K Bartels, Ryan M Boehler, Brian J Cummings, Aileen J Anderson, and Lonnie D Shea. Multifunctional, multichannel bridges that deliver neurotrophin encoding lentivirus for regeneration following spinal cord injury. *Biomaterials*, 33(5):1618–1626, February 2012.

[173] Mark H Tuszynski and Oswald Steward. Concepts and methods for the study of axonal regeneration in the CNS. *Neuron*, 74(5):777–791, June 2012.

[174] M.H. Tuszynski and J H Kordower. CNS Regeneration: basic science and clinical applications. San Diego, CA: Academic Press, 1999.

[175] T Ueyama. The topography of root fibres within the sciatic nerve trunk of the dog. *Journal of anatomy*, 127(Pt 2):277, October 1978.

[176] A Wang, Q Ao, W Cao, M Yu, Q He, L. Kong, L Zhang, Y. Gong, and X Zhang. Porous chitosan tubular scaffolds with knitted outer wall and controllable inner structure for nerve tissue engineering. *Journal of Biomedical Materials Research Part A*, 79(1):36–46, 2006.

[177] Liyan Wang, Zhiqiuang Wang, Xi Zhang, Jiacong Shen, Lifeng Chi, and Harald Fuchs. A new approach for the fabrication of an alternating multilayer film of poly(4-vinylpyridine) and poly(acrylic acid) based on hydrogen bonding. *Macromolecular Rapid Communications*, 18(6):509–514, June 1997.

[178] X Wang. Dog sciatic nerve regeneration across a 30-mm defect bridged by a chitosan/PGA artificial nerve graft. *Brain*, 128(8):1897–1910, May 2005.

[179] P Weiss. *NERVE FIBER COUNTS AND MUSCLE TENSION AFTER NERVE REGENERATION IN THE RAT*. Trans. Amer. neurol. Ass, 1943.

[180] Paul Weiss and A Cecil Taylor. Further experimental evidence against "neurotropism" in nerve regeneration. *Journal of Experimental Zoology*, 95(2):233–257, March 1944.

[181] X Wen. Fabrication and characterization of permeable degradable poly (dl-lactide- co-glycolide)(PLGA) hollow fiber phase inversion membranes for use as nerve tract .... *Biomaterials*, 2006.

[182] Kevin J Whittlesey and Lonnie D Shea. Nerve growth factor expression by PLG-mediated lipofection. *Biomaterials*, 27(11):2477–2486, 2006.

[183] J M Williams, A Adewunmi, R M Schek, and C L Flanagan. Bone tissue engineering using polycaprolactone scaffolds fabricated via selective laser sintering. *Biomaterials*, 2005.

[184] F E Wiria, K F Leong, C K Chua, and Y Liu. Poly-ε-caprolactone/hydroxyapatite for tissue engineering scaffold fabrication via selective laser sintering. *Acta biomaterialia*, 3(1):1–12, January 2007.

[185] St phane Woerly, Van Diep Doan, F Evans-Martin, Christopher G Paramore, and Jean D Peduzzi. Spinal cord reconstruction using NeuroGel? implants and functional recovery after chronic injury. *Journal of Neuroscience Research*, 66(6):1187–1197, 2001.

[186] Fan Yang, Christopher G Williams, Dong-an Wang, Hyukjin Lee, Paul N Manson, and Jennifer Elisseeff. The effect of incorporating RGD adhesive peptide in polyethylene glycol diacrylate hydrogel on osteogenesis of bone marrow stromal cells. *Biomaterials*, 26(30):5991–5998, October 2005.

[187] W Y Yeong, N Sudarmadji, H Y Yu, C K Chua, K F Leong, S S Venkatraman, Y C F Boey, and L P Tan. Porous polycaprolactone scaffold for cardiac tissue engineering fabricated by selective laser sintering. *Acta biomaterialia*, 6(6):2028–2034, June 2010.

[188] Leroy Young, R Chris Wray, and Paul M Weeks. A Randomized Prospective Comparison of Fascicular and Epineural Digital Nerve Repairs. *Plastic and Reconstructive Surgery*, 68(1):89–93, July 1981.

[189] X Yu. Tissue-engineered scaffolds are effective alternatives to autografts for bridging peripheral nerve gaps. *Tissue Engineering*, 2003.